THE UNIVERSITY OF MICHIGAN

COLLEGE OF ENGINEERING

DEPARTMENT OF ELECTRICAL ENGINEERING

Radiation Laboratory

TV AND FM INTERFERENCE BY WINDMILLS

FINAL REPORT

1 January 1976 - 31 December 1976

February 1977

Contract No. E(11-1)-2846

by: Thomas B.A. Senior, Dipak L. Sengupta and
Joseph E. Ferris

Prepared for:

Energy Research and Development Administration
20 Massachusetts Avenue, N.W.
Washington, D.C. 20001

14438-1-F = RL-2273

Ann Arbor, Michigan

014438-1-F

TV and FM Interference by Windmills

by

Thomas B.A. Senior, Dipak L. Sengupta and Joseph E. Ferris
The University of Michigan
Radiation Laboratory
Ann Arbor, Michigan 48109

Final Report

1 January 1976 - 31 December 1976

February 1977

Contract No. E(11-1)-2846

Prepared for

Energy Research and Development Administration
20 Massachusetts Avenue, N.W.
Washington, D.C. 20001

ABSTRACT

The report describes a preliminary but wide ranging investigation of the effects of a horizontal axis windmill on the reception of TV and FM signals in its vicinity. It is shown that the rotating blades produce a time varying amplitude modulation of the total signal received, and that for an antenna so located as to pick up the specular or forward scattering off the blades, the modulation can produce severe distortion of the video portion of a TV signal reproduction. The distortion is worst at the higher frequencies, and therefore poses more of a problem at UHF than at VHF. No interference to the audio signal nor to any FM transmission has been observed. Based on laboratory studies as well as field tests, a modulation level has been established at which the video interference is judged "severe" (or objectionable), and this threshold of interference is substantially independent of the primary field strength. A theory has been developed to compute the interference zone about a windmill for any given TV transmitter, and the results are in good agreement with those obtained from field tests using the operational windmill at the NASA Plum Brook Facility.

TABLE OF CONTENTS

TABLE OF CONTENTS (Continued) Page No.

TABLE OF CONTENTS (Continued)

TABLE OF FIGURES

Page No.

TABLE OF FIGURES (Continued)

TABLE OF TABLES

TABLE OF TABLES (Continued)

INTRODUCTION

1. Background

It is possible that in the years to come large windmills will be used to generate power not only for rural communities but as input to the National Grid, thereby bringing about a revival of one of mankind's earliest methods of harnessing nature. Although the first conversion of wind power is lost in antiquity, a sailboat is depicted on a Egyptian urn circa 4000 BC and there were references to millwrights in Persia some 1300 years ago. Among the westerners sent back to Mongolia by Genghis Kahn were Persian millwrights and Mongolia has maintained its interest in wind-generated power since that time. Horizontal shaft windmills appeared in northwestern Europe 900 years ago and then spread rapidly, remaining common-place throughout the entire continent for over 700 years. It was mostly the power of wind and water that fed the early stages of the industrial revolution, but with the advent of the steam engine and the abundant, reliable and inexpensive power that it provided, the wind soon lost its major role, and windmills lingered on only in regions where steam was unobtainable or impractical, principally for pumping water. Nevertheless, prior to the construction of area-wide electrical power grids in the U.S., propeller-type mills consisting of 20 to 24 galvanized steel blades mounted around a wheel were often used in rural areas to power small electrical generators. These charged batteries that in turn supplied electricity to the house and farm, and by the early 1950's, such units were commonly available in sizes up to 10 kW.

Although winds at ground level come and go in a most unreliable way, even places without strong prevailing surface winds may have strong winds at rather low altitudes, and measurements at three Texas towers off the eastern U.S. have shown annual average wind speeds as high as 20 mph at 100 m above the sea. The World Meterological Association has estimated the wind power in those parts of the lower

atmosphere accessible to man and his machines to be 20 TW, ten times the estimated total power available from flowing streams. But hydro generating capacity in the U.S. is presently around 53 GW, from approximately 30 percent of the potential sites that are available, whereas the wind is contributing nothing.

Experimental work on large scale electrical energy conversion from wind began in France in the 1920's with the construction of a 20 m diameter two-bladed propeller. Work next developed in Russia, Mongolia and Western Europe, but one of the most successful models to date was that constructed in 1941 under the Smith-Putnam project [1] . It was a 53 m diameter, two-bladed propeller mounted on top of Grandpa's Knob near Rutland, Vermont and used to power a 1.25 MW electrical generator. Once a mechanical difficulty associated with a main bearing had been overcome, the machine ran successfully for four years, but when one of the blades failed, the experiment ended for lack of financial support. For all practical purposes, the subject of power generation from the wind lay dormant in the U.S. through two decades of ever increasing power consumption, but was revived by Heronemus as a means of providing power for New England. His initial concept was the placement of wind power systems on offshore banks and in floating positions off the coast, and in 1972 he proposed [2] the construction of 83 clusters of offshore stations to generate an annual average power of 38.2 GW. Each cluster would be 55 km in diameter and consist of 165 towers, with each tower supporting three 60 m diameter rotors driving a 2 MW generator, to produce an average of 900 kW.

Heronemus also proposed a wind-generator network for Eastern Wisconsin to achieve an annual average output of 7.4 GW by extracting about 0.25 percent of the available wind energy over the area. Some of the stations would be floated offshore in Lakes Michigan and Superior, while most would be tower-mounted straddling highways.

Were it not for the power shortages of the last few years and the rapidly increasing costs of fuel, many of these schemes would have remained the pipedreams of an inspired visionary, but as the costs of other power sources escalated, the "clean' energy that is available in the wind has seemed ever more attractive. In 1973 a wind

energy program was initiated jointly by the National Science Foundation and the NASA Lewis Research Center and in 1975 the responsibility for planning and executing a sustained wind energy program was transferred from NSF to the newly formed Energy Research and Development Administration. As part of the program, a 100 kW wind turbine (or windmill) generator has been designed and fabricated, and is now in operation at the Plum Brook facility near Sandusky, Ohio. The rotor consists of two blades of aerofoil shape with a total diameter of 37. 5 m and a fixed coning angle of 7 degrees. The rotor is mounted atop a tower 30 m in height (see Figure 1) and is intended to produce 133 kW of power (100 kW at the actual generator) when rotating at 40 rpm in an 18 mph wind [3, 4] .

With the knowledge gained from this prototype machine, other and larger generators are being developed, and the national goal of energy sufficiency by the 1980's could well see the rapid deployment of this nonpolluting and not visually unattractive system of electrical power generation throughout the United States. Even as presently conceived these windmills could have two or three-blade rotors up to 60 m in diameter [5] . The blades themselves may be twisted and tapered from root to tip, consisting of a metallic skin on a framework of girders or made of fiberglass, and with their aerofoil shape, they would be rather similar to the wings of an aircraft. It is therefore obvious that blades such as these could produce the same type of radio interference as a low-flying aircraft, and could adversely affect both TV and FM reception. Indeed, the problem may be more severe. Whereas aircraft interference is a transitory phenomenon, a windmill would be fixed in its location, and since the blades would be in a plane which is close to the vertical, any windmill could drastically interfere with all forms of radio and TV in that sector of space where signals are received that are specularly reflected from the surfaces of the blades.

If a windmill is to be effective it must be elevated, and to obtain the full advantages of the distributed means of power generation that windmills could provide, most should be located close to the communities which use the power to minimize transmission losses. Communities, both rural and urban, could then find themselves exposed to windmills in the same manner that they are now exposed to radio and TV (transmitting) antennas and at the outset of this study it was not obvious how compatible the two are.

Figure 1. Model of 100 kW wind turbine generator.

2. Purpose and Nature of the Study

Based on preliminary analyses we had performed as well as the observed fact that an aircraft passing nearby could distort a TV picture, it seemed possible that the rotating blades of a windmill could interfere with TV reception. If this was indeed so, it could impact on the allowable siting of a windmill vis-a-vis the community it was designed to serve, and the main objective of the study were therefore as follows:

(i) determine if such interference could exist,

(ii) quantify the levels of interference that were found,

and (iii) assess the impact of these levels on the siting of windmills.

Since the time-varying multipath attributable to the blades would be a source of both amplitude and frequency modulation of the total signal received, it was required that we also consider the possibility of interference with FM (radio) transmissions.

To meet these objectives a rather comprehensive program was developed involving laboratory measurements and simulation, field testing using the existing windmill at the NASA Plum Brook Facility, and rigorous analyses and computations. To complete the investigations within a time span of one year required that many of the tasks be carried on in parallel, but it was nevertheless our hope that by careful coordination each task could be timed so that its findings would have maximum impact on the others. In this at least we were not entirely successful. Due in part to adverse wind conditions, the windmill was seldom in full operation throughout the first half of the year, and it was not until the tenth month of our study that we were able to obtain data with the blades rotating. Several months prior to this our laboratory simulations had indicated that interference did exist and was of sufficient magnitude to pose a problem. This added urgency to the completion of the analytical investigations, and by late summer the computer programs that had been developed were being fully exercised in the assessment of the interference levels at various (potential) windmill sites. It is not inappropriate to add that when the operational tests were finally carried out at Plum Brook, the interference observed was in excellent agreement with the prediction.

In a later part of this report we summarize the work performed in several different categories and cite the main conclusions reached, but to better appreciate how the various tasks impacted upon one another, it may be helpful to start with a chronological survey.

At the beginning of the program it seemed probable that the frequency modulation attributable to the rotating blades of the windmill would be the prime source of interference, and that the problem would be most severe in fringe areas of reception where the primary (direct) signal was already weak. At large distances from a transmitter, the presence of the earth has a substantial effect on the field strength, and it was therefore decided that all calculations would be carried out for the transmitting and receiving antennas and the windmill located on or above a homogeneous smooth spherical earth of arbitrary electrical properties. This required the development of a computer program adequate to determine the field at any point due to a transmitter at another, and though we were fortunate to obtain a program previously compiled by Berry [6], substantial time was taken to 'de-bug' the program and get it working for the situations of concern to us.

Meanwhile a series of laboratory simulation experiments had commenced using two identical 1976 Zenith color television sets selected because of their highly rated [7] capability for interference rejection. A simple signal analysis had indicate the general character of the phase (or frequency) and amplitude modulations which a windmill could impose on the signal reaching the antenna of a TV receiver. The impact that this has on the quality of reception obviously depends on the receiver characteristics, and though there is a high degree of commonality among the receiver in use today, the complexity of their circuitry is such that it is difficult to predict the degradation of the receiver output from a knowledge of the input signal perturbation. We therefore chose to rely on measurements using devices attached to the input terminals of one television set to simulate the modulation that a windmill would provide. Phase and amplitude modulation devices were constructed capable of imposing an adjustable level and frequency of modulation on any VHF channel TV signal received. Reception with and without modulation was compared for a sequence of modulation levels and for frequencies of the (sinusoidal) modulation that would be reasonable for

a windmill to generate. It was immediately found that phase (or frequency) modulation had almost no effect. Not surprisingly (since the video signal is in the form of amplitude modulation), the TV picture was quite immune, and only at the very highest levels of modulation was it possible to detect some audio interference in the form of "clicking". This finding was later substantiated by a signal analysis of the basic TV reception process. It also suggested that the interference would not be a problem with FM (radio) transmissions and, indeed, no interference of any magnitude was found then or later. On the other hand, amplitude modulation did have a noticeable effect on the TV picture. Even at quite low levels, distortion of parts of the picture could be seen with (depending on frequency) grey bands moving up the screen. As the modulation level increased, the bands darkened with (perhaps) "snow" accompanying them, and it was now painful to try to watch the picture. Occasional flipping of the picture occurred due to the breakdown of the vertical hold, and with further increase of modulation the picture disintegrated completely.

It was now evident that the time-varying amplitude modulation produced by a windmill could be a source of major concern to TV reception. Further simulation tests were performed with a unidirectional rectangular pulse type of amplitude modulation and, in particular, a detailed series of measurements was carried out as the level and width of the pulses were increased in steps. At each step the quality of the TV picture was rated by two or more observers. It was found that the modulation level at which the distortion became severe (and "unacceptable") remained reasonably constant at about 20 percent and showed no significant dependence on the TV signal strength. The pictures were also recorded on video tape, but unfortunately the concept of a 'reference tape' proved less effective than we had hoped because of the degradation introduced by the video recording system.

These findings added urgency to our theoretical investigations. The sensitivity of a TV receiver to time-varying amplitude modulation was confirmed by a detailed signal analysis and we also pushed forward with our analysis of windmill scattering in the presence of the earth. A computer program to find the field at any point due to a transmitter at another point was now in operation. This could also serve to find the field incident on the windmill and by using a simple (physical optics) scattering

model in which a windmill blade was approximated by a plane rectangular metal plat of equivalent dimensions, the windmill-scattered field could be found. According tc this model, the scattering is significant only in directions near those of specular an forward scattering from the blades. A program was developed to compute the prim (direct) field of a linearly-polarized transmitting antenna as well as the secondary (windmill scattered) field, and to do so at a sequence of distances from the windmil in front and behind. Based on the conclusion that the interference would be objectio able for a modulation index $m \geq 0.2$ and the fact that, in the large, m is a decrea ing function of distance from the windmill, the (maximum) distances from the windn at which $m = 0.2$ could be found. The distances correspond to a receiving antenna the same great circle path as the transmitter and the windmill and either nearer or further from the transmitter than the windmill. The average then serves to specify the radius of an equivalent circular zone of interference about the windmill.

There are, however, three points that should be noted. Firstly, the computations were carried out on the assumption of an omnidirectional receiving antenna, it is possible that in any given situation the interference could be substantially redu by using a high performance directional antenna. Secondly, the interference zone i not actually circular (see Appendix VII) and this also could reduce the practical con sequence of the interference; and lastly, the interference level is computed on the assumption that the windmill is so pointed as to direct the maximum blade-scattere signal to the receiving antenna. It therefore follows that even within the interferenc zone, TV reception will be affected only when the winds are from the appropriate direction. This could be a small fraction of the total viewing time for that channel.

This program was our basic tool for interference prediction but it was still rather inefficient one requiring the manual comparison (and interpolation) of long strings of computer outputs which were themselves costly to obtain. It had not beer our intent to use it in this form, but this was forced by the urgent need to assess potential windmill sites for interference. In practice, it remained our only tool throughout the entire study and has been used to survey more than a dozen different locations for as many as 20 TV channels in each case.

This effort was carried out in parallel with field tests at the NASA Plum Brook Facility, but our hopes to coordinate the field tests with the laboratory simulations and computer analyses proved largely unattainable. By late Spring we had mapped out a series of field tests whose objective was to develop data for comparison with the findings of the laboratory work. Sites were physically located at Plum Brook, the necessary equipment assembled in a portable package, and a sequence of visits made. It was confirmed that the blades did act as specular reflectors as regards the TV signals incident upon them, and that the magnitude of the scattered signal was comparable to that predicted by our simple scattering model. These were only static tests and, unfortunately, mechanical difficulties prevented the full speed operation of the windmill. By the time these difficulties were overcome, the wind no longer cooperated, and such windy times as did exist were so ephemeral that we were unable to catch them. In this manner, Summer dragged on to Fall, and the overall program advanced only through analytical studies of, for example, the modulation spectrum of rotating point and distributed scatterers.

It was not until late September that the wind conditions improved. Fearing that we might now have only a single opportunity to observe the interference, we therefore selected a site where our theory has predicted that the interference would be significant for a given TV channel with the windmill slewed appropriately in azimuth. On our next visit, we went immediately to this site (number 14), and interference was indeed observed at a level comparable to that predicted. When the windmill was driven out of the azimuthal plane that would direct a scattered signal to the receiving antenna, the distortion disappeared. Video tape recordings were made of the distorted and undistorted pictures. The output of a spectrum analyzer was also recorded to show the modulation waveform, which was a series of sinc-like pulses occurring with every half-revolution of the blades. Since most of our laboratory simulations had been carried out using sinusoidal modulating waveforms, it is noteworthy (and not a little fortuitous!) that the predicted interference based on the selection $m = 0.2$ for the modulation index was in such good agreement with observation.

For the most part the rest of the program was anti-climatic. The field test data were analyzed and their implications determined as regards the calculation of

interference zones. The nature of the modulation waveform was confirmed using a small blade rotating in an anechoic room, and preliminary analyses performed to determine what effect such modulation might have on other microwave systems. Suffice to say that the main objectives of the study had been achieved.

3. Task Summary

In the appendices to this report we detail the work performed in seven different areas constituting the main lines of investigation. These are summarized in the following.

3.1 Signal Analysis of TV Reception (Appendix I)

For a TV signal corrupted by arbitrary amplitude and phase modulation such as may be introduced by a windmill, the output of the first detector of a TV receiver is analyzed. It is shown that amplitude modulation has the most effect. It could therefore cause video distortion, whereas the audio information, being transmitted using frequency modulation, will be relatively unaffected.

3.2 Windmill Modulation (Appendix II)

The amplitude modulation of the signal scattered by a slowly rotating object is studied analytically using two simple models:

(i) A rotating point scatterer for which the modulation waveform is sinusoidal with variable frequency. Only a few discrete frequency components have significant magnitude.

(ii) A rotating linear (extended) scatterer for which a scalar analysis indicates that the modulation waveform consists of sinc-type pulses in time whose spectrum is (ideally) a band of equal amplitude frequencies.

The dominant frequencies can be many times larger than the rotation frequency, and the highest frequency (for the point scatterer) and spectral width (linear scatterer) are determined by the largest (effective) dimension of the scatterer. The implications of these results on the modulation produced by a windmill are discussed.

3.3 Propagation and Scattering Analysis (Appendix III)

Expressions for the primary (direct) field of the transmitter at the receiver are taken from the work of Fock [8] and Wait [9] on the diffraction of electromagnetic waves by a homogeneous smooth spherical earth, and these also serve to determine the field falling on the windmill. The blades are treated as rectangular metal plates lying in the (vertical) plane of rotation: a more realistic approximation would have them twisted out of this plane and, indeed, some such deformation is necessary to account for the observed modulation. The scattered field can be attributed to induced electric dipoles whose moment(s) are obtained using the physical optics approximation, and a further application of the propagation equations then leads to an expression for the secondary (scattered) field at the receiver. The approach is quite general and valid for arbitrary transmitter and receiver locations with respect to both the location and pointing direction of the windmill. The implications as regards the magnitude and modulation of the scattered field are discussed.

3.4 Computer Program (Appendix IV)

An available [6] computer program has been adapted and extended to compute the primary and secondary fields at the receiver in accordance with the expressions in Appendix III. The program is completely general, and from a knowledge of the primary and secondary field strengths at the receiver, the modulation depth (or index) can be found. This is required to determine the maximum distance from the windmill at which interference may occur.

3.5 Laboratory Simulation (Appendix V)

Laboratory simulation tests demonstrated that amplitude modulation of the general level that a windmill could create does produce video distortion of TV reception. The modulation waveform was initially a sinusoid whose frequency and amplitude were adjustable, but later we also used unidirectional rectangular pulses. Based on these experiments it was concluded that a modulation index $m \geq 0.2$ would cause "objectionable" video interference, regardless of the incident field strength.

3.6 Field Tests (Appendix VI)

The tests were all conducted at Plum Brook and were of two main types. For the scattering tests the windmill blades were locked in a horizontal position and the entire turbine was then rotated in azimuth. Using one of the Cleveland or Toledo TV transmitters as the signal source, the field that was scattered off the blades was observed. It was found that the scattering was primarily in the specular direction and that the blades contributed singly. The field strengths were in good agreement with those predicted using the physical optics approximation.

As a result of the theoretical and scattering test data, a site was selected to observe the signals when the windmill was in operation. The site was approximatel 0.5 km from the windmill. Using TV Channel 43 (whose transmitter is 79 km away) and with the windmill slewed to direct the specular scattering to the receiver, video distortion was observed and recorded. This was in spite of using a directional receiving antenna pointed towards the transmitter, thereby discriminating against the source of interference.

3.7 Analysis of Results (Appendix VII)

As a consequence of the laboratory simulations it was concluded that a modulation index $m \geq 0.2$ would cause video distortion that was judged "objectionable". On the assumption that for any given location of the receiver the windmill is so oriented as to direct the maximum blade scattering to this point, the region where $m \geq 0.2$ is defined as the interference zone. That portion of the zone which is produced by specular reflection off the blades is a cardioid centered on the windmill and with its maximum directed towards the transmitter. There is also a narrow lobe directed away from the transmitter resulting from forward scattering, and this generally provides the maximum distance from the windmill at which objectionable interference can occur. In site surveys we have usually quoted a single interference distance equal to the average of the maximum distances ascribed to the cardioid and the forward lobe

The field test results have been analyzed in the light of the theoretical predictions. The key findings are:

(i) the blade scattering is predominantly specular with the blades contributing singly : however, the sites used were not such that any forward scattering would have been observed;

(ii) the rotating blades produce impulsive ('sinc-type') modulation; and

(iii) the threshold of modulation for severe video distortion with impulsive modulation is approximately $m = 0.1$.

Overall, the agreement between the calculated and observed results is remarkably good. The theory has been found capable of predicting all of the major features of the observed phenomena, and is quantitatively accurate as regards the interference zones associated with windmills.

4. Conclusions

The dominant conclusion is that the rotating blades of a horizontal axis wind turbine or windmill can interfere with TV reception by producing video distortion. The interference is predicted theoretically and has been measured experimentally using the operating windmill at Plum Brook. It increases with increasing frequency and is therefore worst on the Upper UHF channels. It decreases with increasing distance from the windmill, but in the worst cases could still produce objectionable video distortion at distances up to a few miles. There does not seem to be any significant dependence on the primary field strength, and no audio distortion has been observed.

Using the theory that has been developed, it is possible to compute the distance from a windmill at which the interference to reception of a given TV channel changes from "severe" to "acceptable": in effect, to compute the zone of interference about a windmill. These calculations are based on a windmill having metallic blades of the same size as the Plum Brook machine. For blades of smaller size or made of a material which does not reflect all of the energy incident upon it, the interference zone would be proportionately smaller. We also remark that the receiving antenna has been assumed omnidirectional with the windmill blades so positioned as to direct the maximum scattered signal to the receiver. In circumstances other than this, the

interference will be less, and the local topography about a given site could also reduc (or increase) the actual level of interference experienced.

5. Recommendations for Future Work

The study that has been carried out is only the first step, and in order to explore ways of reducing the interference that a windmill will produce, it is necessary to have as much information about the interference as possible. To this end and confining attention to the problem only as it relates to TV reception, the following are recommended:

1) Laboratory simulation tests should be performed with sinc-type modulation pulses to establish threshold modulation levels for a number of commercially available TV receivers, old as well as new. These tests should also explore the dependence (if any) on primary field strength.

2) More extensive field tests should be conducted using the existing windmill at Plum Brook and, if possible, a completely mobile receiving system, to trace the interference zone with particular reference to directions near back and forward scattering from the blades. The effects of blade coning and rotation speed should also be explored.

3) To better understand the modulation produced by a rotating scatterer, theoretical and (small scale) experimental investigations should be initiated.

4) The reduced scattering that would result from blades which are not metallic should also be explored, and attempts made to minimize the scattering by appropriate choice of blade material and/or treatment.

6. Acknowledgements

It is a pleasure to acknowledge the assistance of the following members of the Radiation Laboratory who participated in various phases of the study: Professors R.E. Hiatt and E.L. McMahon, Messrs. W.F. Parsons and F.P. Rhine; and Dr. V.V. and Mrs A. Liepa. We are also grateful for the support, moral as well as

financial, of the ERDA Wind Energy Projects Office, and the advice and encouragement of Drs. L.V. Divone and D.D. Teague was much appreciated. Mr. J. Glassco of the NASA Lewis Research Center was instrumental in coordinating our field tests, and we acknowledge the assistance provided by Messrs. D. Cooksey and H. Phanner of the Plum Brook Facility.

7. References

1. Putnam, P.C. (1948), Power from the Wind, Van Nostrand Co., New York.

2. Heronemus, W.E.(1972), "Pollution-free Energy from Offshore Winds", 8th Annual Conference and Exposition, Marine Technology Society, Washington, D.C.

3. Puthoff, R.L. and P.J. Sirocky (1974), "Preliminary Design of a 100 kw Wind Turbine Generator", NASA Technical Memorandum X-71585.

4. Thomas, R., R. Puthoff, J. Savino and W. Johnson (1975), "Plans and Status of the NASA-Lewis Research Center Wind Energy Project", NASA Technical Memorandum X-71701.

5. _____ (1975), "A 3-MW Windmill that would blow good", Electronic Design 23(1), p. 68.

6. Berry, L.A., Fortran Program for Calculating Ground Wave Propagation over Spherical Earth, National Bureau of Standards, Boulder, Colorado.

7. _____(1976), Consumer Report 1976 Buyer Guide, p. 221; Consumers Union, Mount Vernon, New York.

8. Fock, V.A. (1965), Electromagnetic Diffraction and Propagation Problems, Pergamon Press, New York.

9. Wait, J.R. (1964), "Electromagnetic Surface Waves", in Advances in Radio Research, (edited by J.A. Saxon), Vol. 1, pp. 157-217, Academic Press, London.

Appendix I

SIGNAL ANALYSIS OF TV RECEPTION

I.1. Introduction

The present chapter discusses theoretically the general mechanisms by which a windmill may produce undesirable interference effects on television (TV) reception. In the neighborhood of a windmill, a TV receiver would receive the signals scattered by the windmill in addition to the desired direct signals. If sufficiently strong, the former may produce adverse effects on reception. To investigate the problem rigorously, it is necessary to have a detailed knowledge of the scattering behavior of the windmill and the detection characteristics of a TV receiver. To simplify the analysis, it is assumed that the windmill acts as a time varying multipath source producing both amplitude and phase (or frequency) modulation of the signals at the input of the receiver. In the following sections, we discuss the general effects of such extraneous modulations on the output of the first detector of a TV receiver.

The principles of operation of a TV receiver receiving only the direct signals from a desired TV station are well known. Nearby stationary multipath sources like buildings, water-towers, bridges, even static windmills, and other large reflecting objects may cause time delayed signals to reach the receiver. If sufficiently strong, these signals would produce multiple images or so-called "ghosts" on the TV screen, even when the receiving antenna is matched. However, the use of matched directional receiving antenna usually corrects the situation unless the receiver is located in a region of strong multipath sources or such interfering sources lie in the general direction of the desired TV station. For this reason, the present analysis ignores the effects of stationary windmills on TV reception. It is clear from the discussion that the time varying nature of the windmill scattering makes it a potential source capable of producing adverse effects other than "ghosts" on TV reception.

2. Basic TV Detection Process

In the absence of multipath sources, the composite signal at the input f a TV receiver may be represented by:

$$y(t) = \left[1 + f_v(t)\right] \cos(\omega_c t + \phi_1) + B \cos\left[(\omega_c + \Delta\omega)t + \phi_A(t) + \phi_2\right], \quad (I.1)$$

here $f_v(t)$ is the video information transmitted in the form of amplitude modulation of a carrier of radian frequency ω_c,

$\phi_A(t)$ is the audio information transmitted in the form of frequency modulation of an audio carrier of radian frequency $(\omega_c + \Delta\omega)$;

$\Delta\omega$ is called the audio subcarrier and normally $\frac{\Delta\omega}{2\pi} = 4.5$ MHz,

B is the amplitude of the audio carrier with respect to that of of the video carrier, usually $B << 1$,

ϕ_1, ϕ_2 are the phases of the video and audio carriers respectively and are assumed to be constants for the present.

The first detector of a TV receiver envelope detects the signal given by q. (I.1). The output of the first detector consists of the video information $f_v(t)$ and a requency-modulated audio subcarried signal which on second detection yields the esired audio information $\phi_A(t)$. To see this process clearly, let us rewrite Eq. (I.1) n the following form:

$$y(t) = r(t) \cos\left[\omega_c t + \phi_1 + \alpha(t)\right], \quad (I.2)$$

here $$r(t) = \left[A(t)^2 + B^2 + 2A(t)B \cos\left\{\Delta\omega t + \phi_A(t) + \phi_2 - \phi_1\right\}\right]^{1/2}, \quad (I.3)$$

$$\tan \alpha(t) = \frac{B \sin\left\{\Delta\omega t + \phi_A(t) + \phi_2 - \phi_1\right\}}{A(t) + B \cos\left\{\Delta\omega t + \phi_A(t) + \phi_2 - \phi_1\right\}}, \quad (I.4)$$

$$A(t) = 1 + f_v(t). \quad (I.5)$$

From the transmitted TV signal characteristics it is known that $B \ll A(t)$ and thus we can approximate Eqs. (I.3), (I.4) as follows:

$$r(t) \simeq A(t) + B \cos\left\{\Delta\omega t + \phi_A(t) + \phi_2 - \phi_1\right\}$$

$$= 1 + f_v(t) + B \cos\left\{\Delta\omega t + \phi_A(t) + \phi_2 - \phi_1\right\}, \qquad \text{(I.6)}$$

$$\alpha(t) \simeq \frac{B}{A(t)} \sin\left\{\Delta\omega t + \phi_A(t) + \phi_2 - \phi_1\right\}$$

$$= \frac{B}{1 + f_v(t)} \sin\left\{\Delta\omega t + \phi_A(t) + \phi_2 - \phi_1\right\} \qquad \text{(I.7)}$$

Under these approximations, the signal at the input of the first detector may be written as:

$$y(t) = \left[1 + f_v(t) + B \cos\left\{\Delta\omega t + \phi_A(t) + \phi_2 - \phi_1\right\}\right]\left[\cos\left\{\omega_c t + \phi_1 + \alpha(t)\right\}\right] \qquad \text{(I.8)}$$

It is now easy to see that the envelope detection of Eq. (I.8) yields the video signal $f_v(t)$ and a constant amplitude subcarrier signal frequency modulated by the audio signal $\phi_A(t)$. A low pass and a band pass filter at the output of the envelope detector separates the video and audio signals and directs them to the appropriate channels of the TV receiver for further processing. The basic first detection system may be shown in the form of a block diagram given by Figure I.1. Note that the output of the low pass filter is the undistorted video signal, as it should be. In the present case, the phase term $(\phi_2 - \phi_1)$ in the output signal of the band pass filter is constant. Consequently, the undistorted audio signal would be recovered from it on second detection at a later stage.

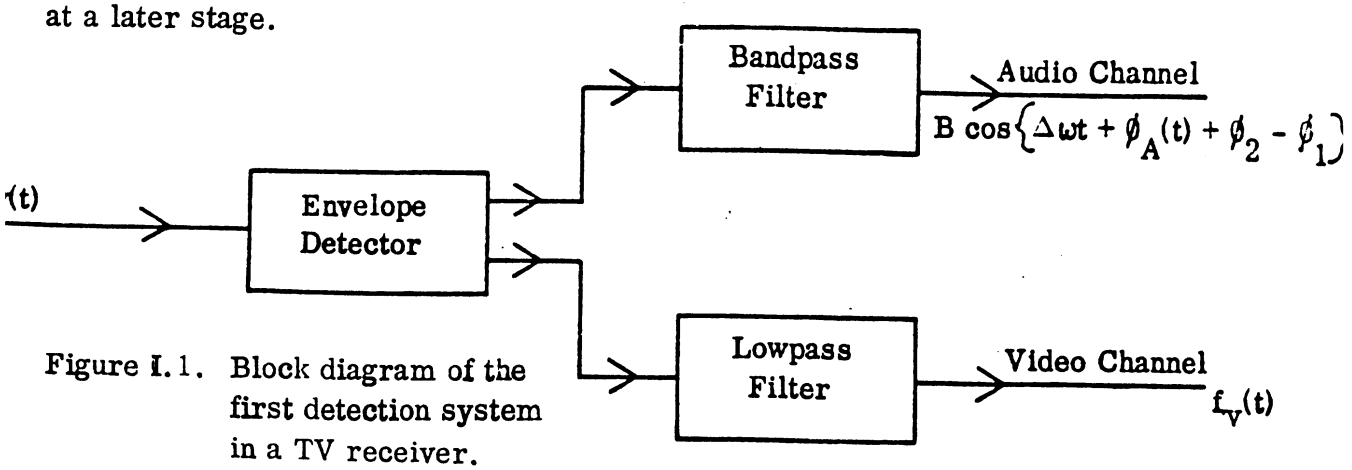

Figure I.1. Block diagram of the first detection system in a TV receiver.

I.3. Artificially Corrupted TV Signal

In this section we investigate the outputs of the first detector when the input signal is artificially corrupted. Some of the results of this section may be useful to explain the few observations made during the experiment on the sensitivities of TV receivers to laboratory-injected modulations applied to the input signals.

For generality, it is assumed that the video and audio carriers are amplitude and phase modulated by $f_{m_1}(t)$, $\phi_1(t)$ and $f_{m_2}(t)$, $\phi_2(t)$ respectively. These modulations may be artificially introduced at the input of the receiver in a laboratory environment in which case $f_{m_1}(t) = f_{m_2}(t)$ and $\phi_1(t) = \phi_2(t)$. In the general case, the corrupt signal at the input of the first detector may be written as:

$$y_c(t) = \left[1 + f_v(t) + f_{m_1}(t) + B\left\{1 + f_{m_2}(t)\right\} \cos\left\{\Delta\omega t + \phi_A(t) + \phi_2(t) - \phi_1(t)\right\}\right] \cdot \cos\left\{\omega_c t + \phi_1(t) + \alpha'(t)\right\}, \qquad (I.9)$$

where

$$\alpha'(t) \simeq \frac{B\left\{1 + f_{m_2}(t)\right\}}{1 + f_v + f_{m_1}(t)} \sin\left\{\Delta\omega t + \phi_A(t) + \phi_2(t) - \phi_1(t)\right\} . \qquad (I.10)$$

The following observations can be made from a study of Eq. (I.9):

(i) The video channel output consists of $f_v(t) + f_{m_1}(t)$ which implies a possible distortion of the picture signal. The artificially injected phase modulations have no effects on the video output.

(ii) The audio channel output is $B\left[1 + f_{m_2}(t)\right] \times \cos\left\{\Delta\omega t + \phi_A(t) + \phi_2(t) - \phi_1(t)\right\}$. The audio subcarrier is now also amplitude modulated; the implication of this is that if $f_{m_2}(t)$ is sufficiently large it may affect the efficiency of the second detection and thereby affect the audio signal output. If $\phi_1(t) = \phi_2(t)$, the phase modulation will not affect the audio signal output. If $\phi_1(t) \neq \phi_2(t)$, the audio signal will be distorted as indicated above.

(iii) In the special case when $f_{m_1}(t) = f_{m_2}(t) = 0$ and $\phi_1(t) = \phi_2(t) \neq 0$, both the video and audio signal outputs are unaffected by the extraneous phase modulations.

The above observations are summarized in the block diagram given in Figure I.2.

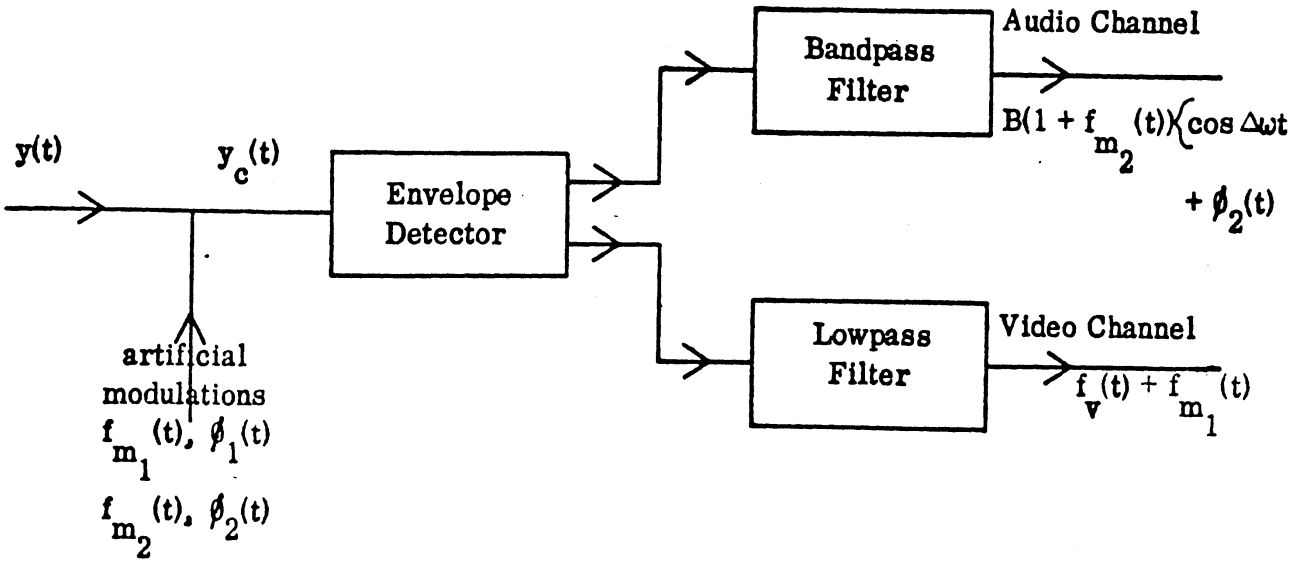

Figure I.2. Block diagram of the first detection system for an artificially corrupted signal.

I.4. Multipath Effects

In this section we study the first detector outputs when the input signal consists of the direct TV signal and a multipath signal. We need not concern ourselves here about the nature of the multipath sources. It is assumed that the multipath source introduces both amplitude and phase modulations to the signal incident on it and the delayed multipath signal then enters the input of the receiver. Thus, the combined direct and simulated multipath signal at the input of the first detector may be written as:

$$\begin{aligned} y_d(t) &= y(t) + y_m(t) \\ &= A(t) \cos \omega_c t + B \cos\{\omega_c t + \Delta\omega t + \phi_A(t)\} \\ &+ \beta[A'(t) \cos(\omega_c t + \phi_1(t)) \\ &\qquad + B(t) \cos\{\omega_c t + \Delta\omega t + \phi_A(t) + \phi_2(t)\}] \end{aligned} \tag{I.11}$$

where

$$\left.\begin{aligned} A(t) &= 1 + f_v(t) \\ A'(t) &= 1 + f_v(t) + f_{m_1}(t) \\ B'(t) &= \left[1 + f_{m_2}(t)\right] B \end{aligned}\right\} , \tag{I.12}$$

β may be identified with the amplitude of the scattering coefficient of the multipath source, $f_{m_1}(t)$, $f_{m_2}(t)$ are the equivalent amplitude modulations introduced by the multipath source, $\phi_1(t)$, $\phi_2(t)$ are the equivalent phase modulations introduced by the multipath source; note that $\phi_1(t)$ and $\phi_2(t)$ may contain static terms to account for the phase delay of the multipath signal,

and the other symbols are as explained before.

As before Eq.(I.11) may be rewritten in the following approximate form:

$$\begin{aligned} y_d(t) \simeq & \left[A(t) + B\cos\left\{\Delta\omega t + \phi_A(t)\right\}\right]\cos\left\{\omega_c t + \alpha_1(t)\right\} \\ & + \beta\left[A'(t) + B'(t)\cos\left\{\Delta\omega t + \phi_A(t) + \phi_2(t) - \phi_1(t)\right\}\right] \\ & \cdot \cos\left\{\omega_c t + \phi_1(t) + \alpha_2(t)\right\} , \end{aligned} \tag{I.13}$$

where

$$\left.\begin{aligned} \tan\alpha_1(t) &= \frac{B\sin\left\{\Delta\omega t + \phi_A(t)\right\}}{A(+) + B\cos\left\{\Delta\omega t + \phi_A(t)\right\}} \\ \text{or} \\ \alpha_1(t) &\simeq \frac{B}{A(t)}\sin\left\{\Delta\omega t + \phi_A(t)\right\} \end{aligned}\right\} \tag{I.14}$$

$$\left.\begin{aligned} \tan\alpha_2(t) &= \frac{B'(t)\sin\left\{\Delta\omega t + \phi_A(t) + \phi_2(t) - \phi_1(t)\right\}}{A'(t) + B'(t)\cos\left\{\Delta\omega t + \phi_A(t) + \phi_2(t) - \phi_1(t)\right\}} \\ \alpha_2(t) &\quad \frac{B'(t)}{A'(t)}\sin\left\{\Delta\omega t + \phi_A(t) + \phi_2(t) - \phi_1(t)\right\} \end{aligned}\right\} . \tag{I.15}$$

Finally, we express Eq. (I.13) in the following form:

$$\begin{aligned} y_d(t) = & \left[F(t) + G(t)\cos\left\{\phi_1(t) + \alpha_2(t) - \alpha_1(t)\right\}\right] \\ & \cdot \cos\left\{\omega_c t + \alpha_1(t) + \alpha_3(t)\right\} , \end{aligned} \tag{I.16}$$

where $$F(t) = A(t) + B\cos\left\{\Delta\omega t + \phi_A(t)\right\} \tag{I.17}$$

$$G(t) = \beta\left[A'(t) + B'(t)\cos\left\{\Delta\omega t + \phi_A(t) + \phi_2(t) - \phi_1(t)\right\}\right] , \tag{I.18}$$

$$\left.\begin{aligned} \tan\alpha_3 &= \frac{G(t)\sin\left\{\phi_1(t) + \alpha_2(t) - \alpha_1(t)\right\}}{F(t) + G(t)\cos\left\{\phi_1(t) + \alpha_2(t) - \alpha_1(t)\right\}} \\ \text{or}\qquad \alpha_3 &\simeq \frac{G(t)}{F(t)}\sin\left\{\phi_1(t) + \alpha_2(t) - \alpha_1(t)\right\} \end{aligned}\right\} . \tag{I.19}$$

Grouping the video and audio components in the amplitude of Eq. (I.16) we obtain the input signal in the following form:

$$\begin{aligned} y_d(t) = &\Big[A(t) + \beta A'(t)\cos\left\{\phi_1(t) + \alpha_2(t) - \alpha_1(t)\right\}\Big) \\ &+ \left\{B\cos\left(\Delta\omega t + \phi_A(t)\right) + \beta B'(t)\cos\left(\phi_1(t) + \alpha_2(t) - \alpha_1(t)\right)\right\} \\ &\cdot \cos\left(\Delta\omega t + \phi_A(t) + \phi_2(t) - \phi_1(t)\right)\Big] \\ &\cdot \cos\left(\omega_c t + \alpha_1(t) + \alpha_3(t)\right) . \end{aligned} \tag{I.20}$$

The first detection of the signal given by Eq.(I.20) yields the video and audio channel outputs denoted by f_{video}, f_{audio} respectively and are given by:

$$f_{video} = f_v(t) + \beta\left\{1 + f_v(t) + f_{m_1}(t)\right\}\cos\left\{\phi_1(t) + \alpha_2(t) - \alpha_1(t)\right\} , \tag{I.21}$$

$$\begin{aligned} f_{audio} = &B\cos\left\{\Delta\omega t + \phi_A(t)\right\} \\ &+ \beta B\left\{1 + f_{m_2}(t)\right\}\cos\left\{\phi_1(t) + \alpha_2(t) - \alpha_1(t)\right\} \\ &\cdot \cos\left\{\Delta\omega t + \phi_A(t) + \phi_2(t) - \phi_1(t)\right\} . \end{aligned} \tag{I.22}$$

In particular, if $f_{m_1}(t) = f_{m_2}(t) = f_m(t) << f_v(t)$ and $\phi_1(t) = \phi_2(t)$, then it can be seen from (I.14 and 15) that $\alpha_1(t) \simeq \alpha_2(t)$. Under these conditions it is found that the video and audio channel outputs are:

$$f_{video} = f_v(t) + \beta\left\{1 + f_v(t) + f_m(t)\right\}\cos\phi_1(t) \tag{I.23}$$

$$f_{audio} = B\left[1 + \beta\left\{1 + f_m(t)\right\}\cos\phi_1(t)\right]\cos\left\{\Delta\omega t + \phi_A(t)\right\} . \tag{I.24}$$

Eq. (I.24) indicates that audio channel output is amplitude modulated due to the multipath effects. If the amount of this modulation is not strong enough, the audio channel signal on second detection would yield undistorted audio output. However, the video output, as given by Eq. (I.23), appears to be affected by both the amplitude and phase modulations due to the multipath source; the effects of amplitude modulation would be dominant. The block diagram given in Figure I.3 summarizes the main effects of multipath.

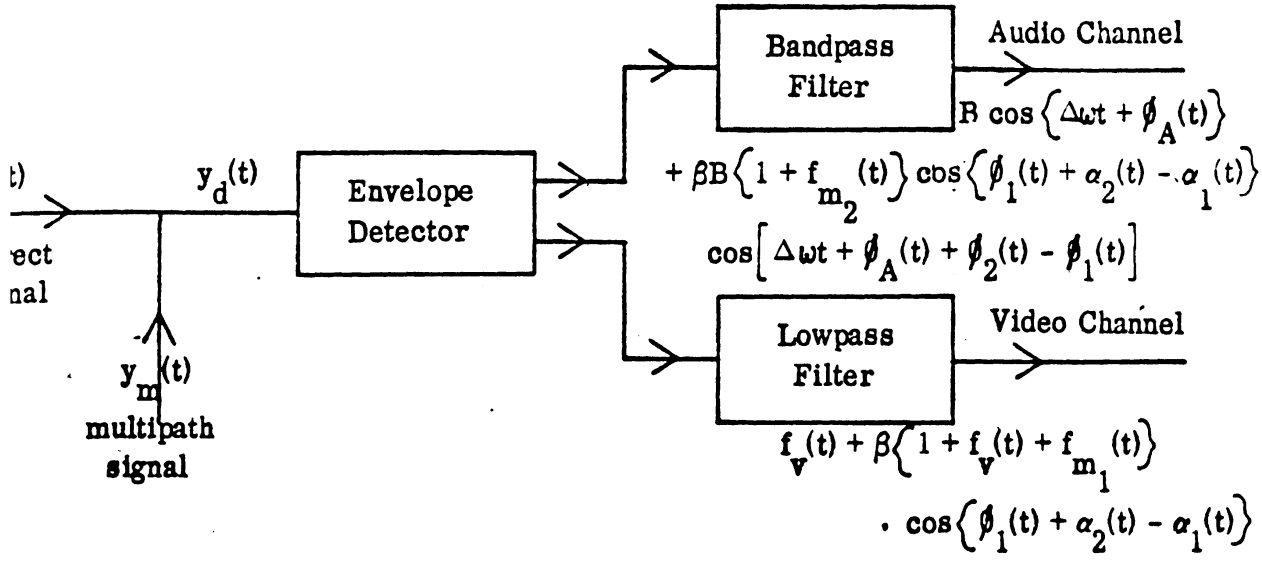

Figure I.3. Block diagram of the first detection system in the presence of multipath interference.

I.5 Discussion

The present analysis indicates that the extraneous amplitude modulation of the signals is more serious and is liable to produce distortion in the picture reception. To the first order, the phase modulation effects may be neglected. Unless the interfering signals are very large, the audio reception may be assumed to be unaffected. Thus it is important to study the nature of amplitude modulation produced by a windmill.

Appendix II

SIGNAL MODULATION BY A WINDMILL

II.1. Introduction

Generally the scattering effect of windmill blades is to produce both amplitude and phase modulation of the incident signal. In Appendix I it has been found that extraneous amplitude modulation is likely to distort video reception. The present Appendix is therefore addressed to the general nature of the amplitude modulation caused by a windmill.

Physically it is clear that such modulation is primarily due to the rotation of the windmill blades. The blades rotate at a variable speed, the typical speed being 30 rpm ($\frac{1}{2}$ Hz). If the blade rotation were to produce continuous amplitude modulation only at the rotation frequency, the AGC circuit in the TV receiver might be able to handle such low frequency modulation, in which case there would not be any appreciable video distortion. But if the modulation waveform is discontinuous (like some sort of repetitive pulse waveform), it may contain larger frequencies which could then adversely affect the video reception. It is therefore of considerable interest to ascertain the modulation waveform produced by the windmill. The nature of this waveform and its frequency spectrum depend, in a complicated manner, on the electromagnetic scattering properties of the windmill blades.

The geometry of the problem characterizing the scattering of TV signals by windmill blades is a difficult electromagnetic boundary value problem and will be discussed in Appendix III. Here, we shall adopt a simpler approach. We first discuss theoretically the scattering characteristics of some idealized rotating scatterers illuminated by electromagnetic waves. Emphasis is given to the time waveforms and the frequency spectrum of the scattered fields. Secondly, the results of an experimental investigation of the scattered fields produced by a rotating linear scatterer are discussed. From these results some of the characteristics of the modulation wav form produced by the windmill are ascertained.

II.2. Rotating Point Scatterer

We start by examining the scattering of a scalar wave by a rotating isotropic point scatterer. Although this is a highly idealized model, the results will have relevance to the windmill problem when the scattering centers are associated with the windmill blades.

Consider a transmitter T located on the negative y-axis at $y = -y_0$ and a receiver R located in the x-y plane at (r, θ, ϕ) with respect to a spherical coordinate system with origin O as shown in Figure II.1. Assume an isotropic point scatterer S located at (ℓ, θ_s, ϕ_s) and rotating in the plane $\phi = \phi_s$ at an angular frequency Ω_s such that

$$\theta_s = \Omega_s t = 2\pi f_s t. \tag{II.1}$$

It is assumed that both T and R are in the far zones with respect to each other and with respect to S. For simplicity it is assumed that the transmitter is an isotropic source producing a spherically symmetric field.

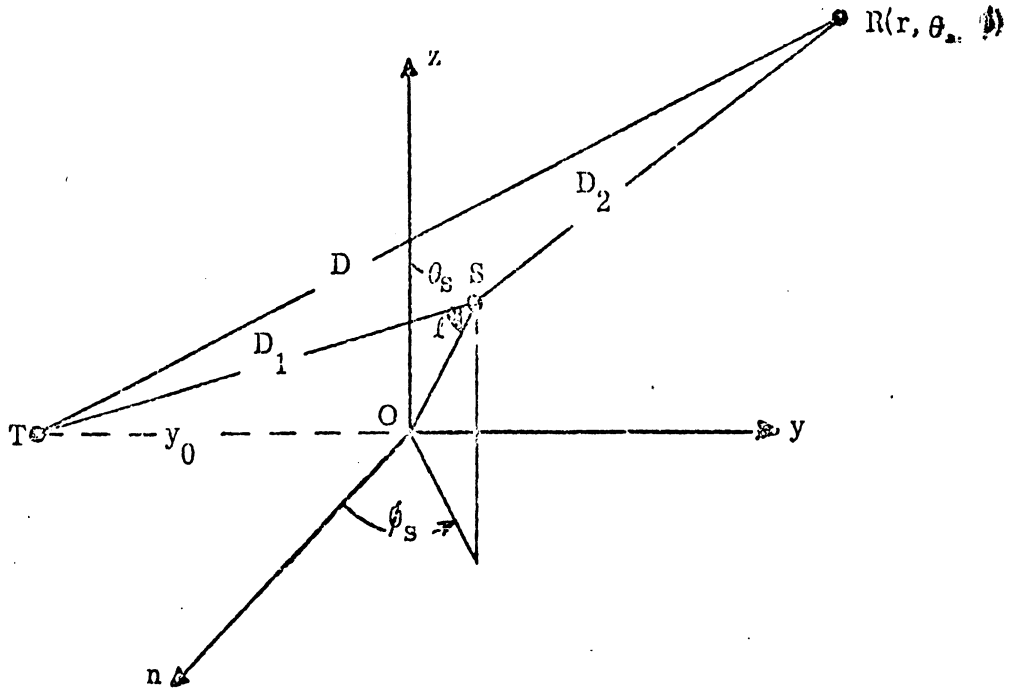

Figure II.1. Transmitter and receiver in the presence of a rotating point scatterer.

The distance D between the transmitter and the receiver is given by

$$D^2 = r^2 + y_0^2 + 2ry_0 \sin \phi \tag{II.2}$$

and the other two distances D_1 and D_2 in Figure II.1 may be approximated as follows:

$$D_1 = TS \simeq y_0 + \ell \sin \theta_s \sin \phi_s, \qquad \ell << y_0 \tag{II.3}$$

$$D_2 = SR \simeq r - \ell \sin \theta_s \cos (\phi - \phi_s), \qquad \ell << r. \tag{II.4}$$

The field at the receiver consists of the direct field and the field scattered by S, and can be expressed as

$$E(R) = E_0 \left[1 + \Gamma e^{i\delta - ik\ell p \sin \theta_s} \right], \tag{II.5}$$

where

$$E_0 = K \frac{e^{i(\omega_c t - D)}}{D} \quad \text{(K is a constant)}, \tag{II.6}$$

ω_c is the radian frequency of the video carrier,

$k = 2\pi/\lambda$ is the propagation constant at the carrier frequency,

$\Gamma e^{i\delta}$ is the scattering coefficient of the scatterer S,

and

$$p = \sin \phi_s - \cos (\phi - \phi_s) . \tag{II.7}$$

The complete expressions for the amplitude and phase of the received signal may be obtained from (II.5) and are

$$\left|E(R)\right| = \left|E_0\right| \left[1 + \Gamma^2 + 2\Gamma \cos(k\ell p \sin \theta_s - \delta) \right]^{1/2}, \tag{II.8}$$

$$\arg E(R) = \arg E_0 + \tan^{-1} \frac{\Gamma \sin(k\ell p \sin \theta_s - \delta)}{1 + \Gamma \cos(k\ell p \sin \theta_s - \delta)} . \tag{II.9}$$

Assuming $\delta = 0$, $\Gamma << 1$ and using (II.1) we can write (II.8) as

$$\left|E(R)\right| = \left|E_0\right| \left[1 + f_m(t) \right] \tag{II.10}$$

where the amplitude modulation introduced by the scatterer is

$$f_m(t) = \Gamma \cos(k\ell p \sin \Omega_s t) \tag{II.11}$$

Note that if the center of rotation of the scatterer, the transmitter and the receiver are in line, then $f_m(t)$ becomes independent of time for all values of ϕ_s. It can be seen from (II.11) that as a function of time $f_m(t)$ varies at a variable angular frequency given by

$$\nu_m(t) = k\ell|p|\Omega_s \cos \Omega_s t = k\ell\Omega_s \left|\sin \phi_s - \cos(\phi - \phi_s)\right| \cos \Omega_s t. \tag{II.12}$$

By considering the average number of oscillations of $f_m(t)$ in a time equal to the period of the rotation frequency Ω_s, it can be shown from (II.11) that the average frequency of oscillations in $f_m(t)$ is approximately

$$\Omega_{av} = \frac{2}{\pi} k\ell|p|\Omega_s. \tag{II.13}$$

Observe that (II.13) may also be obtained by taking the average of $\nu_m(t)$, given by (II.12), over a half-period of Ω_s.

In fact, $f_m(t)$ contains an infinite number of components whose frequencies are harmonically related to Ω_s. The characteristics of these components may be understood clearly if we express (II.11) in the following form:

$$f_m(t) = \Gamma J_0(k\ell p) + 2\Gamma \sum_{n=1}^{\infty} J_{2n}(k\ell p) \cos 2n\Omega_s t, \tag{II.14}$$

where J_n is the Bessel function of the first kind and order n. The number of significant terms for different values of $k\ell p$ can be found from plots of the Bessel functions, from which it is seen that $J_{2n}(k\ell p)$ decreases rapidly for $2n > k\ell|p|$, particularly if $k\ell\, p \gg 1$. Thus, for large values of $k\ell p$, the significant frequencies of amplitude modulation are

$$\Omega_{mn} = 2n\Omega_s, \quad n = 1, 2, \ldots\ldots, \simeq \frac{1}{2} k\ell p, \tag{II.15}$$

whose amplitudes are

$$A_{mn} = 2\Gamma \left| J_{2n}(k\ell p) \right| , \tag{II.16}$$

with n varying as before. For large $k\ell|p|$, only a few components at the upper range of n will be significant. From this it follows that the frequency and amplitude of the largest frequency component in the amplitude modulation are approximately

$$\tilde{\Omega} = k\ell\, p\, \Omega_s = k\ell \left| \sin \phi_s - \cos(\phi - \phi_s) \right| \Omega_s, \tag{II.17}$$

$$\tilde{A} = 2\Gamma \left| J_{2n'}(2n') \right| , \tag{II.18}$$

where $2n' \simeq k\ell|p|$ is the even integer nearest to $k\ell|p|$. It is interesting to observe that the largest frequency $\tilde{\Omega}$ given by (II.17) is exactly equal to the maximum frequency of variation predicted by (II.12). $\tilde{\Omega}$ may be many times larger than the rotation frequency of the scatterer if $k\ell$ is large. For example, if $\phi_s = 0$ and $\phi = \pi/4$,

$$\tilde{\Omega} = \frac{k\ell}{\sqrt{2}}\, \Omega_s = \sqrt{2}\frac{\pi\ell}{\lambda}\, \Omega_s, \tag{II.19}$$

where λ is the wavelength corresponding to the carrier frequency ω_c.

Figure II.2 shows a plot of $\left[1 + f_m(t)\right]$ versus θ_s, as obtained from (II.10) for $\phi_s = 0$, $\phi = \pi/4$, $k\ell = 60$ and $\Gamma = 0.5$. This large value of Γ may be unrealistic and it is assumed here for ease of computation and to enhance the effects. Note that the spacings between the maxima and minima in Figure II.2 are not uniform, showing that a single frequency cannot be assigned to the oscillations. However, from Figure II.2 $\Omega_{av}/\Omega_s = 28$, whereas $\Omega_{av}/\Omega_s \simeq 27$ as predicted by (II.13). Figure II.3 shows a plot of $\left|J_{2n}(20)\right|$ versus n which may be considered as the frequency spectrum diagram for the case when $k\ell p = 20$. Observe that the frequency components are $2n\Omega_s$ and are negligible for $n > 10$. The edge of the frequency spectrum is approximately at $2n = k\ell p = 20$, i.e. at $n = 10$. Within the frequency band only selected frequencies have significant amplitudes, and in the present case the frequency component for

Figure II.2. $\left[1 + \Gamma\cos(k\ell p \sin \Omega_s t)\right]$ versus $\theta_s = \Omega_s t$ for $k\ell = 60$, $\Gamma = 0.5$, $\phi_s = 0$ and $\phi = \pi/4$.

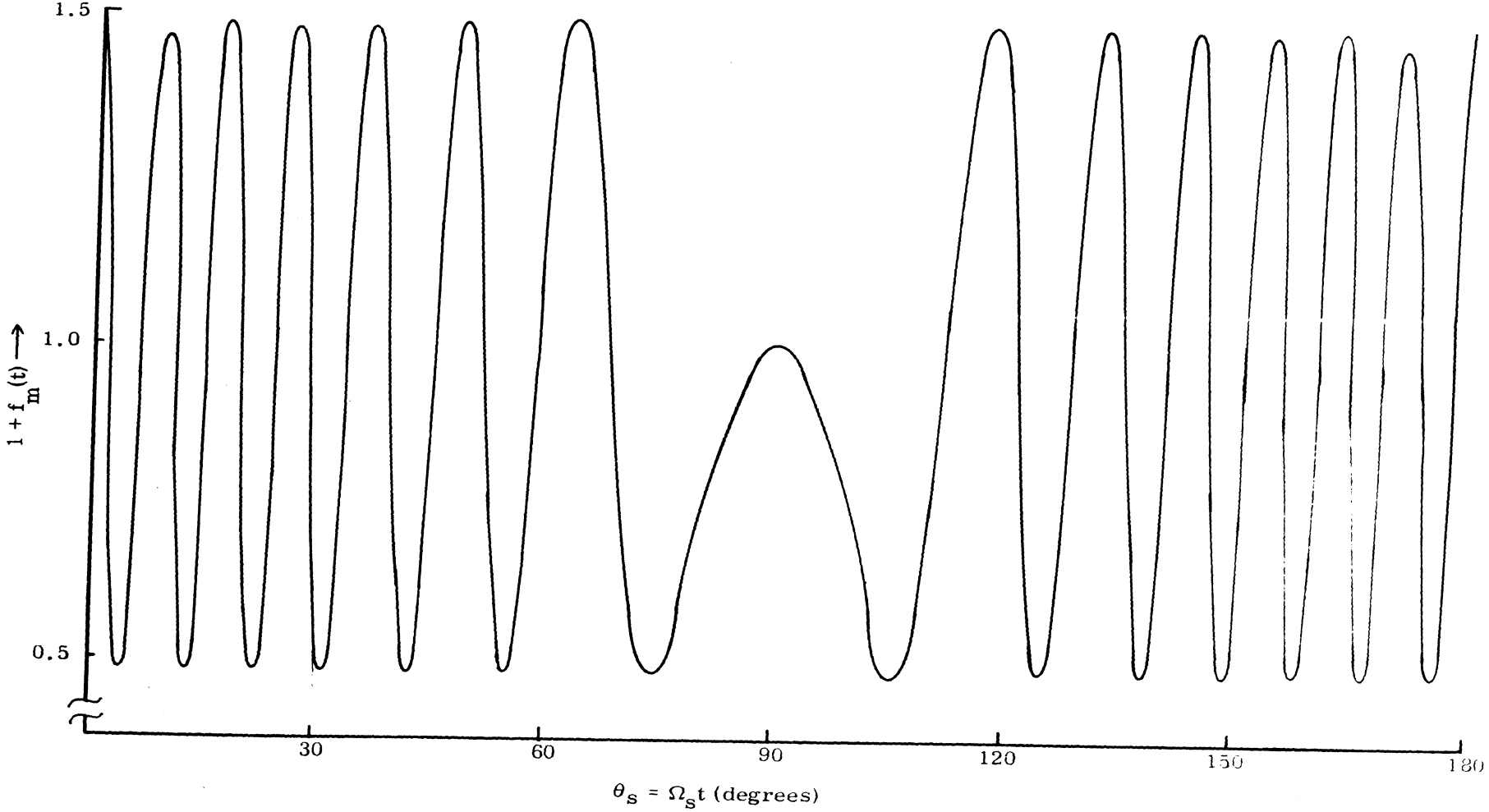

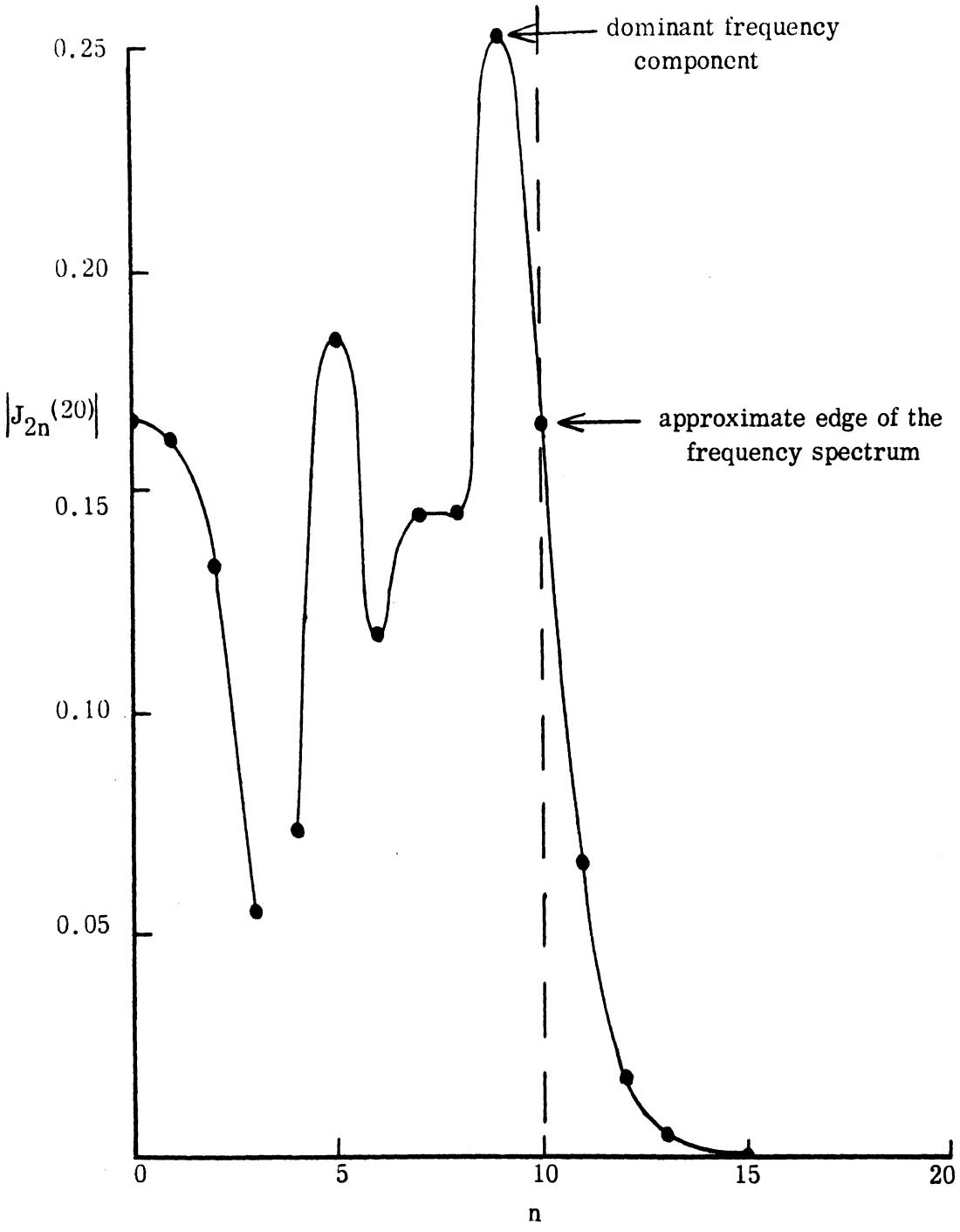

Figure II.3. Frequency spectrum diagram for the modulation produced by a rotating point scatterer, $k\ell p = 20$.

$n = 9$ seems dominant. For future reference the largest frequency of amplitude modulation normalized to the rotating frequency is

$$\frac{\tilde{\Omega}}{\Omega_s} = \frac{\pi}{2}\left(\frac{\Omega_{av}}{\Omega_s}\right) = \frac{2\pi\ell}{\lambda}\left|\sin\phi_s - \cos(\phi - \phi_s)\right| . \qquad \text{(II.20)}$$

Figure II.4 shows the plots of (II.20) versus ℓ/λ for the case $\phi_s = 0$ and $\phi = \pi/4$. For $\phi_s = 0$ the maximum values of the normalized frequencies are obtained when $\phi = 0$ or and are $\sqrt{2}$ times the values shown in Figure II.3. For example, if $\phi = 0$ or π, $\frac{\tilde{\Omega}}{\Omega_s} \simeq 1.4 \times 44.4 = 62.8$, and $\frac{\Omega_{av}}{\Omega_s} = 1.4 \times 28.3 \simeq 40.02$ for $\ell/\lambda = 10$.

II.3. Rotating Linear Scatterer

We now turn to the scattering of a scalar wave by a rotating linear scatterer. Consider a scatterer consisting of a continuous distribution of point scatterers along a length L, centered on S and aligned along ℓ as in Figure II.1. The linear scatterer is assumed to rotate in the plane $\phi = \phi_s$ at the angular frequency (II.1). After redefining the scattering coefficient per unit length as $\frac{\Gamma}{L} e^{i\delta}$ where $\Gamma e^{i\delta}$ is now the total scattering scattering coefficient of the scatterer, it can be shown that the scattered field at R for the geometry shown in Figure II.1 is given by

$$E_s(R) = E_0 \Gamma e^{i\delta} \int_{\ell - L/2}^{\ell + L/2} e^{-ik\ell p \sin\theta_s}\, d\ell ,$$

$$= E_0\, \Gamma e^{i\delta} e^{-ik\ell p \sin\theta_s} \operatorname{sinc}\left(\frac{kL}{2} p \sin\theta_s\right), \qquad \text{(II.21)}$$

where $\operatorname{sinc}(x) = \frac{\sin\pi x}{\pi x}$, $\qquad$ (II.22)

and the other parameters are as before. The total field at R is then

$$E(R) = E_0 + E_s(R)$$

$$= E_0 \left[1 + e^{i\delta} e^{-ik\ell p \sin\theta_s} \operatorname{sinc}\left(\frac{kL}{2} p \sin\theta_s\right)\right] . \qquad \text{(II.23)}$$

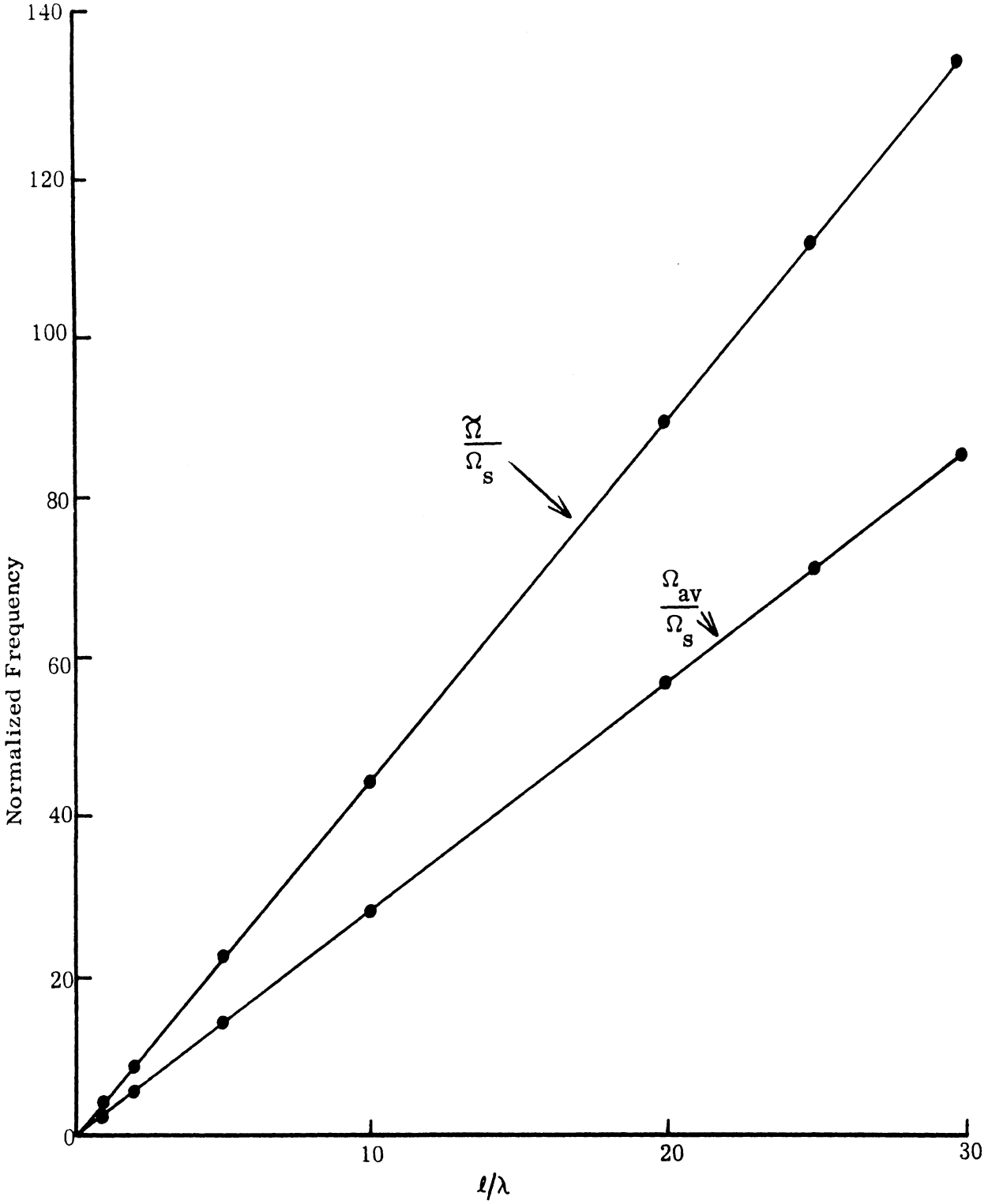

Figure II.4. $\frac{\tilde{\Omega}}{\Omega_s}$ or $\frac{\Omega_{av}}{\Omega_s}$ versus ℓ/λ for the rotating point scatterer:

$\phi_s = 0$ and $\phi = \pi/4$.

Assuming $\delta = 0$ and $\Gamma \ll 1$, the amplitude modulation function introduced by a linear scatterer of length L is

$$f_m(t) = \Gamma \text{sinc}\left(\frac{kL}{2} p \sin \Omega_s t\right) \cos(kp\ell \sin \Omega_s t). \tag{II.24}$$

Note that for $L = 0$, (II.24) reduces to the point scatterer result given in (II.11).

For $\ell = L/2$, i.e. a linear scatterer extending from $\ell = 0$ to $\ell = L$, the modulation function is

$$f_m(t) = \Gamma \text{sinc}(kLp \sin \Omega_s t). \tag{II.25}$$

For $\ell = 0$, i.e. if the scatterer is symmetrically located with respect to the origin O, the modulation function is

$$f_m(t) = \Gamma \text{sinc}\left(\frac{kL}{2} p \sin \Omega_s t\right). \tag{II.26}$$

(II.26) may be identified with the modulation produced by a pair of rotating windmill blades.

Figure II.5 shows a plot of $\left[1 + f_m(t)\right]$ versus $\theta_s = \Omega_s t$, with $f_m(t)$ given by (II.26), for $kL = 60$, $\phi_s = 0$, $\phi = \pi/4$ and $\Gamma = 0.5$. Notice that $1 + f_m(t)$ repeats itself for $\theta_s = n\pi$. This is because $f_m(t)$ is a periodic function of period $T_s/2 = \pi/\Omega_s$, i.e. its frequency is $2\Omega_s$. To obtain the frequency spectrum of $f_m(t)$ we assume that it may be approximated by the following:

$$f_m(t) \simeq \Gamma \text{sinc}\left(\frac{kL}{2} p \Omega_s t\right) \tag{II.27}$$

and $f_m(t + T_s/2) = f_m(t)$, i.e. $f_m(t)$ is a periodic function with period $T_s/2$. For large values of the argument this approximation should be good.

The Fourier transform of $\text{sinc}\left(\frac{kL}{2} p \Omega_s t\right)$ is (II.28)

$$\mathcal{F}\left\{\text{sinc}\left(\frac{kL}{2} p \Omega_s t\right)\right\} = \int_{-\infty}^{\infty} \text{sinc}\left(\frac{kL}{2} p \Omega_s t\right) e^{-i\omega t} dt = \frac{G_{kL}}{2} p \Omega_s (\omega),$$

Figure II.5. $1 + \Gamma S_a(\frac{kL}{2} \; p \sin \Omega_s t)$ versus $\theta_s = \Omega_s t$ for $kL = 60$, $\Gamma = 0.5$, $\phi_s = 0$ and $\phi = \pi/4$

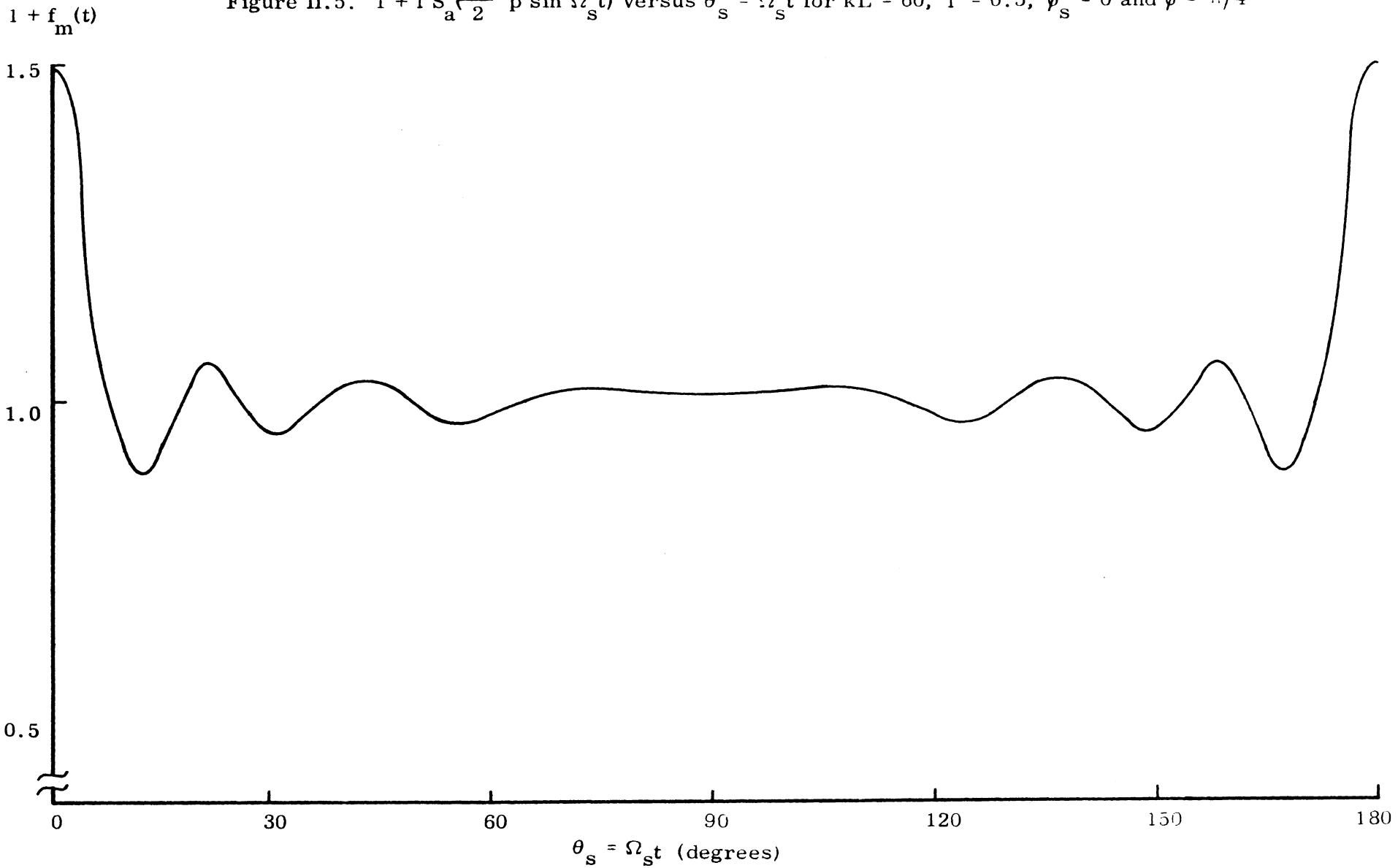

where the gate function G (ω) is defined as

$$G_\tau(\omega) = \begin{cases} 1 & \omega \leq \tau \\ 0 & \omega > \tau. \end{cases} \tag{II.29}$$

Using the concepts of the Fourier series expansion of a periodic function we obtain the following expansion of $f_m(t)$:

$$f_m(t) = \Gamma \frac{\Omega_0}{2\pi} \sum_{-\infty}^{\infty} \frac{\pi}{\tau} G(n\Omega_0) e^{in\Omega_0 t}, \tag{II.30}$$

where $$\Omega_0 = 2\Omega_s, \quad \tau = \frac{kL}{2} p \Omega_s \tag{II.31}$$

As $$\frac{kL}{2} p \Omega_s \to 0, \quad \frac{1}{\tau} G_\tau(n\Omega_0) \to 2\delta(n\Omega_0) \tag{II.32}$$

implying

$$f_m(t) \to \Gamma \frac{1}{2\pi} \int_{-\infty}^{\infty} 2\pi\delta(n\omega_0) e^{in\omega_0 t} d(n\omega_0) = \Gamma.$$

For convenience we rewrite (II.30) as follows:

$$f_m(t) = \Gamma \sum_{-\infty}^{\infty} \frac{1}{\tau} G_\tau(2n\Omega_s) e^{i2n\Omega_s t}. \tag{II.33}$$

Eq. (II.33) indicates that the modulation contains even harmonics of Ω_s each of constant amplitude of $\frac{1}{\tau}$, and that the spectrum extends up to $2n\Omega_s \simeq \frac{kL}{2} p \Omega_s$. A sketch of the spectral components of $f_m(t)$ is shown in Figure II.6. In contrast to the point scatterer case, the results in Figure II.6 show that all the frequency components within the band are of equal amplitude and theoretically no frequency component exists beyond the value $\frac{kL}{2} p \Omega_s$.

The modulation frequency spectrum shown in Figure II.6 is based on the approximation given by (II.27) which assumes that $\frac{kL}{2} p$ is a large quantity. When p is small this maybe a poor approximation even when $\frac{kL}{2}$ is large.

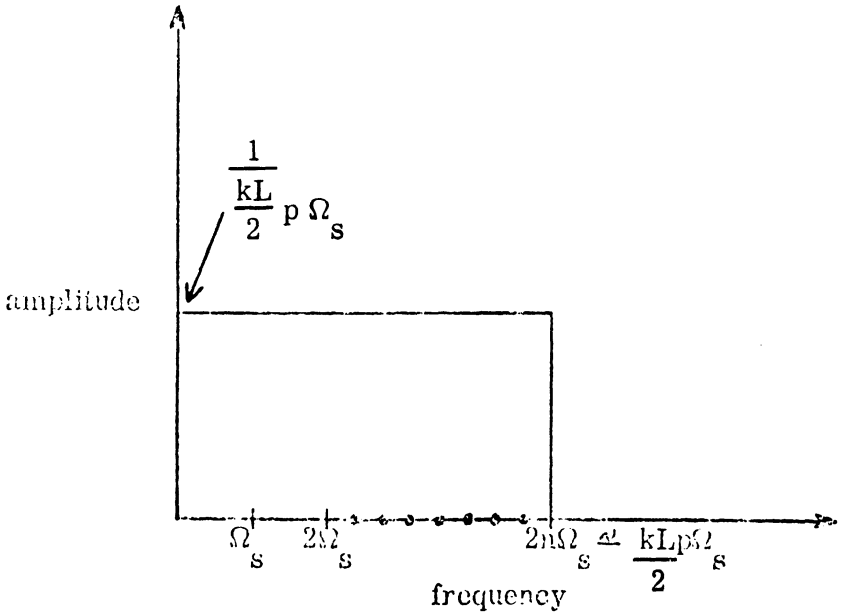

Figure II.6. Frequency spectrum of the modulation function produced by a rotating extended scatterer of length L.

Under such conditions the modulation function $f_m(t)$ given by (II.26) should be examined more carefully. To do this we use the following expansion:

$$\sin\left(\frac{kL}{2}p \sin \Omega_s t\right) = 2 \sum_{o}^{\infty} J_{2n+1}\left(\frac{kL}{2}p\right) \sin\left[(2n+1)\,\Omega_s t\right], \qquad \text{(II.34)}$$

to obtain

$$f_m(t) = 2\Gamma \sum_{o}^{\infty} \frac{J_{2n+1}\left(\frac{kL}{2}p\right)}{\frac{kL}{2}p} \cdot \frac{\sin\left\{(2n+1)\,\Omega_s t\right\}}{\sin \Omega_s t}. \qquad \text{(II.35)}$$

For integral values of n,

$$\frac{\sin\left\{(2n+1)\,\Omega_s t\right\}}{\sin \Omega_s t} = 1 + 2\sum_{m=1}^{n} \cos 2m\Omega_s t, \qquad \text{(II.36)}$$

and (II.35) then gives

$$f_m(t) = 2\sum_{0}^{\infty} \frac{J_{2n+1}(\frac{kL}{2}p)}{\frac{kL}{2}p} + \sum_{n=1}^{\infty}\left\{\sum_{m=n}^{\infty} \frac{4\,J_{2m+1}(\frac{kL}{2}p)}{(\frac{kL}{2}p)}\right\}\cos 2n\Omega_s t. \qquad \text{(II.37)}$$

The amplitudes of the various modulation frequency components are therefore

$$A_n = \sum_{m=n} \frac{4\,J_{2m+1}(\frac{kL}{2}p)}{\frac{kL}{2}p}, \quad n = 1, 2, 3, \ldots. \qquad \text{(II.38)}$$

As expected, the calculation of the frequency spectrum from (II.38) is much more complicated than in the approximate case discussed earlier. However (II.38) does indicate the existence of a band of frequencies, the highest frequency being determined by the parameter $\frac{kL}{2}p$, as before. Figure II.7 shows $\sum_{m=n}^{\infty} J_{2m+1}(\frac{kL}{2}p)$ versus n for two values of $\frac{kL}{2}p$. The band-limited nature of the modulation waveform is evident in Figure II.7. In contrast to the ideal case (Figure II.6), the amplitudes of the various frequencies within the band now fluctuate about some constant value and the band-edges are less sharp.

II.4. Further Discussion of the Modulation Waveform

For the purpose of the present section the modulation function $f_m(t)$ given by (II.26) is rewritten as

$$f_m(t) = \Gamma \frac{\sin\left[\frac{kL}{2}\cos\phi \sin\Omega_s t\right]}{\left[\frac{kL}{2}\cos\phi \sin\Omega_s t\right]}, \qquad \text{(II.39)}$$

where it is assumed that the rotating scatterer is in the xz plane and the receiver is in the xy plane and at an angle ϕ from the x-axis. (II.39) indicates the $f_m(t)$ is a periodic function of period $T_s/2$ where $T_s (= 2\pi/\Omega_s)$ is the time period of rotation of the scatterer (see Figure II.5). More importantly, for large $\frac{kL}{2}\cos\phi$ and small Ω_s, $f_m(t)$ consists of a series of pulses (of $\frac{\sin x}{x}$ form) repeating at intervals of $T_s/2$.

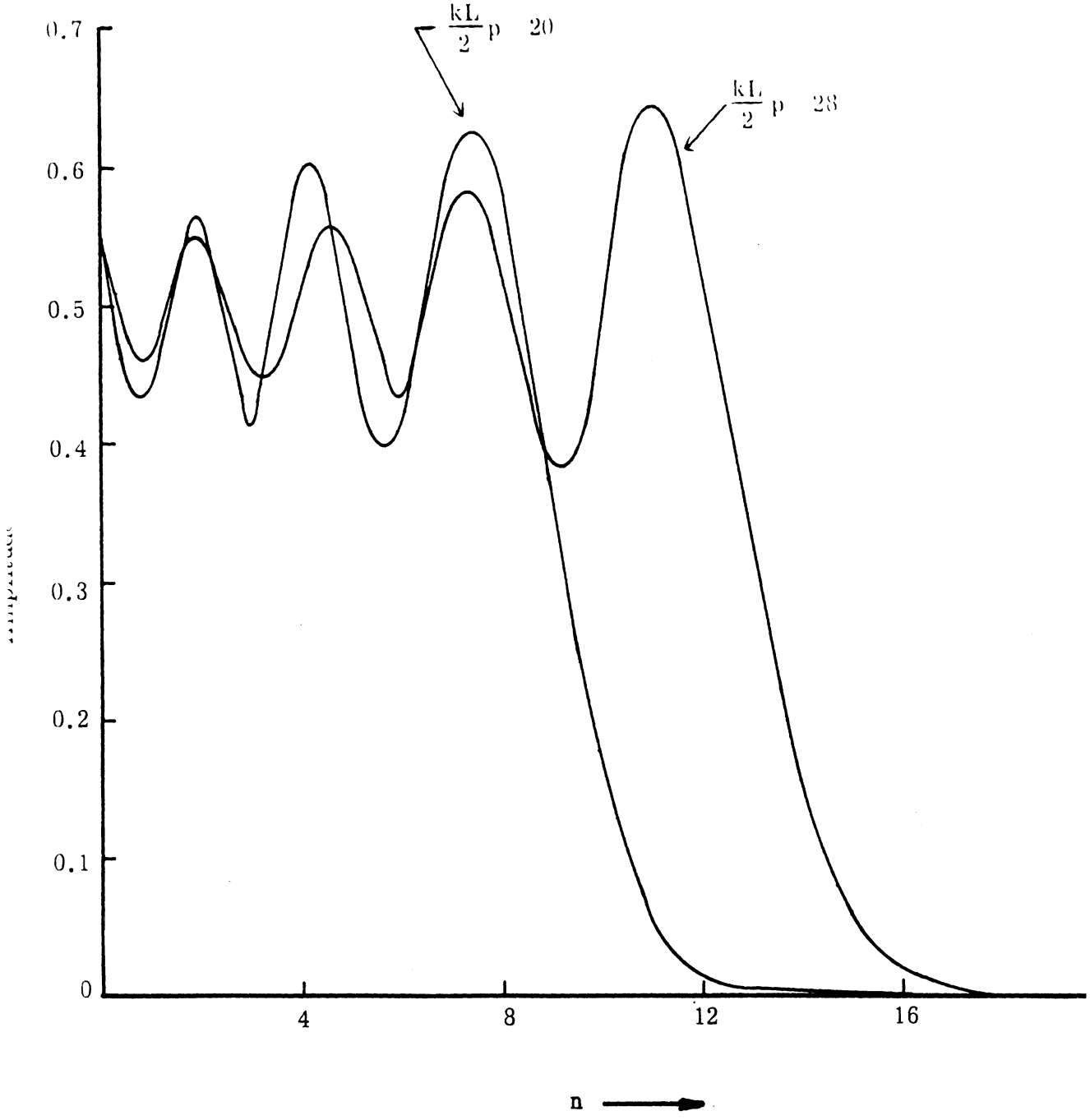

Figure II.7. Spectral distribution curve for the rotating linear scatterer. n = 1 corresponds to the frequency $f_1 = 2f_s$, f_s is the rotation frequency.

One of these modulation pulses is sketched in Figure II.8. For large values of $\frac{kL}{2}\cos\phi$ the pulse width may be defined as $2t_1$, (see Figure II.8) where

$$t_1 = \frac{1}{2\pi f_s}\sin^{-1}\left[\frac{1\cdot 5}{\frac{L}{\lambda}\cos\phi}\right] \simeq \frac{1}{2\pi f_s}\,\frac{1\cdot 5\lambda}{L\cos\phi}\,, \qquad \text{(II.40)}$$

for $\frac{L}{\lambda}\cos\phi \gg 1$, f_s being the rotation frequency. As discussed earlier the modulation function $f_m(t)$ contains a band of frequencies harmonically related to the rotation frequency. The largest modulation frequency is determined by the parameter $\frac{kL}{2}\cos\phi$ and the amplitude of the various frequency components fluctuate about some constant value.

The above expression for the modulation function needs to be modified by taking into account the vector nature of electromagnetic waves. Assume that a z-polarized electromagnetic field is incident on the linear scatterer rotating in the xz plane. The current induced on the scatterer is proportional to the component of the incident field parallel to the scatterer. Assuming that the induced current distribution on the scatterer is of the form $\cos\frac{\pi\ell}{L}$, it can be shown that the modulation waveform at the z-polarized receiver, located in the x-y plane and at an angle ϕ from x-axis is:

$$f_m(t) = C\,(1+\cos 2\Omega_s t)\,\frac{\pi}{4}\left[\frac{\sin\left\{\frac{\pi L}{\lambda}(\cos\gamma+\frac{\lambda}{2L})\right\}}{\left\{\frac{\pi L}{\lambda}(\cos\gamma+\frac{\lambda}{2L})\right\}} + \frac{\sin\left\{\frac{\pi L}{\lambda}(\cos\gamma-\frac{\lambda}{2L})\right\}}{\left\{\frac{\pi L}{\lambda}(\cos\gamma-\frac{\lambda}{2L})\right\}}\right]$$

$$= C\,(1+\cos 2\Omega_s t)\,\frac{\pi^2}{4}\,\frac{\cos\left(\frac{\pi L}{\lambda}\cos\gamma\right)}{\frac{\pi^2}{4}-\frac{\pi^2 L^2}{\lambda^2}\cos^2\gamma}\,, \qquad \text{(II.41)}$$

where $\cos\gamma = \cos\phi\sin\Omega_s t$. (II.42)

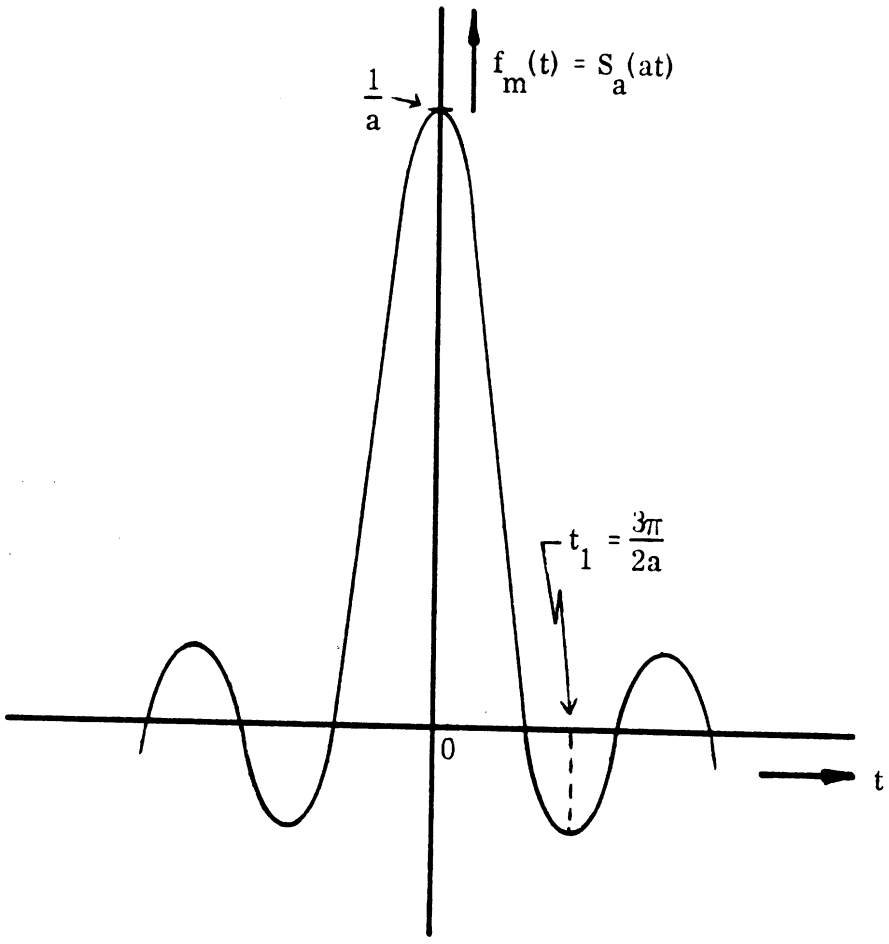

Figure II. 8. A single modulation pulse.

(II.41) is again a periodic function of period $T_s/2$. For sufficiently large $\frac{L}{\lambda}\cos\phi$ and small Ω_s, $f_m(t)$ will consist of a series of pulses repeating at $T_s/2$. The general shape of the pulse is as sketched in Figure II.8 but the width of the pulse will be wider than that given by (II.40). For sufficiently large $\frac{L}{\lambda}\cos\phi$ the width of the pulse may be obtained from:

$$t_1 = \frac{1}{2\pi f_s} \sin^{-1}\left[\frac{2\lambda}{L\cos\phi}\right], \qquad \text{(II.43)}$$

valid for $\frac{L}{\lambda}\cos\phi >> 1$. For small and intermediate values of $\frac{L}{\lambda}\cos\phi$, t_1 can be obtained by numerically computing (II.41).

The general nature of the frequency spectrum of $f_m(t)$ given by (II.41) is similar to that in (II.39) except that the fundamental component of frequency $2f_s$ now has much larger amplitude than the others. It can also be seem from (II.41) that as the length of the scatterer is reduced, the modulation waveform changes from repetitive pulse type to a continuous sinusoidal waveform of frequency $2f_s$.

II.5. Experimental Investigation

The present section discusses the results of an experimental investigation of the amplitude modulation produced by a rotating linear scatterer illuminated by linearly polarized electromagnetic waves. Figure II.9(a) is a sketch of the complete experimental arrangement. A rectangular metallic scatterer of length $L = 6.32\lambda$, width $w = 0.173\lambda$ and thickness $d = 0.028\lambda$ at $\lambda = 21.4$ cm (f = 1.4 GHz) rotates in the xz plane at an angular frequency Ω_s. A transmitting horn illuminates the scatterer at an angle ϕ with z-polarized electromagnetic waves. A similar horn receives the scattered field at an angle $(\pi - \phi)$ as shown. The center of the rotating scatterer and the two horns are placed in the xy plane. The two horns are located 12'4" from the center of the scatterer and are displaced 14'4" in the x direction. Figure II.9(b) gives the block diagram of the receiving arrangement. The received signal is first fed to a spectrum analyzer, the output of which is connected to the vertical input to an oscilloscope where the modulation waveform in the received scattered field is observed. The output of the spectrum analyzer is then fed to a cascade of two band-pass filters whose output is in turn connected to an oscilloscope. This arrangement

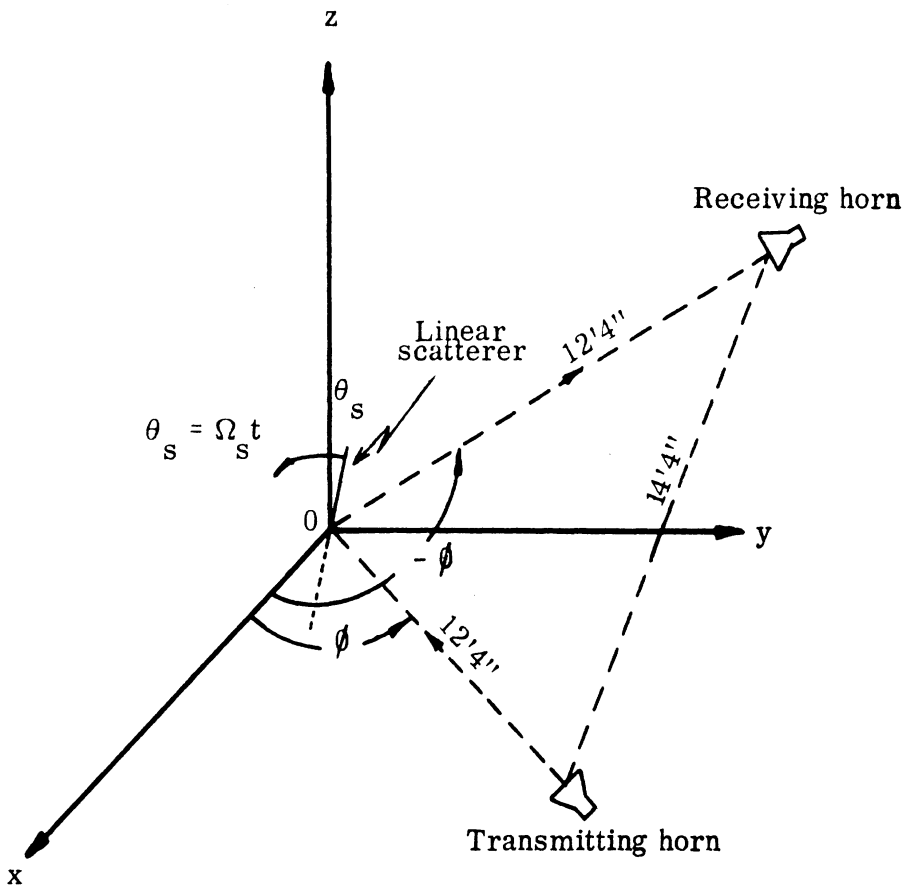

Figure II.9(a). Sketch of the experimental set-up.

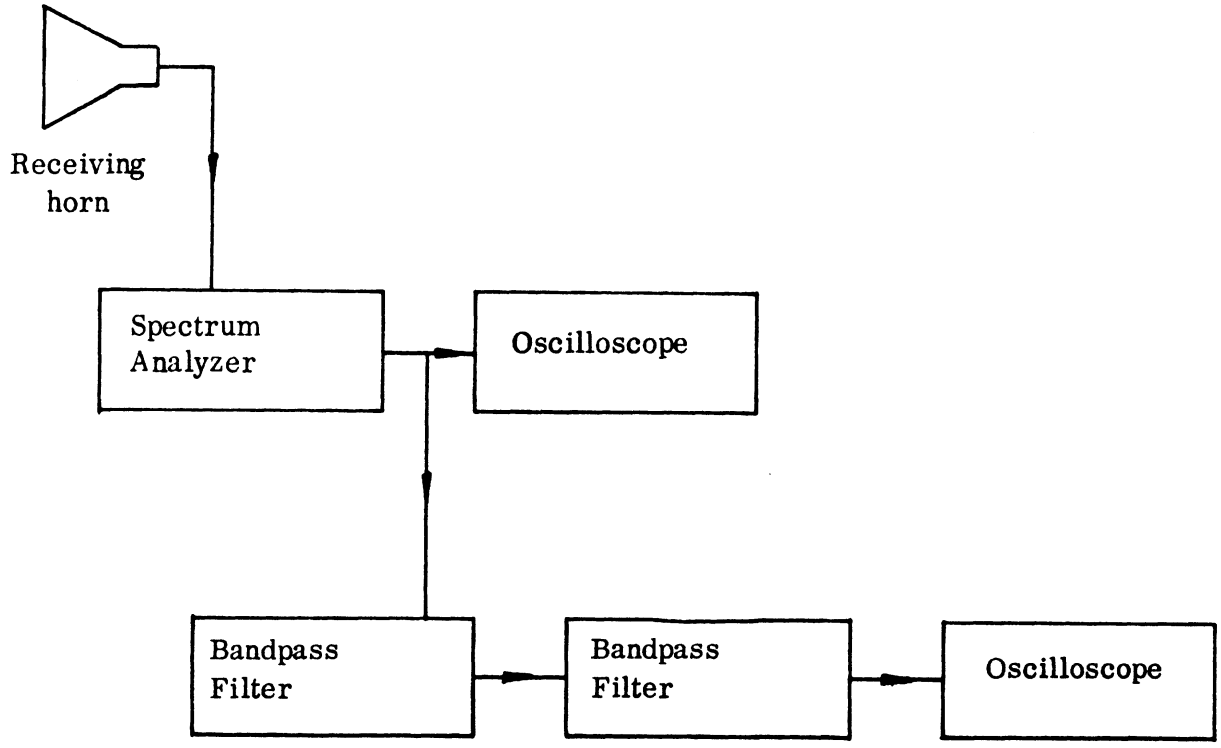

Figure II.9(b). Block diagram of the receiving system.

is used to measure the amplitude of the various frequency components of the modulation waveform. The desired frequency component is selected by properly adjusting the band width and the center frequency of the two bandpass filters.

Figures II.10(a) and (b) show the observed modulation waveforms for $L = \lambda/2$ and λ when the scatterer is rotating at $f_s = 30.83$ Hz. Note that the repetition period of 16.2 ms in Figure 9(a) is exactly half the time period (32.4 milliseconds) of rotation. For $\frac{L}{\lambda} = 0.5$ the observed modulation waveform is sinusoidal as predicted by the theory. For $\frac{L}{\lambda} = 1.0$ the lower halves of the waveforms are distorted (Figure II.10(b)) indicating the existence of harmonics.

Figures II.11(a) - (e) show the observed modulation waveforms for some selected values of $\frac{L}{\lambda}$. Observe that in case (a) the rotation frequency is $f_s = 6.1$ Hz and in all other cases the rotation frequency is 5 Hz. The repetitive pulse-like nature of the modulation waveforms is particularly evident for larger $\frac{L}{\lambda}$. For large values of $\frac{L}{\lambda}$ the waveforms resemble the shape sketched in Figure II.8.

The width ($2t_1$) of the modulation pulses (defined as the time interval between the two minima of the mainlobe of the waveform) obtained from Figures II.10(a) - (e) are shown in Table II.1. The corresponding pulse widths obtained numerically from (II.41) are also shown in Table II.1. Considering the approximate nature of the theory the overall agreement between the measured and theoretical results in Table II.1 is very satisfactory. The somewhat poorer agreement between the results for $\frac{L}{\lambda} = 6.32$ is due to the fact that the receiving and transmitting horns were not located in the far zone of the scatterer in this case.

$\frac{L}{\lambda}$	Measured $2t_1$ in milliseconds	Theoretical $2t_1$ in milliseconds
6.32	50	39
5.32	58	50
4.32	65	62
3.32	70	78
2.32	95	100

Table II.1. Modulation pulse widths produced by a rotating linear scatterer: $\phi \simeq 60$ degrees.

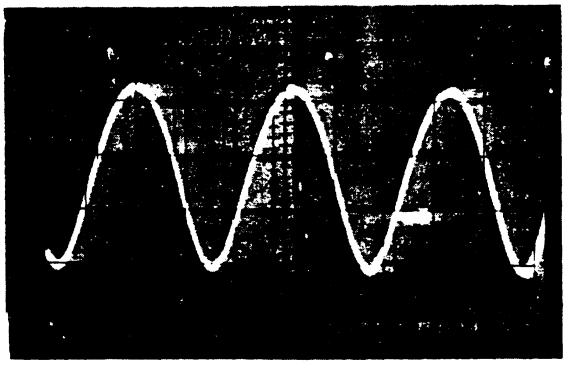

Figure II.10a. Modulation waveform for L = 0.5λ, ϕ = 60 degrees, f_s = 30.83 Hz
Vertical scale 10 mv/division; Horizontal scale 5 ms/division.

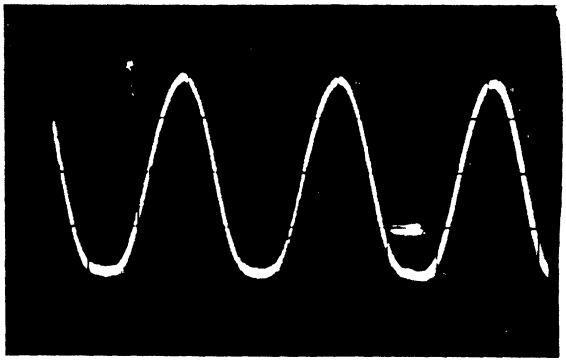

Figure II.10b. Modulation waveform for L = λ, ϕ = 60 degrees, f_s = 30.83 Hz
Vertical scale 10 mv/division; Horizontal scale 5 ms/division.

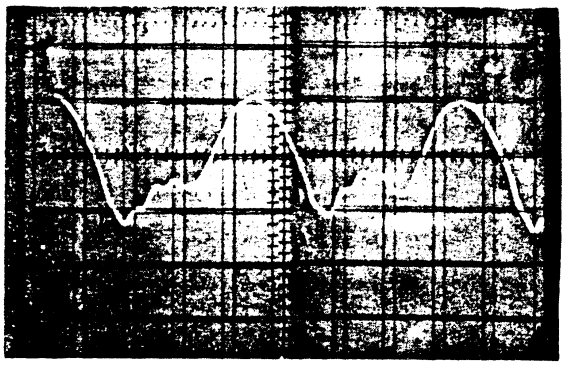

Figure II.11a. Modulation waveform for L = 6.32λ, ϕ = 60 degrees, f_s = 6.1 Hz
Vertical scale 50 mv/division; Horizontal scale 20 ms/division.

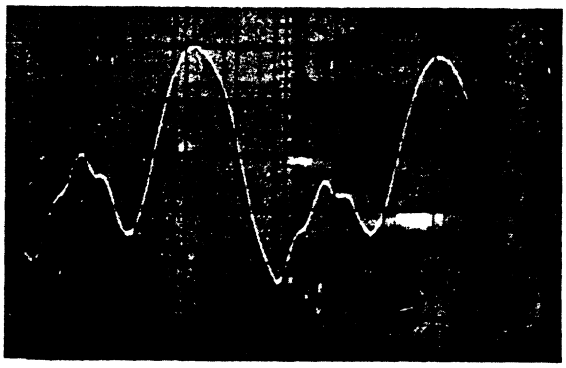

Figure II.11b. Modulation waveform for L = 5.32λ, ϕ = 60 degrees, f_s = 5 Hz
Vertical scale 20 mv/division; Horizontal scale 20 ms/division.

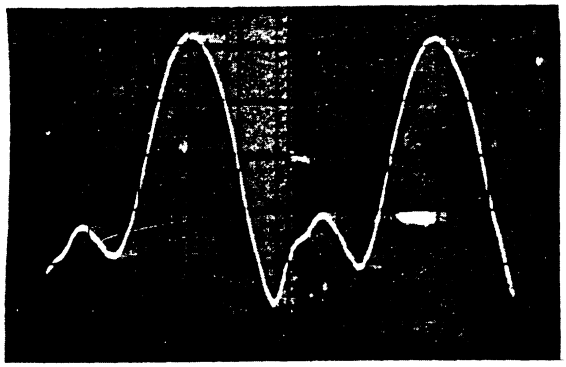

Figure II.11c. Modulation waveform for L = 4.32λ, ϕ = 60 degrees, f_s = 5 Hz
Vertical scale 20 mv/division; Horizontal scale 20 ms/division.

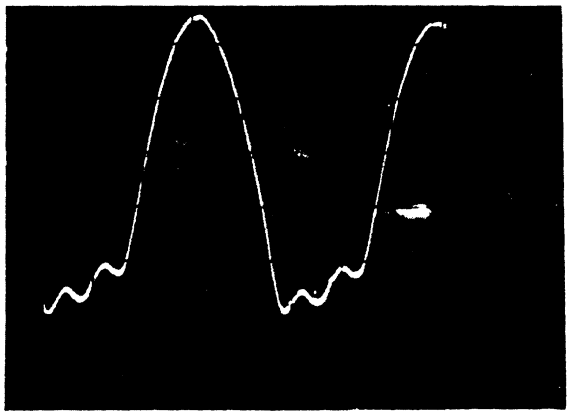

Figure II.11d. Modulation waveform for L = 3.32λ, ϕ = 60 degrees, f_s = 5 Hz
Vertical scale 20 mv/division; Horizontal scale 20 ms/divisio

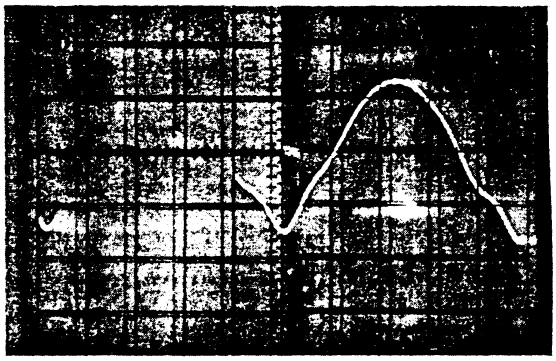

Figure II.11e. Modulation waveform for L = 2.32λ, ϕ = 60 degrees, f_s = 5 Hz
Vertical scale 10 mv/division; Horizontal scale 20 ms/division.

As mentioned earlier the modulation waveform was fed to a cascade of band-pass filters to single out the harmonic content of interest. The peak-to-peak amplitudes, in millivolts of the harmonic output from the filters were measured using an oscilloscope, and Table II.3 lists the results for different $\frac{L}{\lambda}$. The maximum peak-to-peak amplitude values in millivolts are also shown in Table II.2. Due to diminished accuracy, results below 0.5 millivolts have not been included. Because of the response characteristics of the filters and the oscilloscope and the low rotation frequency (5 Hz) used, the determination of the amplitudes of the frequency components near the fundamental was quite difficult.

The results in Table II.2 show that the waveform contains a band of frequencies harmonically related to the rotation frequency. There are also certain general trends: the band becomes wider as $\frac{L}{\lambda}$ is increased, and the frequency components near the fundamental become stronger as $\frac{L}{\lambda}$ is decreased. For large $\frac{L}{\lambda}$ there exists a group of higher frequency components which are of approximately equal amplitudes. Qualitatively at least, the measured data are in agreement with the theory.

II.6. Discussion

The scattering of electromagnetic waves by a rotating linear scatterer has been studied both theoretically and experimentally. Based on the results discussed in the earlier sections, the following observations are made about the general effects produced by such scatterers.

(i) The rotating scatterer produces amplitude modulation of the incident signal. The waveform of the modulation depends critically on the parameter $\frac{L}{\lambda}$. For $\frac{L}{\lambda} \simeq 1/2$ the modulation waveform is pure sinusoid having a frequency twice the rotation frequency of the scatterer. For large $\frac{L}{\lambda}$ and sufficiently low rotation frequency the modulation waveform becomes pulse-like, repeating at twice the rotation frequency.

$\frac{L}{\lambda} \rightarrow$	6.32	5.32	4.32	3.32	2.32
$V_{pp} \rightarrow$	74.0	80.0	100.0	110.0	150.0
n ↓ \ $a_{pp} \rightarrow$					
1	41.4	51.7	48.3	113.8	131.0
2	38.5	41.3	37.3	16.0	11.5
3	9.6	13.9	17.4	15.2	8.7
4	6.8	5.5	5.5	7.3	12.7
5	4.8	4.4	4.4	8.9	12.7
6	2.9	2.9	5.4	9.6	9.6
7	2.5	3.6	5.4	7.1	4.6
8	3.2	5.0	5.4	5.4	3.1
9	4.1	4.8	4.5	3.1	1.7
10	5.2	4.1	3.5	2.1	1.1
11	5.0	2.7	2.3	1.3	0.5
12	4.5	2.1	1.5	0.9	----
13	3.1	1.2	1.0	0.5	----
14	2.2	0.7	0.7	----	----
15	1.5	0.6	0.6	----	----
16	1.2	0.5	0.5	----	----
17	0.8	----	----	----	----
18	0.7	----	----	----	----
19	0.5	----	----	----	----
20	----	----	----	----	----

Table II.2. Measured frequency spectrum of the modulation waveform produced by a linear rotating scatterer: $\phi \simeq 60^{o}$, f_s = 5 Hz.

Note: V_{pp} is the maximum peak-to-peak amplitude of the waveform in millivolts.

a_{pp} is the peak-to-peak amplitude of the harmonic in millivolts.

n is the harmonic number: n = 1 corresponds to 10 Hz.

(ii) The width of the modulation pulse decreases with increasing $\frac{L}{\lambda}\cos\phi$, implying that for a given $\frac{L}{\lambda}$, the pulse width will decrease with increasing observation angle ϕ.

The theory we have developed is only approximate, but it has been found to be sufficient to obtain an engineering understanding of the scattering of an electromagnetic wave by a rotating object. The simple theory explains, with reasonable accuracy, the behavior of the modulation waveforms produced. It is recommended that further theoretical and experimental work be performed to develop a better quantitative understanding of the problem.

II.7. Windmill Modulation

If a pair of windmill blades is replaced by a rotating linear scatterer of equivalent area, the above results can be applied to study the modulation waveform produced by the windmill. On the basis of the rotating linear scatterer model of the windmill blades the following comments can be made about the general nature of the modulation waveform produced by the windmill:

(i) The modulation waveform is a series of pulses repeating at intervals $T_s/2$ where T_s is the rotation period of the blades. For sufficiently large T_s the frequency spectrum of the waveform will be a band of discrete frequencies harmonically related to the rotation frequency of the blades. The spectrum will extend from DC to a maximum angular frequency $\simeq \frac{\Omega_s L}{\lambda}\cos\phi$. Depending on the parameter $\frac{L}{\lambda}\cos\phi$, the maximum modulation frequency maybe many times larger than the blade rotation frequency.

(ii) The width of the modulation pulse becomes smaller at higher frequencies. Thus in the UHF band the modulation waveform will contain a substantial number of high modulation frequencies. It is also expected that at UHF frequencies the scattering from the windmill blades will be large. This would imply that the interference problem is strongest at the UHF channels.

(iii) For receivers located in a direction normal to the plane of rotation of the blades the modulation waveform will contain very low frequency components and hence the interference effects will be less severe.

For future reference we give in Table II.3 the widths of the modulation pulses at three selected TV channel frequencies produced by a rotating linear scatterer of length L = 30.48 m (100'). The dimensions and frequencies are those appropriate to the windmill at Plum Brook. The pulse widths have been obtained using (II.43). The missing values in Table II.3 are when (II.43) cannot be used to obtain the modulation pulse widths. It implies that at these points the modulation waveform is almost sinusoidal at a frequency $2f_s$.

TV Channel No.	Frequency MHz	Wavelength λ in m	$\frac{L}{\lambda}$	Pulse width in milliseconds for $f_s = 1/2$		Pulse width in milliseconds for $f_s = 1/3$	
				$\phi = 60^o$	$\phi = 75^o$	$\phi = 60^o$	$\phi = 75^o$
43	647	0.46	66.3	38	74	57	111
11	200	1.5	20.3	126	249	189	373
4	70	4.29	7.1	381	---	571	---

Table II.3. Modulation pulse widths produced by a linear rotating scatterer of length L = 30.48 m (= 100').

Appendix III

PROPAGATION ANALYSIS

III.1. Introduction

The present Appendix develops the theoretical expressions necessary for computing the TV signals received by a given antenna in the presence of a large windmill. It is assumed that the transmitting antenna is an elementary electric dipole and the receiving antenna is isotropic. The present results can be easily adapted to the case of non-isotropic receiving antennas.

In general, the field which reaches the receiving antenna consists of two distinct parts: the primary or direct field of the transmitting antenna in the presence of the earth, and the field originating from the transmitter and scattered by the windmill, also with the earth present. The latter field will be referred to as the scattered or secondary field. It is assumed that the transmitter, the receiver and the windmill are located in the far zones of each other.

Theoretical expressions for the primary fields are obtained from the work of Fock [1] and Wait [2] on the propagation of radio waves over a smooth homogeneous spherical earth with arbitrary ground constants. As these results are well-known, we shall merely quote the appropriate expressions without derivation.

Since the time varying portions of the windmill scattered fields are of interest, we seek the fields scattered by the windmill blades only. To simplify the electromagnetic scattering problem, each windmill blade is replaced by a narrow rectangular metallic plate of equivalent area. The method of obtaining the scattered fields is as follows. Concepts of physical optics are used to determine the dipole moments induced on the metallic plate by the incident (direct) field. The windmill blades are then replaced by a dipole of equivalent moment, and the secondary field which this produces are found by re-applying Fock theory.

A detailed computer program has been developed by Berry [3] to determine the fields of elementary electric dipoles located above a homogeneous spherical earth. In the following sections, expressions for the primary and secondary fields are presented that can be used directly in the computer program developed in [3]. The computer program itself is discussed in Appendix IV.

III.2. The Primary Field

III.2.1. General Expressions

Consider a current element $\vec{Id\ell}$ of dipole moment $\vec{p} = \frac{\vec{Id\ell}}{i\omega}$ located at T and oriented either along the z-axis or the x-axis (vertical or horizontal) as shown in Figure III.1. It is assumed that the time dependence is $e^{i\omega t}$. The origin of the spherical coordinate system (r, θ, ϕ) is taken to be at the center of the earth of radius a. The electric and magnetic fields at R may be obtained from the following:

$$\vec{E} = \nabla \times \nabla \times \vec{\pi}, \tag{III.1}$$

$$\vec{H} = i\omega\epsilon \nabla \times \vec{\pi}, \tag{III.2}$$

where ϵ is the permittivity of the medium and $\vec{\pi}$ is the Hertz vector produced by the source at the receiving point R. It can be shown [1, 2] that the Hertz vector is given by the following:

$$\vec{\pi} = \frac{\vec{p}e^{-ika\theta}}{4\pi\epsilon a(\theta \sin\theta)^{1/2}} \left(\frac{x}{\pi}\right)^{1/2} e^{i\pi/4} \int_{\Gamma_2} e^{-ixt} F(t, y_1, y_2, q)dt \tag{III.3}$$

where $k = 2\pi/\lambda$ is the propagation constant, Γ_2 consists of the straight line segments from $\infty e^{-i2\pi/3}$ to the origin and out along the real axis to ∞ in the complex t-plane, and the other parameters are defined as follows:

$$F = \frac{1}{2} w_1(t - y_2) \left[w_2(t - y_1) + B(t) w_1(t - y_1) \right], \tag{III.4}$$

$$B(t) = -\left[\frac{w_2'(t) - q w_2(t)}{w_1'(t) \quad q w_1(t)} \right], \tag{III.5}$$

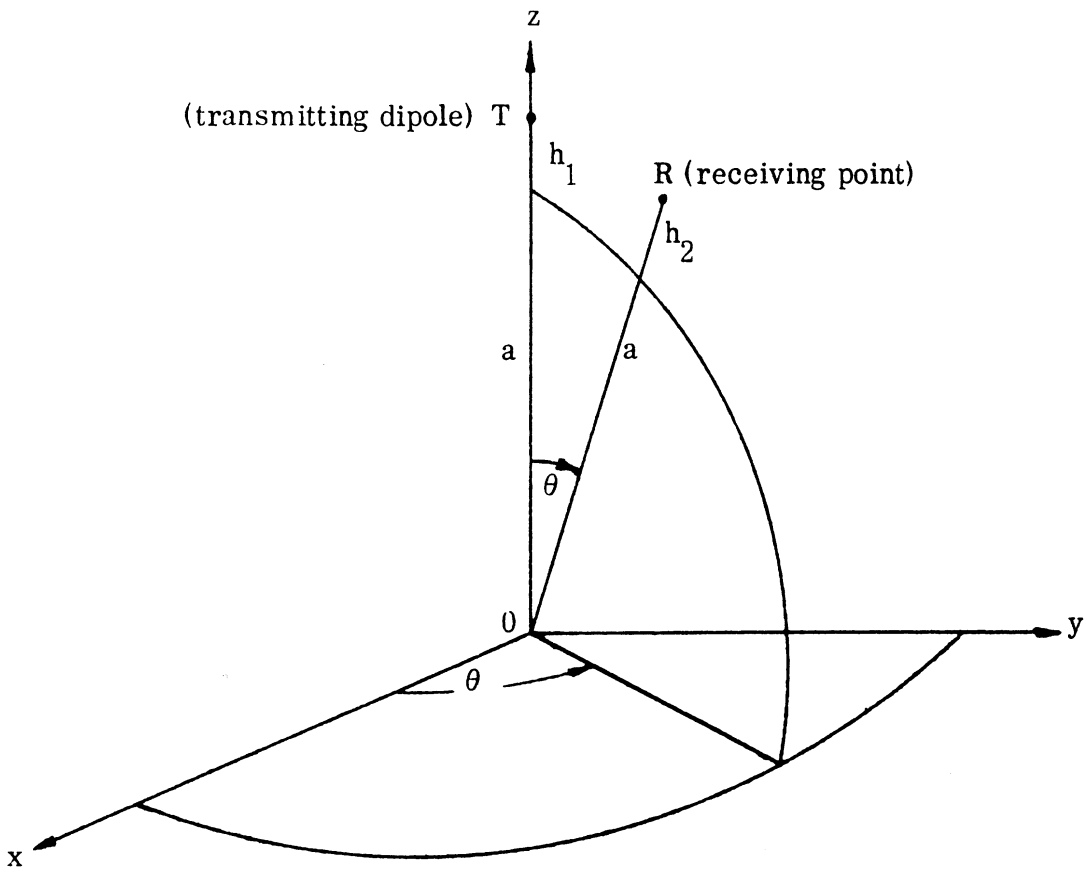

Figure III.1. Coordinate system used for the primary field calculations.

$$y_1 = \left(\frac{2}{ka}\right)^{1/3} kh_1,\ y_2 = \left(\frac{2}{ka}\right)^{1/3} h_2 ,$$

$$x = \left(\frac{ka}{2}\right)^{1/3} \theta = v\theta , \qquad \text{(III.6)}$$

$$q = -i\left(\frac{ka}{2}\right)^{1/3} \delta ,$$

$$\delta = \begin{cases} \sqrt{\eta - 1}/\eta & \text{for vertical polarization} \\ \sqrt{\eta - 1} & \text{for hirozontal polarization} \end{cases} \qquad \text{(III.7)}$$

$$\eta = \epsilon - i\frac{1.8 \times 10^7 \sigma}{f} .$$

where f is the frequency in KHz, σ is the ground conductivity in mho/m and ϵ is the permittivity of the ground relative to that of free space. $w_1(t)$ and $w_2(t)$ are the Airy integral function and the associated Airy integral function respectively defined as follows:

$$w_1(t) = \frac{1}{\pi} \int_{\Gamma_1} \exp(st - s^3/3)ds \qquad \text{(III.8)}$$

$$w_2(t) = \frac{1}{\pi} \int_{\Gamma_2} \exp(st - s^3/3)ds$$

where Γ_1 consists of straight line segments in the complex s-plane from $\infty e^{i2\pi/3}$ to the origin and out along the real axis to ∞ and Γ_2 is as defined before. The expression (III.3) is valid for $y_2 > y_1$ (i.e., $h_2 > h_1$); if $y_1 > y_2$ the quantities y_1 and y_2 in the expression (III.4) for F are to be interchanged.

In Wait's notation [2], (III.3) may be written as follows:

$$\vec{\pi} = \frac{\vec{p}e^{-ika\theta}}{4\pi\epsilon a}\left(\frac{v}{\pi \sin\theta}\right)^{1/2} e^{i\pi/4} \int_{\Gamma_2} e^{-ixt} F_w(q, t)dt, \qquad \text{(III.9)}$$

where

$$F_w(q, t) \quad \frac{H_1(h_1)H_2(h_2)}{\frac{w_1'(t)}{w_1(t)} - q} \tag{III.10}$$

$$H_1(h_1) = \frac{w_1(t - y_1)}{w_1(t)} , \tag{III.11}$$

and

$$H_2(h_2) = 0.5 \left[\left\{ w_1'(t) - q w_1(t) \right\} w_2 (t - y_2) - \left\{ w_2'(t) - q w_2(t) \right\} w_1(t - y_2) \right]. \tag{III.12}$$

For a z-directed dipole $\vec{\pi} = \hat{z}\pi_z$, where

$$\pi_z = \frac{p_z e^{-ika\theta}}{4\pi\epsilon a} \left(\frac{v}{\pi \sin\theta} \right)^{1/2} e^{i\pi/4} \int_{\Gamma_2} e^{-ixt} F_w(q, t) dt \tag{III.13}$$

with $p_z = \frac{Id\ell}{\omega}$ and q given by the form of (III.7) appropriate for vertical polarization. The far zone fields can now be obtained from (III.1) and (III.2) and are

$$E_\theta = - \sin\theta (k^2 \pi_z)$$

$$H_\phi = E_\theta / \eta_0 \tag{III.14}$$

where η_0 is the intrinsic impedance of free space.

Similarly, for an x-directed dipole, $\vec{\pi} = \hat{x}\pi_x$ with

$$\pi_x = \frac{p_x e^{-ika\theta}}{4\pi\epsilon a} \left(\frac{v}{\pi \sin\theta} \right)^{1/2} e^{-i\pi/4} \int_{\Gamma_2} e^{-ixt} F_w(q, t) dt \tag{III.15}$$

where $p_x = \frac{Id\ell}{\omega}$ and q is given by the form of (III.7) appropriate for horizontal polarization. The far zone fields of interest in this case are [1]

$$\left.\begin{aligned} E_\phi &= -k^2 \pi_x \sin\phi \\ H_r &= -\frac{k^2}{\eta_0} \pi_x \sin\phi \end{aligned}\right\} \qquad \text{(III.16)}$$

III.2.2. Check with Berry's Formulation:

For computational purposes Berry [3] takes a contour $\Gamma = -\Gamma_2$ in (III.9) and writes the Hertz vector in the form

$$\pi = \frac{ipe^{-ika\theta}}{4\pi\epsilon a}\left(\frac{v}{\pi \sin\theta}\right)^{1/2} e^{-i3\pi/4}\int_\Gamma e^{-ixt} F_I(q, t)dt \qquad \text{(III.17)}$$

where $F_I(q, t) = -iF_w(q, t)$. With this notation $H_2(h_2)$ is given by (III.12) with - i in front of the right hand side. Thus, in Berry's notation the components of the z- and x-directed Hertz vectors are

$$\pi_{\substack{z \\ x}} = \frac{ip_{\substack{z \\ x}} e^{-ika\theta}}{4\pi\epsilon a}\left(\frac{v}{\pi \sin\theta}\right)^{1/2} e^{-i3\pi/4}\int_\Gamma e^{-ixt} F_I(q, t)dt \qquad \text{(III.18)}$$

with q having the appropriate value. The far fields can now be obtained from (III.14) or (III.16).

Berry's computer program computes the z-component of the field, E_z, for vertical polarization and the x-component of the field, E_x, for horizontal polarization, and the transmitting dipole moment is also expressed in terms of the effective radiated power in free space. For a current element $Id\ell$ (of moment $p = Id\ell/i\omega$) located above a conductive half-space, it can be shown [4] that the total effective power radiated in free space is

$$P_{eff} = 5\omega^2 k^2 \qquad \text{(III.19)}$$

If $P_{eff} = P$ where P is expressed in kW, then $Id\ell$ can be expressed as

$$Id\ell = \frac{5\sqrt{P}}{k}. \qquad \text{(III.20)}$$

To compute the fields it is convenient to divide the entire space into regions. The location and extent of these regions depend on the transmitter and receiver positions, the ground constants and the operating frequency, and are chosen so as to permit different approximations to be made to evaluate the integral in (III.18). Overall there are four regions where four different versions of the potential function obtained from (III.18) are employed to compute the fields. After making use of (III.20), we write below the modified forms of (III.18) appropriate to the four regions, listed in the order of increasing distance from the transmitter.

The radio waves propagate as a surface wave if both antennas are located near the earth. For short distances between the two antennas it is possible and convenient to assume that the earth is flat, enabling the flat earth approximation to (III.18) to be made. The geometry of this situation is shown in Figure III.2. The appropriate expressions for the Hertz vector components are [2]

$$\pi_{z_x} = \frac{300\sqrt{P}}{k^2 d} A(z), \tag{III.21}$$

where A(z) is the flat earth attenuation function defined as

$$A(z) = 1 - R_0 \delta e^{z^2} \operatorname{erfc}(z) \tag{III.22}$$

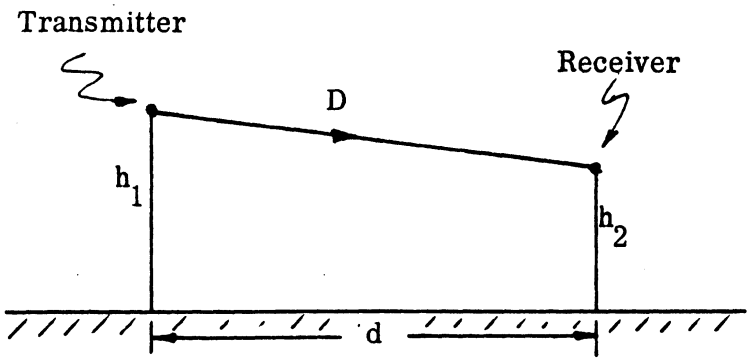

Figure III.2. Geometry of the flat earth case.

where

δ is the surface impedance of the ground (see III.7)

$$R_0 = e^{i\pi/4} \frac{\pi k D}{2}, \tag{III.23}$$

$$D = \left\{ d^2 + (h_1 - h_2)^2 \right\}^{1/2}, \tag{III.24}$$

$$z = e^{i\pi/4} \sqrt{\frac{kD}{2}} \, \delta \, 1 + \frac{h_1 + h_2}{\delta D}, \tag{III.25}$$

$$\operatorname{erfc}(z) = \frac{2}{\pi} \int_z^\infty e^{-t^2} dt. \tag{III.26}$$

Geometrical optics approximations can be used to simplify (III.18) if the receiving point is located well above the radio horizon when viewed from the transmitter. The geometry of the problem in this region, called the interference region, is sketched in Figure III.3. The Hertz vector components then have the expression[1, 2]

$$\pi_{\substack{z \\ x}} = \frac{300\sqrt{P}}{k^2} \frac{e^{-ik(D - d)}}{2D} \left[1 + R_g e^{-ik(D_1 + D_2 - D)} \right] \tag{III.27}$$

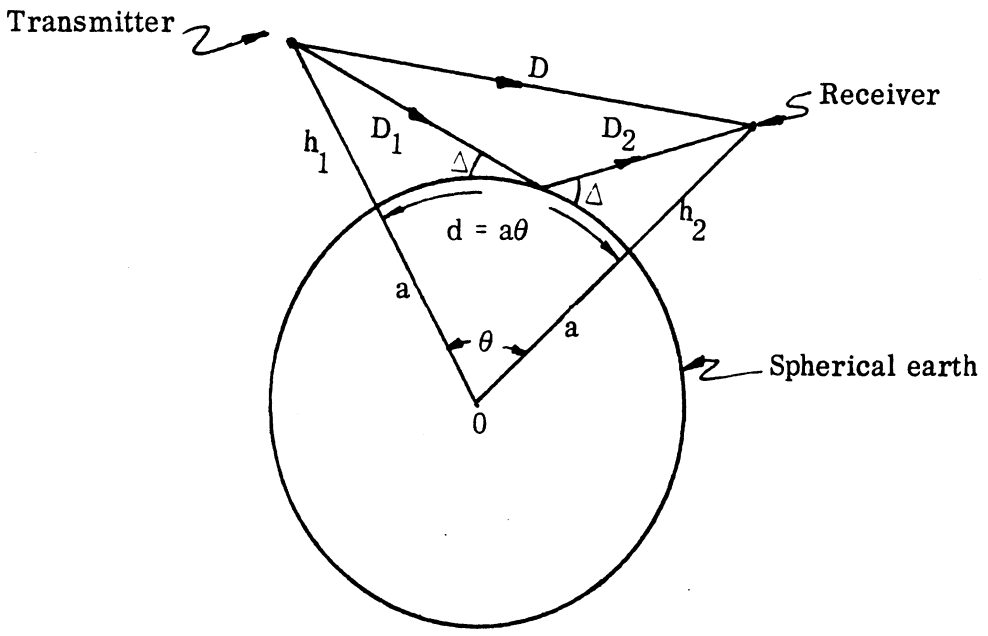

Figure III.3. Geometry of the problem in the interference region.

where

$$R_g = \frac{\sin\Delta - \bar{\delta}}{\sin\Delta + \bar{\delta}}\ , \tag{III.28}$$

$$\bar{\delta} = \begin{cases} \sqrt{\eta - \cos^2\Delta}/\eta & \text{for vertical polarization} \\ \sqrt{\eta - \cos^2\Delta} & \text{for horizontal polarization} \end{cases}\ , \tag{III.29}$$

$$D = \left\{ \left[2a^2 + 2a(h_1 + h_2) \right] (1 - \cos\theta) + h_1^2 + h_2^2 - 2h_1 h_2 \cos\theta \right\}^{1/2}\ , \tag{III.30}$$

$$D_i = \left\{ a^2 \sin^2\Delta + A_i \right\}^{1/2} - a\sin\Delta, \qquad i = 1, 2\ , \tag{III.31}$$

$$A_i = 2ah_i + h_i^2\ , \quad i = 1, 2, \tag{III.32}$$

$$(D_1 + D_2)^2 + 4 D_1 D_2 \sin^2\Delta - D^2 = 0. \tag{III.33}$$

Observe that (III.27) assumes the divergence factor to be unity.

The next region is known as the transition region where the receiving point is near but not beyond the radio horizon of the transmitting antenna. This is the most difficult region in which to compute the fields since the integral in (III.18) must now b evaluated numerically. For this purpose (III.18) is written in the following modified form:

$$\pi_{\substack{z \\ x}} = \frac{300\sqrt{P}}{k^2 a}\, e^{-ika\theta} \left(\frac{v}{4\pi \sin\theta} \right)^{1/2} e^{-i3\pi/4} \int_\Gamma e^{-ixt} F_I(q, t)\, dt, \tag{III.34}$$

where q is given the value appropriate to the polarization.

The shadow region is farthest from the transmitter and corresponds to a receiving point located beyond the radio horizon of the transmitting antenna. The integral in (III.18) can then be evaluated using its residue series to give

$$\pi_{\substack{z \\ x}} = \frac{300\sqrt{P}}{k^2}\,\frac{\pi}{a}\,e^{-ika\theta}\left(\frac{v}{\pi \sin\theta}\right)^{1/2} e^{-i\pi/4}$$

$$\times \sum_j e^{-ixt_j}\,\frac{H_1(h_1)\,H_1(h_2)}{t_j - q^2}\,, \qquad \text{(III.35)}$$

where t_j are the poles of $F_I(q, t)$, i.e. the solutions of

$$w_1'(t) - q\, w_1(t) = 0 \qquad \text{(III.36)}$$

The exact conditions under which the various approximations are employed will be discussed along with the computer program in a later Appendix.

After using (III.14) and (III.34) the z-component of the E-field in the transition zone produced by a vertically polarized ($\hat{z}$-directed) electric dipole is obtained as

$$E_z = k^2 \pi_z = \frac{300\sqrt{P}}{a}\, e^{-ika\theta}\left(\frac{v}{4\pi \sin\theta}\right)^{1/2} e^{-i3\pi/4} \int e^{-ixt}\, F_I(q, t)\,dt \qquad \text{(III.37)}$$

where q corresponds to vertical polarization. Similarly in the horizontal polarization case, the x-component of the E-field in the transition zone produced by a horizontally polarized ($\hat{x}$-directed) electric dipole may be obtained using (III.16) and (III.34) and is

$$E_x = k^2 \pi_x = \frac{300\sqrt{P}}{a}\, e^{-ika\theta}\left(\frac{v}{4\pi \sin\theta}\right)^{1/2} e^{-i3\pi/4} \int_\Gamma F_I(q, t)\,dt \qquad \text{(III.38)}$$

where q corresponds to horizontal polarization. Apart from the term $e^{-ika\theta}$, (III.37) and (III.38) agree with Berry's expressions [3].

III.3. Field Expressions for the Present Problem

III.3.1. Geometry of the Problem

A spherical polar coordinate system (r, θ, ϕ) is chosen with its origin 0 located at the center of the spherical earth of radius a and its polar axis z aligned along

the windmill tower (see Figure III.4). The windmill tower height is C'C = ρ_0. It is assumed that the windmill blades lie and rotate in the x-z plane. The location of a typical blade area element dS' at B is identified by the coordinates ℓ, Ω where Ω is measured from the z-axis and ℓ is the distance from the top of the tower to the center of the area element. With this choice of coordinates, the rotation of the windmill blades can be simulated by making the parameter Ω time varying. The locations of the phase centers of the transmitting and receiving antennas are at T and R respectively.

With respect to the basic spherical coordinate system, the coordinates of B, R and T are respectively $(a + h_3, \theta_3, 0)$, $(a + h_2, \theta_2, \phi_2)$ and $(a + h_1, \theta_1, \phi_1)$ where h_3, h_2 and h_1 are as shown in Figure III.4. The various great circle distances between these three points, measured along the surface of the earth are represented by:

$$\begin{aligned} &\text{transmitter-to-receiver:} && d_{12} = a\theta_{12} \\ &\text{transmitter-to-windmill blade point:} && d_{13} = a\theta_{13} \\ &\text{windmill blade point-to-receiver:} && d_{23} = a\theta_{23} \end{aligned} \qquad \text{(III.39)}$$

where θ_{12}, θ_{13} and θ_{23}, as shown in Figure III.4, are given by

$$\begin{aligned} \cos\theta_{12} &= \cos\theta_1 \cos\theta_2 + \sin\theta_1 \sin\theta_2 \cos(\phi_1 - \phi_2) \\ \cos\theta_{13} &= \cos\theta_1 \cos\theta_3 + \sin\theta_1 \sin\theta_3 \cos\phi_1 \\ \cos\theta_{23} &= \cos\theta_2 \cos\theta_3 + \sin\theta_2 \sin\theta_3 \cos\phi_2 \end{aligned} \qquad \text{(III.40)}$$

with

$$\sin\theta_3 = \frac{\ell\,|\sin\Omega|}{\left[(a+\rho_0)^2 + \ell^2 + 2(a+\rho_0)\,\ell\cos\Omega\right]^{1/2}} . \qquad \text{(III.41)}$$

The parameter h_3 for the area element dS' is obtained from the following relation:

$$h_3 = -a + \sqrt{(a+\rho_0)^2 + \ell^2 + 2(a+\rho_0)\,\ell\cos\Omega}$$

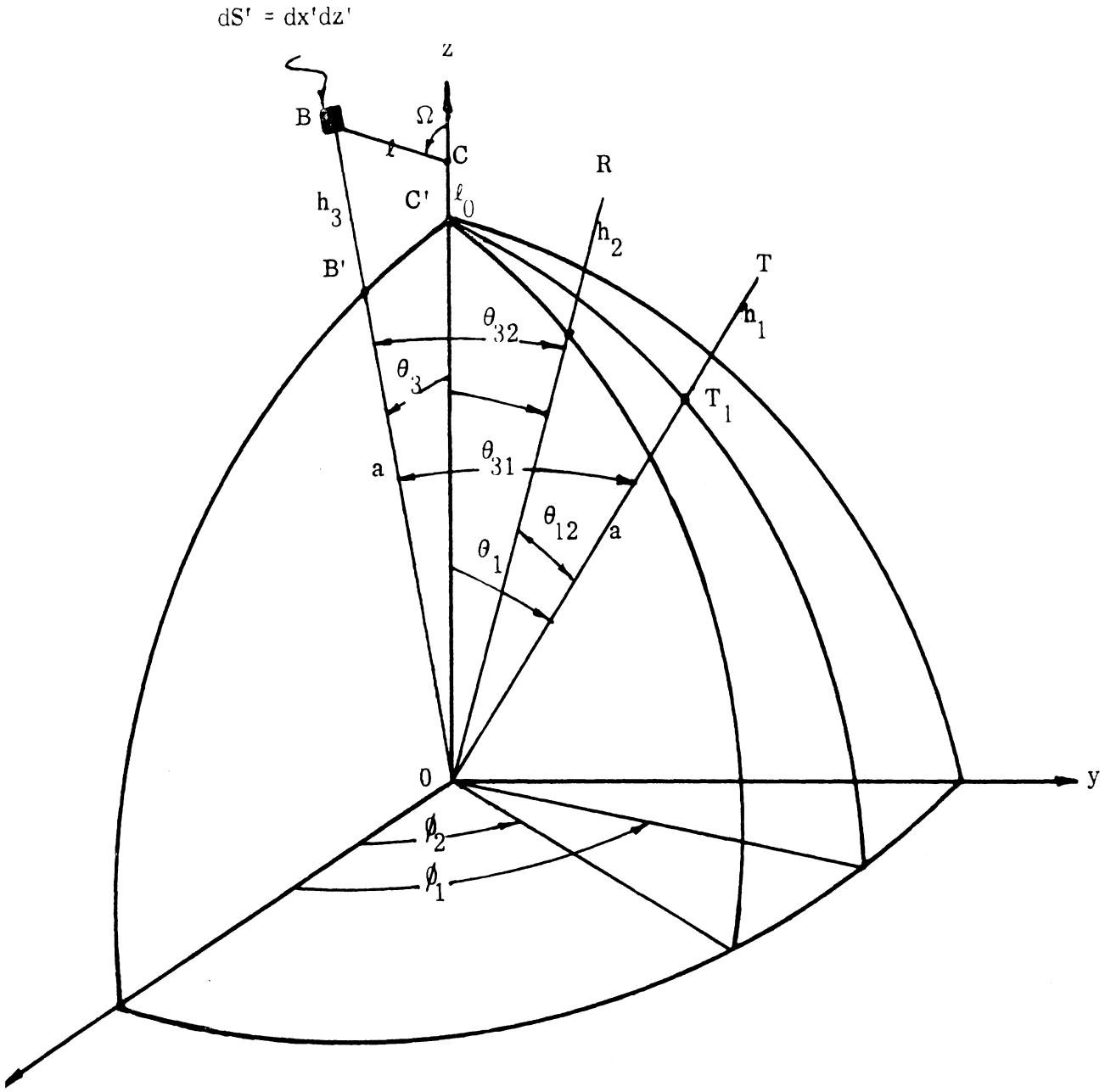

Figure III.4. The geometry and the coordinate system used for the windmill, transmitter and receiver located above a spherical earth.

If T, R and B are within the line-of-sight of each other, the three relevant line-of-sight distances D_{12} (transmitter-to-receiver), D_{13} (transmitter-to-windmill blade point) and D_{23} (receiver-to-windmill blade point) are given by

$$D_{12}^2 = (a + h_1)^2 + (a + h_2)^2 - 2(a + h_1)(a + h_2) \cos \theta_{12} \tag{III.43}$$

$$D_{13}^2 = (a + h_1)^2 + \left[(\rho_0 + 2)^2 + \ell^2 \right. 2(\rho_0 + a)\, \ell \cos \Omega$$
$$- 2(a + h_1)^2 \left[\ell \sin \Omega \sin \theta_1 \cos \phi_1 + (\ell \cos \Omega + \rho_0 + a)\cos \theta_1\right] \tag{III.44}$$

$$D_{23}^2 = (a + h_2)^2 + \left[(\rho_0 + a)^2 + \ell^2 + 2(\rho_0 + a)\, \ell \cos \Omega\right]$$
$$- 2(a + h_2) \left[\ell \sin \Omega \sin \theta_2 \cos \phi_2 + (\ell \cos \Omega + \rho_0 + a) \cos \theta_2\right] \tag{III.45}$$

To find the reflected fields it is necessary to know the length of the reflected path and the grazing angle. This is shown in Figure III.5 for the transmitter and receiver combination where the reflected path length is $D_1 + D_2$ and the grazing angle is Δ. These parameters may be obtained from the following:

$$D_1 = \sqrt{2ah_1 + h_1^2 + a^2 \sin^2 \Delta} - a \sin \Delta \tag{III.46}$$

$$D_2 = \sqrt{2ah_2 + h_2^2 + a^2 \sin^2 \Delta} - a \sin \Delta \tag{III.47}$$

$$D_{12}^2 = (D_1 + D_2)^2 - 4D_1 D_2 \sin^2 \Delta. \tag{III.48}$$

For TB and BR combinations, the required parameters may be obtained from (III.46) - (III.48) by appropriate change of subscripts.

III.3.2. Field Incident at B

Assume that an x-directed current element $Id\ell$ of moment $\hat{x}p_{Tx} = \hat{x}\frac{Id\ell}{\omega}$ is located at the transmitter point T. The fields produced by the transmitter at the windmill blade point B may be obtained using (III.16) and (III.18) and are

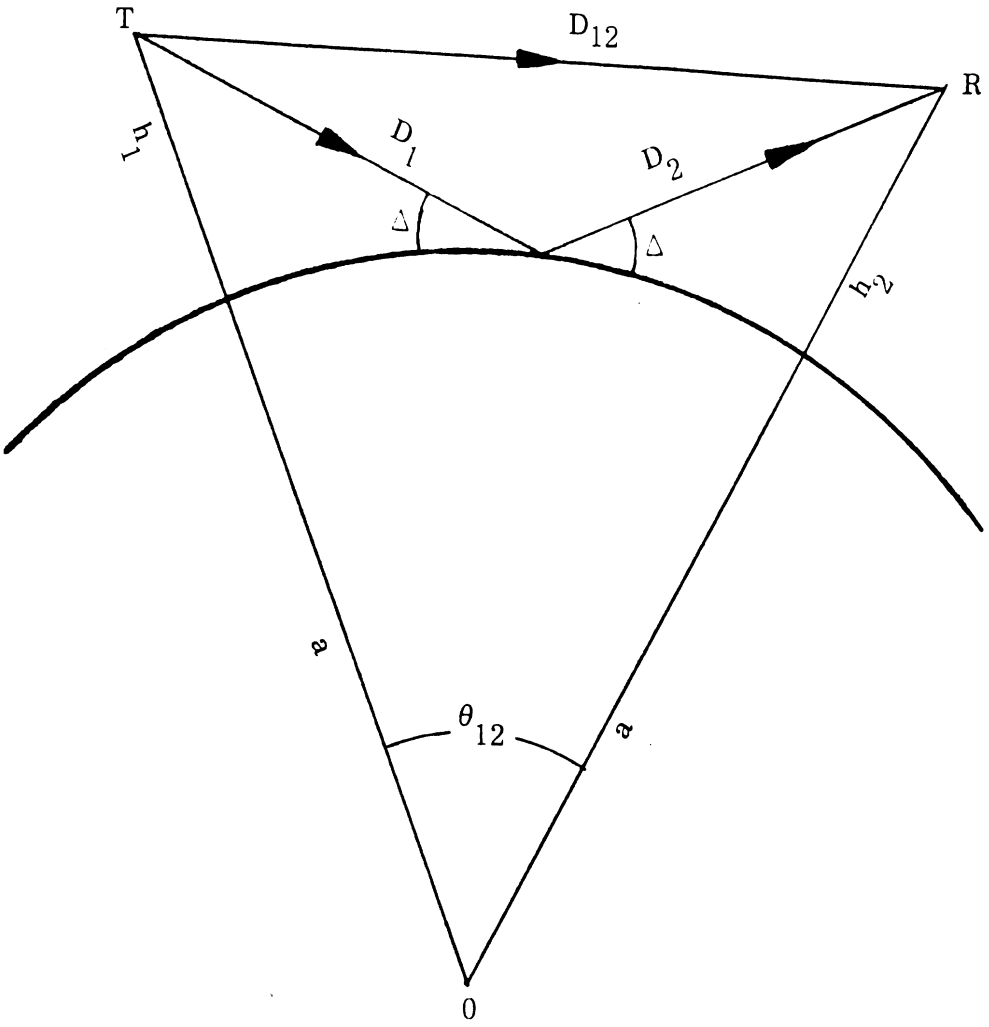

Figure III.5. Reflected path and grazing angle for the transmitter-receiver combinations.

$$E_{\phi}^{T}(B) = -\frac{k^2 \sin \phi_1}{4\pi\epsilon a} \, ip_{Tx} e^{-ika\theta_{13}} \left(\frac{v}{\pi \sin \theta_{13}}\right)^{1/2} I_1 , \qquad \text{(III.49)}$$

$$H_r^T(B) = \frac{E_{\phi}^{T}(B)}{\eta_0} , \qquad \text{(III.50)}$$

where

$$I_1 = e^{-i3\pi/4} \int_{\Gamma} e^{-ix_{13}t} F_I(q, t)dt , \qquad \text{(III.51)}$$

with q specified appropriately for horizontal polarization. In terms of the effective radiated power P (in kW), (III.49) may be written as

$$E_{\phi}^{T}(B) = - \frac{300\sqrt{P}\sin\phi_1}{a} e^{-ika\theta_{13}} \left(\frac{v}{4\pi\sin\theta_{13}}\right)^{1/2} I_1 . \qquad \text{(III.52)}$$

The incident field $E_{\phi}^{T}(B)$, $H_{r}^{T}(B)$ will induce currents on the windmill blade at B which in turn will produce the scattered or secondary field at the receiving point. The induced current density and hence the induced dipole moment on the blade surface is discussed in the next section.

III.3.3 Induced Dipole Moment on the Blade

It is assumed that the windmill blades are perfectly conducting. The induced surface current density on the windmill blade at the point B can be approximated as

$$\vec{K}(B) = 2(\hat{n} \times \vec{H}^{i}) , \qquad \text{(III.53)}$$

where $\hat{n}$ is the unit outward vector normal to the blade surface at the point B and $\vec{H}^{i}$ is the incident magnetic field at that point. For the present case $\hat{n} = \hat{y}$ and $\vec{H}^{i} = \hat{r}E_{\phi}^{T}(b)/\eta_0$ and from (III.53) we then have

$$\vec{K}(B) = \frac{2E_{\phi}^{T}(B)}{\eta_0}\left[\hat{x}\cos\theta_3 - \hat{z}\sin\theta_3\right] . \qquad \text{(III.54)}$$

The current on the surface element dS' induces a dipole of moment $\vec{p}_B$ which may be written as

$$\vec{p}_B = \frac{\vec{K}(B)}{i\omega} dS' = p_{Bx}\hat{x} + p_{Bz}\hat{z} , \qquad \text{(III.55)}$$

where

$$p_{Bx} = \frac{2E_{\phi}^{T}(B)}{i\omega\eta_0} \cos\theta_3 \, dS' , \qquad \text{(III.56)}$$

$$p_{Bz} = -\frac{2E_{\phi}^{T}(B)}{i\omega\eta_0} \sin\theta_3 \, dS' . \qquad \text{(III.57)}$$

It can be seen from (III.55) to (III.57) that the field of a horizontally polarized transmitter induces both horizontally and vertically polarized dipoles on the windmill blade. This indicates that the scattered field will contain both horizontal and components in general. However, in a practical situation $\theta_3 \simeq 0$ and hence the contributions due to the vertical dipole are negligible. We shall therefore confine our attention to the horizontally polarized scattered field.

III.3.4. Scattered or Secondary Field at the Receiver

The horizontally polarized secondary field at the receiver is produced by the x-directed dipole induced in the windmill blade. Using (III.16), (III.18) and (III.56), the secondary field at a receiver R located at $(a + h_2, \theta_3, \phi_3)$ is

$$E_{\phi}^{B}(R) = - \frac{2E_{\phi}^{T}(B) \sin \phi_2 \cos \theta_3}{\lambda a} dS' \, e^{- ika\theta_{32}} \left(\frac{v}{4\pi \sin \theta_{32}} \right)^{1/2} \cdot e^{- i3\pi/4} \int_{\Gamma} e^{- ix_{32}t} F_I(q, t) \, , \tag{III.58}$$

where

$$x_{32} = \left(\frac{ka}{2} \right)^{1/3} \theta_{32} = v\theta_{32} \tag{III.59}$$

and the other parameters are as defined before.

The total scattered field produced by the windmill blades can be obtained by integrating (III.58) over the surface area of the equivalent rectangular plate. This integration is difficult to carry out exactly. However, considering the orders of magnitude with respect to the large parameter a of the various parameters identifying the metallic plate, we can make some approximations so that the total scattered field may be estimated with sufficient accuracy without actually carrying out the integration.

The incident field being x-polarized, it is expected that the blades will produce strong scattering when they are parallel to the x-axis (i.e., $\Omega = \pi/2$ in Figure III.4.).

Under this condition, the maximum scattering will occur in a direction normal to the x-axis, and the maximum value of the total scattered field can be obtained by replacing dS' in (III.58) by the area A of the metal plates.

The directional characteristics of the total scattered field can be approximated from the following considerations. The linear dimensions of the blades are small compared to the radius of the earth. Because of this the horizontally polarized incident electric field induces predominantly x-directed dipoles on the metallic plate (see Section III.3.3). Under the physical optics approximation the total scattered field produced by the rectangular plate can be obtained from (III.58) and is written in the following form:

$$E_{\phi}^{B}(R) = - \frac{2E_{\phi}^{T}(B) \sin \phi_2 \cos \theta_3}{\lambda a} dS' \, I_2 , \qquad \text{(III.60)}$$

where

$$I_2 = e^{-ika\theta_{32}} \left(\frac{v}{4\pi \sin \theta_{32}} \right)^{1/2} e^{-3\pi/4} \int_{\Gamma} e^{-ix_{32}t} F_I(q, t)dt , \qquad \text{(III.61)}$$

$$dS' = A \frac{\sin\left\{\frac{kL_1}{2}(\sin\theta_1' \cos\phi_1 + \sin\theta_2' \cos\phi_2)\right\}}{\left\{\frac{kL_1}{2}(\sin\theta_1' \cos\phi_1 + \sin\theta_2' \cos\phi_2)\right\}} \cdot \frac{\sin\left\{\frac{kL_2}{2}(\cos\theta_1' + \cos\theta_2')\right\}}{\left\{\frac{kL_2}{2}(\cos\theta_1' + \cos\theta_2')\right\}}$$

(III.62)

θ_1', θ_2' refer to the elevation coordinates of the incident and receiving directions measu from the z-axis of a local spherical coordinate system with center at C (Figure III.4).

L_1, L_2 are the linear dimensions of the rectangular plate in the x- and z-directions respectively,

and $A = L_1 L_2$ is the physical area of the rectangular plate.

Because the radius of the earth is large compared to other parameters involved it can be seen from (III.39) and (III.40) that θ_1, θ_2 are usually very small. Also, in a practical situation, it is most important to know the scattered field variation in a

plane normal to the plane of rotation of the blades (i.e. $\theta_1' = \theta_2' \simeq \pi/2$), and it is then sufficient to use the following expression instead of (III.62):

$$dS' = A \frac{\sin\left\{\frac{kL_1}{2}(\cos\phi_1 + \cos\phi_2)\right\}}{\left\{\frac{kL_1}{2}(\cos\phi_1 + \cos\phi_2)\right\}} . \qquad \text{(III.63)}$$

(III.60) indicates that the source of the scattered field at the receiver is the electric field $E_\phi^T(B)$ produced by the transmitter at B as given by (III.52). For computational purposes it is convenient to first obtain the field produced at R by an x-directed electric dipole of known strength located at B and then obtain the desired scattered field from this with the help of an equivalent dipole strength depending on the incident field $E_\phi^T(B)$. Let an x-directed electric dipole with effective radiated power P_B (in kW) be located at B. The field produced at R by this dipole is given by:

$$\tilde{E}_\phi^B(R) = -\frac{300\sqrt{P_B}}{a} \sin\phi_2 \; I_2 , \qquad \text{(III.64)}$$

where I_2 is as defined before. From (III.60) and (III.64) the equivalent strength of the dipole at B (or the normalizing constant) is

$$N = \frac{E_\phi^B(R)}{\tilde{E}_\phi^B(R)} = \frac{2\,dS' \cos\theta_3 \, E_\phi^T(B)}{300\,\lambda\sqrt{P_B}} . \qquad \text{(III.65)}$$

Its maximum value for a given $E_\phi^T(B)$ is

$$|N|_{max} = \frac{2A\,|E_\phi^T(B)|}{300\,\lambda\sqrt{P_B}} , \qquad \text{(III.66)}$$

and the maximum value of the scattered field amplitude at R is therefore

$$\left|E_{\phi}^{B}(R)\right|_{max} = \frac{2A\left|E_{\phi}^{T}(B)\right|}{300\,\lambda\sqrt{P_B}}\,\tilde{E}_{\phi}^{B}(R)\,, \tag{III.67}$$

III.3.5. Direct Field at the Receiver

The direct field at the receiver may be obtained by using (III.16), (III.18) and (III.20) and is

$$E_{\phi}^{T}(R) = -\frac{300\sqrt{P}}{a}\sin\beta\left(\frac{v}{4\pi\sin\theta_{12}}\right)^{1/2} e^{-ika\theta_{12}} \cdot e^{-i3\pi/4}\int_{\Gamma} e^{-ix_{12}t}\,F_I(q,\,t)dt\,, \tag{III.68}$$

where

$$x_{12} = \left(\frac{ka}{2}\right)^{1/3}\theta_{12}\,, \tag{III.69}$$

$$\cos\beta = \frac{\sin\theta_2\cos\phi_2 - \sin\theta_1\cos\phi_1}{\left[2\left\{1 - \sin\theta_1\sin\theta_2\cos(\phi_1 - \phi_2) - \cos\theta_1\cos\theta_2\right\}\right]^{1/2}}\,, \tag{III.70}$$

and the other parameters are as defined before.

III.3.6. Total Field at the Receiver

The total field at the receiver is obtained by adding (III.58) and (III.68) and is

$$E_{\phi}(R) = E_{\phi}^{T}(R) + E_{\phi}^{B}(R) \tag{III.71}$$

where it has been assumed that $E_{\phi}^{B}(R)$ now denotes the total scattered field. Observe that the scattered field given by (III.60) depends on the windmill blade parameter Ω through the parameters θ_3, θ_{32}, etc. For a rotating blade Ω will be a function of time, implying that the scattered field amplitude and phase will also be functions of time. It is therefore expected that the scattered field will be both amplitude and phase modulated by the rotating windmill blades. The modulation characteristics can be found

by studying the time behavior of (III.58) as a function of the parameter Ω, and an approximate analysis of the modulation of the total receiver signal was presented in Appendix II. We shall not repeat any of this here, and will merely indicate how the amplitude modulation index can be determined from a knowledge of $E_{\phi}^{T}(R)$ and $E_{\phi}^{B}(R)$.

The windmill scattered signal is modulated by the rotating blades, and assuming that the maximum value of the scattered signal at the receiver is small compared with the direct one, the modulus of the total signal reaching the receiver can be written as

$$\left|E_{\phi}(R, t)\right| = \left|E_{\phi}^{T}(R)\right| \left[1 + m f_m(t)\right] , \qquad \text{(III.72)}$$

where $E_{\phi}^{T}(R)$ is as before,

$f_m(t)$ is the normalized modulation function of amplitude unity,

and m is the amplitude modulation index:

$$m = \frac{\left|E_{\phi}^{B}(R)\right|}{\left|E_{\phi}^{T}(R)\right|} , \qquad \text{(III.73)}$$

where $E_{\phi}^{B}(R)$ is the maximum scattered field at R. Using (III.67) the expression for the modulation index becomes

$$m = \frac{2}{300\,\lambda\sqrt{P_B}} \frac{\left|E_{\phi}^{T}(B)\right|}{\left|E_{\phi}^{T}(R)\right|} \tilde{E}_{\phi}^{B}(R) , \qquad \text{(III.74)}$$

where $\tilde{E}_{\phi}^{B}(R)$ is the field produced at R by an electric dipole located at B and radiating an effective power P_B in kW.

III.4. Discussion

The theoretical expressions have been derived which are necessary to obtain the primary and secondary signals received by an isotropic receiving antenna in the

presence of a windmill. The field expressions include explicitly the directional properties of the transmitting antenna and the windmill blade scatterer. The directional characteristics of a receiving antenna can be included by multiplying each received signal by the appropriate pattern function of the receiving antenna.

In the present study we are mainly interested in obtaining the maximum scattered signal relative to the direct signal at the receiving antenna. For this purpose it is sufficient to ignore the directional characteristics of the transmitting and receiving antennas and the windmill blade scatterer during the initial calculations of the various field quantities. This is justified also by the following practical considerations. Although the transmitted TV signal is horizontally polarized, it is not known a priori exactly what the polarization of the incident signal is in a given situation. Also the vertical plane of rotation of the windmill blades is arbitrarily oriented with respect to the incident field polarization. Under these conditions it is more appropriate to carry out the initial field calculations on the basis of non-directional transmitting and receiving antennas and the maximum of windmills scattered fields. The assumption of isotropy will therefore yield the maximum values of the various field quantities of interest in a given practical situation.

III.5. References

1. Fock, V.A. (1965), Electromagnetic Diffraction and Propagation Problems, Pergamon Press, New York.

2. Wait, J.R. (1964), "Electromagnetic Surface Waves", in Advances in Radio Research, (edited by J.A. Saxon), Vol. 1, pp. 157-217, Academic Press, London.

3. Berry, L.A., Fortran Program for Calculating Ground Wave Propagation over Spherical Earth, National Bureau of Standards, Boulder, Colorado.

4. Stratton, J.A. (1941), Electromagnetic Theory, McGraw-Hill Book Co. Inc., New York, p. 437.

Appendix IV

COMPUTER PROGRAM

In this Appendix we describe the program used to compute the field of a ıorizontal (or vertical) electric dipole transmitter when a large windmill is present. Γhe transmitter, receiver and windmill are assumed located above a homogeneous ;mooth spherical earth of arbitrary electrical properties. The program is based on :hat developed by Berry, but with the modification necessary to take account of the ;ffects produced by the windmill. The various field expressions derived in Appendix JI have been implemented in an IBM-compatible FORTRAN program which is capable)f providing the following information:

(i) Primary field at the receiver in the absence of the windmill : complex, amplitude and phase.

(ii) Incident field at the windmill : complex, amplitude and phase.

(iii) Secondary, i.e. windmill-scattered, field at the receiver as a function of the blade position : complex, amplitude and phase.

(iv) Total (primary plus secondary) field at the receiver : complex, amplitude and phase.

The above information is obtained for any transmitter and receiver heights and ocations, and for a windmill of arbitrary size and location; however, the program isting presented later shows only those parameters of direct interest in the present ;tudy. Most of the notations used are explained there, and Appendix III should be :onsulted for any that are not clear. On the Amdahl 470 V/6 computer at The Univer-;ity of Michigan, the C.P.U. time to compute a single field quantity averages 0.1 sec. ?low charts of the entire program are shown in Figures IV.1 and IV.2, and a program isting follows.

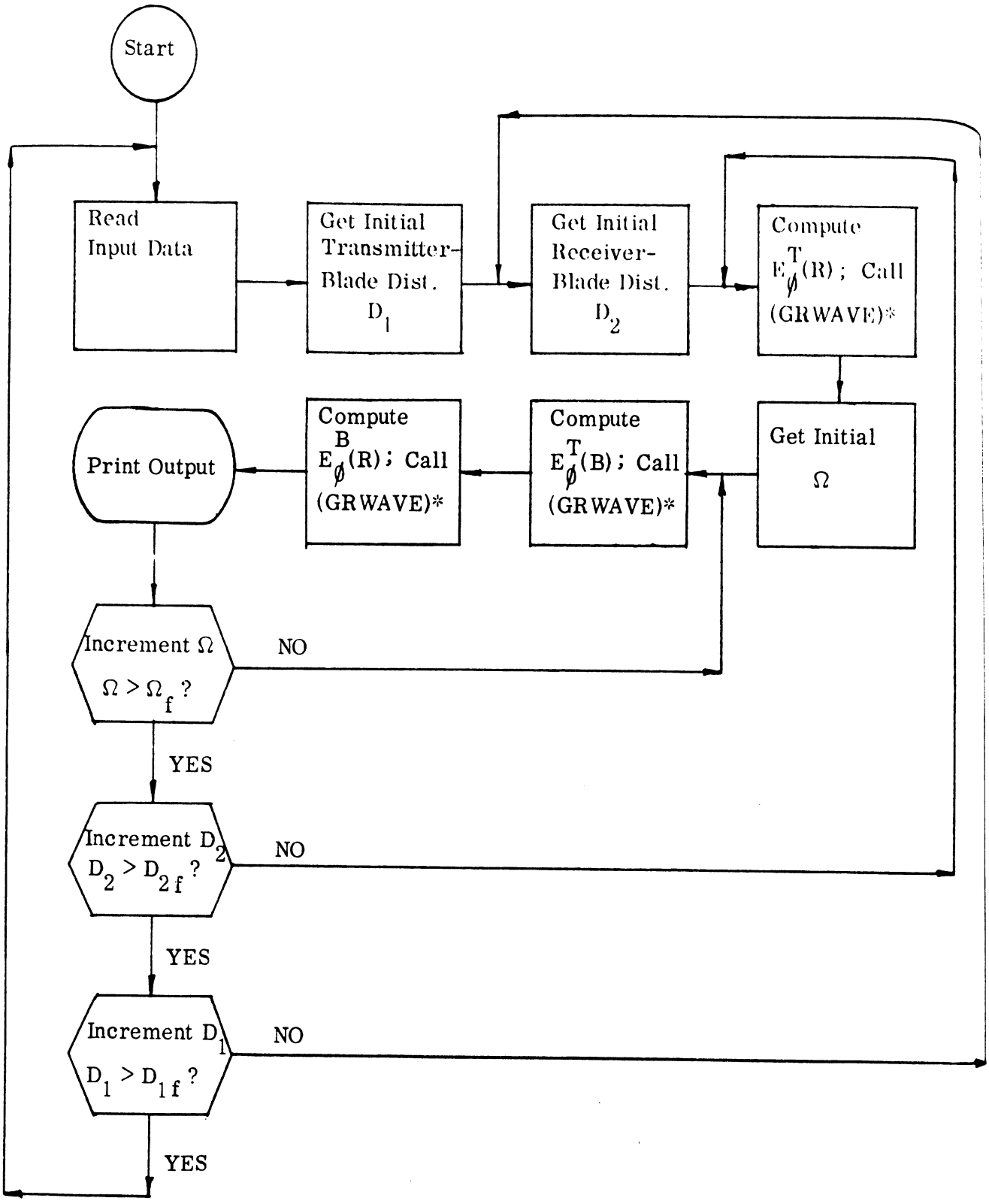

*GRWAVE is a subroutine to compute the ground wave field strength. A flow diagram follows in Figure IV.2.

Figure IV.1. Flow diagram for windmill program.

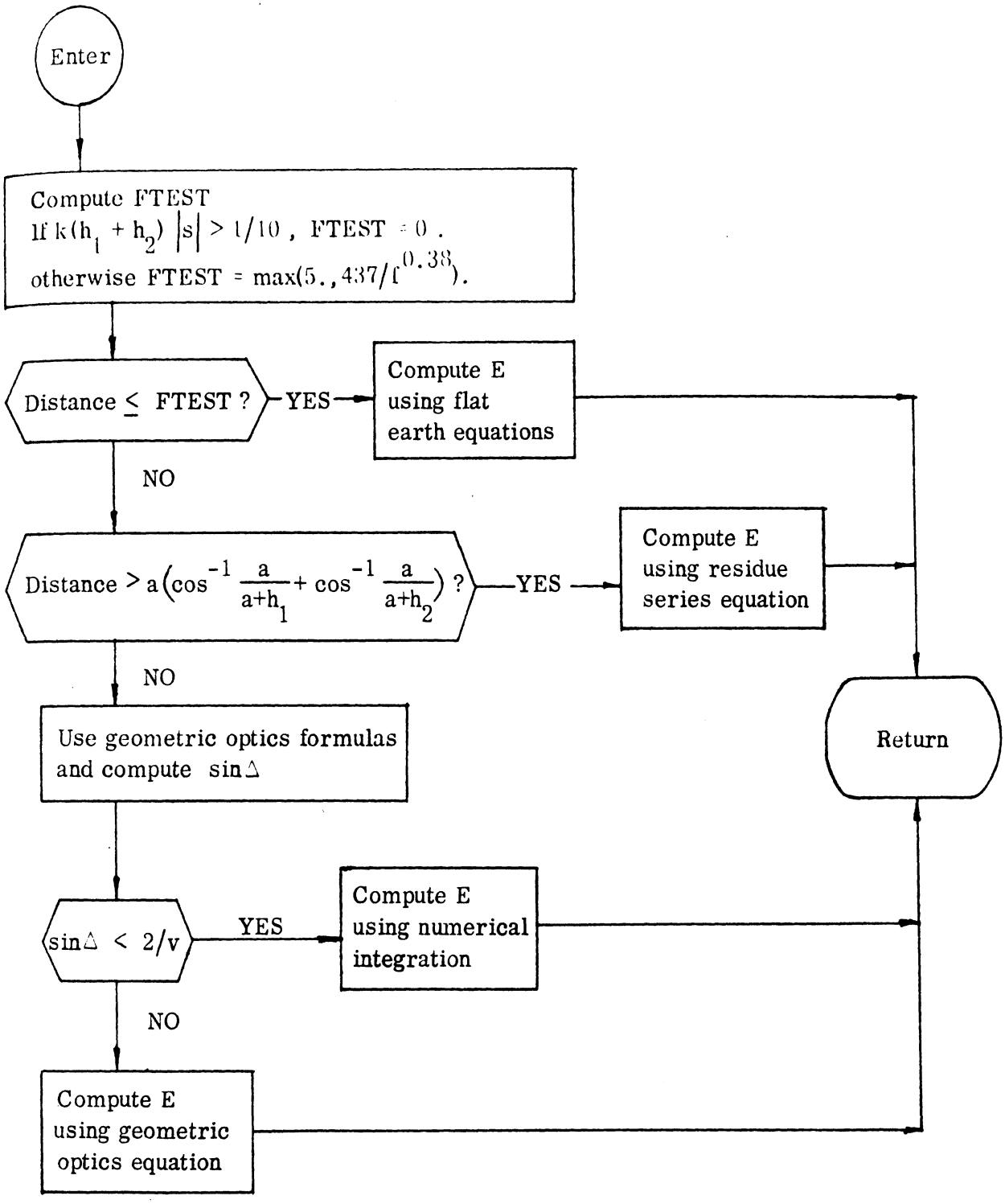

Figure IV.2. Flow diagram for subroutine GRWAVE.

TABLE OF CONTENTS

(Sequential)

```
THIS PROGRAM COMPUTES THE PRIMARY AND SECONDARY FIELDS
AT A RECEIVING POINT PRODUCED BY A TRANSMITTER AND
IN THE PRESENCE OF A LARGE WINDMILL.

INPUT DATA

CARD 1   FORMAT(5F5.0,3F10.5)
     FREQ  = FREQUENCY IN MHZ
     COND  = GROUND CONDUCTIVITY IN MHO/M
     EPS   = GROUND PERMITTIVITY RELATIVE TO FREE SPACE
     ALFA  = EFFECTIVE EARTH RADIUS FACTOR
     POWER = EFFECTIVE RADIATED POWER IN KILOWATTS
     ROEO  = WINDMILL TOWER HEIGHT IN METERS
     H1    = HEIGHT OF THE TRANSMITTER IN METERS
     H2    = HEIGHT OF THE RECEIVER IN METERS
CARD 2   FORMAT(6F5.0,2F10.5,I2)
     PHI1    = AZIMUTHAL ANGLE OF THE TRANSMITTER WITH RESPECT
               TO THE PLANE OF ROTATION OF THE BLADE
     PHI2    = AZIMUTHAL ANGLE OF THE RECEIVER (SEE PHI1 ABOVE)
     OMEGAI = INITIAL ANGLE OF THE BLADE AREA ELEMENT
               MEASURED FROM THE Z-AXIS
     OMINC  = ANGLE INCREMENT OF OMEGA
     OMLAST = FINAL ANGLE OF THE BLADE AREA ELEMENT
     ELI    = DISTANCE IN METERS FROM THE TOP OF THE TOWER
               TO THE CENTER OF THE BLADE AREA ELEMENT
     L1     = LONGER DIMENSION OF THE BLADE IN METERS
     L2     = SHORTER DIMENSION OF THE BLADE IN METERS
     NPOL   = GROUND WAVE POLARIZATION
       1    = VERTICAL POLARIZATION
       2    = HORIZONTAL POLARIZATION
CARD 3   FORMAT(6F10.2)
     D1I    = INITIAL GREAT CIRCLE DISTANCE IN KM BETWEEN
               TRANSMITTER AND BLADE ELEMENT
     D1INC = DISTANCE INCREMENT
     D1F    = FINAL GREAT CIRCLE DISTANCE BETWEEN TRANSMITTER
               AND BLADE ELEMENT
     D2I    = INITIAL GREAT CIRCLE DISTANCE BETWEEN RECEIVER
               AND BLADE ELEMENT
     D2INC = DISTANCE INCREMENT
     D2F    = FINAL GREAT CIRCLE DISTANCE BETWEEN RECEIVER
               AND BLADE ELEMENT

OUTPUT DATA

     D31    = GREAT CIRCLE DISTANCE BETWEEN TRANSMITTER AND
               WINDMILL BLADE POINT
     D32    = GREAT CIRCLE DISTANCE BETWEEN WINDMILL BLADE POINT
               AND RECEIVER
     D12    = GREAT CIRCLE DISTANCE BETWEEN TRANSMITTER AND RECEIVER
```

```
C IN THE FOLLOWING TB,BR,TR REPRESENT:
C    TB = TRANSMITTER-TO-WINDMILL BLADE POINT
     BR = WINDMILL BLADE POINT-TO-RECEIVER
C    TR = TRANSMITTER-TO-RECEIVER
C AMPTB,AMPBR,AMPTR = AMPLITUDES OF FIELDS IN VOLTS/METER AT A
C                     RECEIVING POINT
C DBTB,DBBR,DBTR    = AMPLITUDES IN DB OF FIELDS AT A RECEIVING PO
C MTB,MBR,MTR       = AN INTEGER (1,2,3,4) DESIGNATING THE
C                           METHOD USED TO COMPUTE THE FIELD:
C                       1 = FLAT EARTH
C                       2 = GEOMETRIC OPTICS
C                       3 = NUMERICAL INTEGRATION
C                       4 = RESIDUE SERIES
C
      REAL*8 THETA1,THETA2,COST1,SINT1,COST2,SINT2,ANG,COSP1,COSP2,
     & SINT3,COST3,COSP12,SINP12,PI,RAD,CON1,CON2,COSINE,D31,D32,D1
      REAL*8 A,COSB,SINB,RHOO,WAVE,EL,ROOT,ANGO
      REAL LAMDA,L1,L2
      INTEGER VEBR
      COMPLEX  E,ETB,EBR,ETR,SQPBX
      DATA PI/3.14159265358979/, DS/1.0/
      DATA VEBR/2/
      RAD=PI/180.DO
      READ (5,1) FREQ,COND,EPS,ALFA,POWER,ROEO,H1,H2
   50 READ(5,2) PHI1,PHI2,OMEGAI,OMINC,OMLAST,ELI,L1,L2,NPOL
      READ(5,3) D1I,D1INC,D1F,D2I,D2INC,D2F
      WRITE(6,9)
    1 FORMAT (5F5.0,3F10.5)
    2 FORMAT (6F5.0,2F10.5,I2)
    3 FORMAT(6F10.2)
    9 FORMAT(1H1)
      LAMDA=300./FREQ
      A=6.36739D6*ALFA
      WAVE=2.*PI/LAMDA
      FREQ=1.E3*FREQ
      WRITE(6,10) POWER
      IF (NPOL .EQ. 1.OR.VEBR.EQ.1) WRITE(6,15) FREQ
      IF (NPOL .EQ. 2) WRITE(6,13) FREQ
      WRITE(6,14) EPS,COND,H1,H2,ALFA
      RHOO=ROEO
      WAVEL1=WAVE*L1/2.
      WAVEL2=WAVE*L2/2.
      D1=D1I
CLOOP ON TRANSMITTER-BLADE DISTANCE STARTS HERE
CENDS AT STATEMENT 160
80    CONTINUE
      THETA1=1.D3*D1/A
      COST1=DCOS(THETA1)
      SINT1=DSIN(THETA1)
      D2=D2I
```

```
LOOP ON RECEIVER-BLADE DISTANCE STARTS HERE
ENDS AT STATEMENT 150
0   CONTINUE
    THETA2=1.D3*D2/A
    COST2=DCOS(THETA2)
    SINT2=DSIN(THETA2)
    ANG=PHI1*RAD
    COSP1=DCOS(ANG)
    SINP1=DSIN(ANG)
    IF (ABS(SINP1).LE.1.E-4) SINP1=0.
    ANG=PHI2*RAD
    COSP2=DCOS(ANG)
    SINP2=DSIN(ANG)
    IF (ABS(SINP2) .LE. 1.E-4) SINP2=0.
    ANG=(PHI1-PHI2)*RAD
    COSP12=DCOS(ANG)
    SINP12=DSIN(ANG)
    PP=-SQRT(POWER)*SINP1
    COSB=(SINT1*COSP1-SINT2*COSP2)/(DSQRT(2.D0*(1.D0-SINT1*
   &SINT2*COSP12 -COST1*COST2)))
    SINB=DSQRT(1.D0-COSB*COSB)
    PPP=-SQRT(POWER)*SINB
    PBXCON=-SINP2/(150.*LAMDA)
    EL=ELI
    CON1= (A+RHO0)*(A+RHO0) +EL*EL
    CON2= 2.D0*(A+RHO0)*EL
    WRITE(6,17) D1,D2,EL,RHO0,PHI1,PHI2,L1,L2
C           COMPUTE E FOR TRANSMITTER DIRECT TO RECEIVER
    COSINE=COST1*COST2+SINT1*SINT2*COSP12
    D12=A*DARCOS(COSINE)
    D3=D12/1.D3
    CALL GRWAVE(FREQ,COND,EPS,ALFA,D3,H1,H2,NPOL,E,MTR)
    ETR=E*PPP*CDEXP(DCMPLX(0.D0,-WAVE*D12))
    AMPTR=CABS(ETR)
    PHASTR= ATAN2(AIMAG(ETR),REAL(ETR))
    DBSTR=20.*ALOG10(AMPTR)
    MM=0
    OMEGA=OMEGAI
LOOP ON OMEGA STARTS HERE - ENDS AT STATEMENT 140
00  MM=MM+1
    ANGO=OMEGA*RAD
    ROOT=DSQRT(CON1+CON2*DCOS(ANGO))
COMPUTE E FOR TRANSMITTER TO BLADE
    HP=-A+ROOT
    SINT3=DSIN(ANGO)
    IF (DABS(SINT3).LE.1.D-4) SINT3=0.D0
    SINT3=EL*DABS(SINT3)/ROOT
    COST3=DSQRT(1.D0-SINT3*SINT3)
    COSINE=COST3*COST1+SINT3*SINT1*COSP1
    D31=A*DARCOS(COSINE)
```

```
      D1C=D31/1.D3
      SINSIN=WAVEL1*(SINT1*COSP1+SINT2*COSP2)
      COSCOS=WAVEL2*(COST1+COST2)
      DS=L1*L2*(SIN(SINSIN)/SINSIN * SIN(COSCOS)/COSCOS)
      COSINE=COST3*COST2+SINT3*SINT2*COSP2
      D32=A*DARCOS(COSINE)
      D2C=D32/1.D3
      IF (PP.NE.0.) GO TO 104
      ETB=(0.,0.)
      AMPETB=0.
      DBSETB=1.E-75
      MTB=0
      GO TO 103
  104 CONTINUE
      CALL GRWAVE(FREQ,COND,EPS,ALFA,D1C,H1,HP,NPOL,E,MTB)
      ETB=E*PP*CDEXP(DCMPLX(0.D0,-WAVE*D31))
      AMPETB=CABS(ETB)
      DBSETB=20.*ALOG10(AMPETB)
      SQPBX=PBXCON*ETB*COST3*DS
  103 CONTINUE
C COMPUTE E FOR BLADE TO RECEIVER
      IF (VEBR .EQ. 1) GO TO 105
      IF (AMPETB.EQ.0. .OR. PBXCON.EQ.0.) GO TO 106
      CALL GRWAVE(FREQ,COND,EPS,ALFA,D2C,HP,H2,NPOL,E,MBR)
      EBR= E*SQPBX*CDEXP(DCMPLX(0.D0,-WAVE*D32))
      GO TO 120
C COMPUTE VERTICAL EBF
  105 CONTINUE
      IF (SINT3.NE.0. .OR.AMPETB.NE.0.) GO TO 110
  106 EBR=(0.,0.)
      AMPBR=0.
      PHASBR=0.
      MBR=0
      DBSBR=1.E-75
      GO TO 130
  110 CONTINUE
      CALL GRWAVE(FREQ,COND,EPS,ALFA,D2C,HP,H2,VEBR,E,MBR)
      EBR=-E*ETB*SINT3*DS*CDEXP(DCMPLX(0.D0,-WAVE*D32))/
     & (150.*LAMDA)
  120 CONTINUE
      AMPBR=CABS(EBR)
      PHASBR=ATAN2(AIMAG(EBR),REAL(EBR))
      DBSBR= 20.*ALOG10(AMPBR)
  130 CONTINUE
      WRITE(6,20) OMEGA,D1C,D2C,D3
      WRITE(6,21) AMPETB,DBSETB,MTB
      IF (VEBR.EQ.1) WRITE(6,23) AMPBR,PHASBR,DBSBR,MBR
      IF (VEBR.NE.1) WRITE(6,22) AMPBR,DBSBR,MBR
      WRITE(6,24) AMPTR,DBSTR,MTR
      DIFFDB=DBSBR-DBSTR
      ETRBR= 10.**(DIFFDB/20.)
      OMEGA=OMEGA+OMINC
```

```
140 IF (OMEGA .LE. OMLAST) GO TO 100
    D2=D2+D2INC
150 IF (D2.LE.D2F) GO TO 90
    D1=D1+D1INC
160 IF (D1.LE.D1F) GO TO 80
10  FORMAT( 10X,'GROUND WAVE FIELD STRENGTH FOR ',F8.3,' KW EFFECTIVE
   & RADIATED POWER')
17  FORMAT(1H0,1X,'D1 =',F8.2,3X,'D2 =',F8.2,3X,'L =',F8.2,
   & /2X,'RHO0 =',F8.2,5X,'PHI1 =',F5.1,3X,'PHI2 =',F5.1/
   & 2X,'L1 =',F5.1,3X,'L2 =',F5.1)
13  FORMAT (17X,'HORIZONTAL POLARIZATION,FREQUENCY =',F9.2,' KHZ ,')
15  FORMAT (17X,'VERTICAL POLARIZATION,FREQUENCY =',F9.2,' KHZ ,')
14  FORMAT(14X,'PERMITTIVITY =',F7.2,', EARTH CONDUCTIVITY =',F7.3,
   &' MHOS/M,'/,25X,'HEIGHT OF THE TRANSMITTER =',F7.1, 'M,'/22X,
   & 6X,'HEIGHT OF THE RECEIVER =',F7.1,'M,'/22X,
   & '(EFFECTIVE RADIUS)/(TRUE RADIUS) =',F7.3//)
20  FORMAT(1H0,3X,'OMEGA =',F8.1,/4X, 'D31 =',F10.4,
   & 2X,'D32 =',F10.4,2X,'D12 =',F10.4)
21  FORMAT(1H ,3X,'AMPTB =',E14.7,5X,'DBTB =',F8.2,5X,'MTB =',I2)
22  FORMAT(1H ,3X,'AMPBR =',E14.7,5X,'DBBR =',F8.2,5X,'MBR =',I2)
23  FORMAT(1H ,3X,'AMPBZR =',E14.7,5X,'PHASE BZR =',F8.3,5X,'DBBZR =',F8.2,
   & 5X, 'MBZR =',I2)
24  FORMAT(1H ,3X,'AMPTR =',E14.7,5X,'DBTR =',F8.2,5X,'MTR =',I2)
30  FORMAT(1H ,52X,'DIFF =',F8.2,5X,'ETRBR = ',E14.7)
    GO TO 50
    END


      SUBROUTINE GRWAVE(FREQ,COND,EPS,ALFA,DMIN,HT,HR,NPOL,E,MCASE)
C ******* CALCULATION OF THE GROUND WAVE OVER A FINITELY-CONDUCTING,
C         SPHERICAL EARTH.
C
C ******* INPUT
C     FREQ = FREQUENCY IN KILOCYCLES/SECOND.
C     COND = GROUND CONDUCTIVITY IN MHO/METER (SIEMENS/METER).
C     EPS  = DIELECTRIC CONSTANT RELATIVE TO FREE SPACE.
C     ALFA = EFFECTIVE EARTH RADIUS FACTOR.
C     DMIN = THE MINIMUM DISTANCE IN KILOMETERS BETWEEN THE TRANSMITTER
C            AND RECEIVER.
C     HT   = HEIGHT OF THE TRANSMITTER IN METERS.
C     HR   = HEIGHT OF THE RECEIVER IN METERS.
C     NPOL = 1, THE GROUND WAVE FOR VERTICAL POLARIZATION.
C     NPOL = 2, THE GROUND WAVE FOR HORIZONTAL POLARIZATION.
C ******* OUTPUT
C     E     = FIELD STRENGTH IN VOLTS/METER.
C     MCASE = THE METHOD USED IN CALCULATING E.
C       1 = FLAT EARTH
C       2 = GEOMETRIC OPTICS
C       3 = NUMERICAL INTEGRATION
C       4 = RESIDUE SERIES
```

```
      COMMON /WG/ AK1,V,Q,Y1,Y2,COTH,STH,X,HTKM,HRKM,FLF,A,MRGWD
      COMPLEX ETA,DELTA,Q,RO,U,CZW,E,ECOM,Z2,RR,RGW,PT(96),O(96),W1(96
     &W2(96),DW1(96),DW2(96),WX(96),WW1(96),WW2(96),TS,ZZ,TZ,WY1,WY2
      COMPLEX EEK,EAK,ECK,ZR,ZT,RS,ZC,CZ,ZO
      REAL*8 A1,A2,HT2,HR2,D,D1,D2,SD2,SD,S,SSQ,ASQ,SE,SSE,SA,DT
      DIMENSION G(48),W(48),M1(96),M2(96),MD1(96),MD2(96),MPT(96)
      MRGWD=2
      G(1)=-.9987710073
      G(2)=-.9935301723
      G(3)=-.9841245837
      G(4)=-.9705915925
      G(5)=-.9529877032
      G(6)=-.9313866907
      G(7)=-.9058791367
      G(8)=-.8765720203
      G(9)=-.8435882616
      G(10)=-.8070662040
      G(11)=-.7671590325
      G(12)=-.7240341309
      G(13)=-.6778723796
      G(14)=-.6288673968
      G(15)=-.5772247261
      G(16)=-.5231609747
      G(17)=-.4669029048
      G(18)=-.4086864820
      G(19)=-.3487558863
      G(20)=-.2873624874
      G(21)=-.2247637904
      G(22)=-.1612223561
      G(23)=-.0970046992
      G(24)=-.0323801709 6
      G(25)=.0323801709 6
      G(26)=.0970046992 1
      G(27)=.1612223561
      G(28)=.2247637904
      G(29)=.2873624874
      G(30)=.3487558863
      G(31)=.4086864820
      G(32)=.4669029048
      G(33)=.5231609747
      G(34)=.5772247260
      G(35)=.6288673968
      G(36)=.6778723796
      G(37)=.7240341309
      G(38)=.7671590325
      G(39)=.8070662040
      G(40)=.8435882616
      G(41)=.8765720203
      G(42)=.9058791367
      G(43)=.9313866907
      G(44)=.9529877032
```

G(45) =.9705915925
G(46) =.9841245837
G(47) =.9935301723
G(48) =.9987710073
W(1) =.0C3153346052
W(2) =.0C732755390 1
W(3) =.01147723458
W(4) =.01557931572
W(5) =.01961616046
W(6) =.02357076084
W(7) =.02742650971
W(8) =.03116722783
W(9) =.03477722256
W(10) =.03824135107
W(11) =.04154508294
W(12) =.04467456086
W(13) =.04761665849
W(14) =.05035903555
W(15) =.05289018949
W(16) =.05519950370
W(17) =.05727729210
W(18) =.05911483970
W(19) =.06070443917
W(20) =.06203942316
W(21) =.06311419229
W(22) =.06392423858
W(23) =.06446616444
W(24) =.06473769681
W(25) =.06473769681
W(26) =.06446616444
W(27) =.06392423858
W(28) =.06311419229
W(29) =.06203942316
W(30) =.06070443917
W(31) =.05911483970
W(32) =.05727729210
W(33) =.05519950370
W(34) =.05289018949
W(35) =.05035903555
W(36) =.04761665849
W(37) =.04467456086
W(38) =.04154508294
W(39) =.03824135107
W(40) =.03477722256
W(41) =.03116722783
W(42) =.02742650971
W(43) =.02357076084
W(44) =.01961616046
W(45) =.01557931572
W(46) =.01147723458
W(47) =.00732755390
W(48) =.003153346052

```
      POWER=1.
      A=6.36739E3*ALFA
      WAVE=FREQ*.0209584
      AK1=A*WAVE
      V= (AK1/2.)**0.33333333
      V2=V*V
      Z=.5/V2
      ZC=2.5*Z
      FLF=300.*SQRT(POWER)
      ETA=CMPLX(EPS,-18.E6*COND/FREQ)
      DELTA=CSQRT(ETA-1.)
      IF (NPOL .EQ. 2) GO TO 35
      DELTA=DELTA/ETA
   35 Q=CMPLX(0.,-V)*DELTA
      MM=0
      MGW =1
      TEST=0.
      IF (HR.GE.HT) GO TO 50
      MM=1
      TEMP=HR
      HR=HT
      HT=TEMP
   50 CONTINUE
      HTKM=HT/1000.
      HRKM=HR/1000.
      Y1=WAVE*HTKM/V
      Y2=WAVE*HRKM/V
      IF(HT+HR)70,70,65
   65 B=A+HTKM
      R=A+HRKM
      TEST =  A*(ARCOS( A/R) + ARCOS( A/B))
      CONTINUE
      FTEST=AMAX1(5.,437./(FREQ**.38))
      IF(WAVE*(HTKM+HRKM)*CABS(DELTA) .GT. .1 ) FTEST =0.
      THETA=DMIN/A
      X=V*THETA
      STH= SIN(THETA)
      COTH =COS(THETA)/STH
      E=(0.,0.)
      IF (DMIN .LE. FTEST) GO TO 100
      IF(DMIN .GT. TEST ) GO TO 400
      GO TO 200
  100 CONTINUE
C     COMPUTE GROUND WAVE ASSUMING A FLAT EARTH.
C     USED FOR SHORT DISTANCES.
      R=SQRT(DMIN*DMIN*1.E6+(HT-HR)**2)
      RO=(.886227,.886227)*SQRT(WAVE*R*1.E-3)
      U=R*DELTA*(1.+(HT+HR)/(DELTA*R))
```

```
      CZW=U*(C.5,C.5)*SQRT(WAVE/(R*1.E-3))*.001
      E=(1.-RO*DELTA*ECOM(CZW))*FLF/(1000.*DMIN)
      MCASE=1
      GO TO 600
  200 CONTINUE
C*** COMPUTE GROUND WAVE WITH GEOMETRIC OPTICS.
C     USED FOR HIGH ANTENNAS WELL WITHIN THE LINE-OF-SIGHT.
      HT2=HTKM*HTKM
      HR2=HRKM*HRKM
      A1=2.*A*HTKM+HT2
      A2=2.*A*HRKM+HR2
      D=DSQRT((2.*A*A+2.*A*(HTKM+HRKM))*OMCOS(THETA)+HT2+HR2
     & -2.*HTKM*HRKM*COS(THETA))
      IF (HT .NE. 0.) GO TO 210
      D1=0.DO
      D2=D
      CSQD=(((A+HRKM)*SIN(THETA))/D)**2.
      SD2=1.DO-CSQD
      SD=DSQRT(SD2)
      GO TO 250
  210 CONTINUE
      KOUNT=1
      S=1.DO/SQRT( 1.+(DMIN/(HTKM+HRKM))**2)
      SSQ=S*S
      ASQ=A*A
      D1=DSQRT(ASQ*SSQ+A1)-A*S
      D2=DSQRT( ASQ*SSQ+A2)-A*S
      SE=(D1+D2)**2-4.DO*D1*D2*SSQ-D*D
      SD=S+DSIGN( .01DO,SE)
      SD2=SD*SD
C*** START INTERATION TO FIND RAY PATH DISTANCES.
  220 D1=DSQRT( ASQ*SD2+A1)-A*SD
      D2=DSQRT( ASQ*SD2+A2)-A*SD
      SSE=(D1+D2)**2-4.DO*D1*D2*SD2-D*D
      KOUNT=KOUNT+1
      IF (KOUNT .GT. 20) GO TO 250
      SA=SD+(S-SD)*SSE/(SSE-SE)
      S=SD
      SSQ=S*S
      SE=SSE
      SD=SA
      SD2=SD*SD
      IF (DABS( SSE) .GE. .62831853/WAVE) GO TO 220
      CSQD=1.DO-SD2
  250 CONTINUE
C*** NEAR THE HORIZON(SMALL SD), USE NUMERICAL INTEGRATION.
      IF (SD .LT. 2./V) GO TO 300
      Z2=CSQRT(ETA-CSQD)
      IF (NPOL .EQ. 1) Z2=Z2/ETA
      RR=(SD-Z2)/(SD+Z2)
      DT=4.DO*D1*D2*SD2/(D1+D2+D)
      E=FLF*CDEXP( DCMPLX(0.DO,-WAVE*(D-DMIN)))/(2000.*D)*
     &(1.+RR*CDEXP(DCMPLX(0.DO,-WAVE*DT)))
```

```
      MCASE=2
      GO TO 600
  300 CONTINUE
C***  COMPUTE GROUND WAVE WITH GAUSSIAN NUMERICAL INTEGRATION.
      N=0
      CALL TW (N,Q,TZ,EEK,MZ,EAK,MA,ECK,MZ,ECK,MZ)
      BOT = .5*AIMAG(TZ)
      YONE=BOT
      XONE=REAL(TZ)
      TOP = AMIN1( -AMIN1(6./X,100.),-SQRT(Y1)-SQRT(Y2))
      FTX=.5*(TOP-BOT)
      KK=0
      SGN=1.
      DO 310 I=1,2
      SGN=-SGN
      DO 310 K=1,48
      KK=KK+1
      TX=((TOP-BOT)*G(K)+TOP+BOT)*.5
      O(KK)=CMPLX(XONE+SGN    *(TX-YONE),TX)
  310 CONTINUE
      DO 365 K=1,96
      IF(ABS(REAL(O(K))-Y2).GT. 5. .AND.Y1.GT.0. .AND.
     &CABS(O(K)).GT.5.) GO TO 340
      CALL CWAIRY(1,O(K),W1(K),M1(K),W2(K),M2(K))
      CALL CWAIRY(2,O(K),DW1(K),MD1(K),DW2(K),MD2(K))
      P=2.7182818**(MD1(K)-M1(K))
      WX(K)=P*DW1(K)/W1(K)-Q
  330 CALL CWAIRY(1,O(K)-Y2,WY1,MY1,EEK,M)
      MPT(K) = MY1-M1(K)
      PT(K)=WY1/W1(K) /WX(K)
      IF(Y1.LE.0.) GO TO 365
      WW1(K)=2.7182818**(MD1(K)-M1(K))*DW1(K) -W1(K)*Q
      WW2(K)=2.7182818**(MD2(K)-M2(K))*DW2(K) -W2(K)*Q
      CALL CWAIRY(1,O(K)-Y1,WY1,MY1,WY2,MY2)
      F=2.7182818**(MY1+M2(K))
      FF=2.7182818**(MY2+M1(K))
      PT(K)=(0.,-.5)*(FF*WY2*WW1(K)-F*WY1*WW2(K)) *PT(K)
      GO TO 365
  340 MPT(K) =0
      IF(K.GT.48) GO TO 350
      TS=CSQRT(O(K))
      ZO=.666666667* O(K)*TS
      ZR=CSQRT(O(K)-Y2)
      ZT=CSQRT(O(K)-Y1)
      ZZ=CSQRT(ZR*ZT)
      ZR=.666666667*ZR*(O(K)-Y2)
      ZT=.666666667*ZT*(O(K)-Y1)
      PT(K)=.5*CEXP(ZR-ZT) * (1.+CEXP(2.*(ZT-ZO))*
     & (TS+Q)/(TS-Q))/ZZ
      GO TO 365
```

```
350 TS=CSQRT(-Q(K))
    ZO=-.666666667*Q(K)*TS
    ZR=CSQRT(Y2-Q(K))
    ZT=CSQRT(Y1-Q(K))
    ZZ=CSQRT(ZR*ZT)
    ZR=.666666667*ZR*(Y2-Q(K))
    ZT=.666666667*ZT*(Y1-Q(K))
    PT(K)=.5*CEXP((0.,-1.)*(ZR-ZT))   *(1.+CEXP((0.,-2.)*
   & (ZT-ZO))  *((0.,1.)*TS+Q)/((0.,1.)*TS-Q))/((0.,1.)*ZZ)
365 CONTINUE
380 KK=0
    SGN=1.
    DO 385 I=1,2
    SGN=-SGN
C*** INTEGRATE FOR THIS DISTANCE
    DO 385 K=1,48
    KK=KK+1
    CALL ZEXP(X*AIMAG(Q(KK)),-X*REAL(Q(KK)),TX,TY,MT)
    F=2.718282**(MT+MPT(KK))
385 E=E+W(K)*FTX*F*CMPLX(TX,TY)*CMPLX(1.,SGN)*PT(KK)
    E=FLF*SQRT(V/(6.2831853*STH))/(2000.*A)*E*(-1.,-1.)
    MCASE =3
    GO TO 600
400 CONTINUE
C*** COMPUTE GROUND WAVE WITH THE RESIDUE SERIES.
    E=RGW(MGW)
C*** RGW IS SUBROUTINE TO COMPUTE GROUND WAVE WITH FOK-WAIT SERIES.
    MCASE=4
600 CONTINUE
    IF (MM.EQ.0) RETURN
    HT=HR
    HR=TEMP
    RETURN
    END

    COMPLEX FUNCTION ECOM(Z)

C*** ECOM(Z) = EXP(Z**2)*ERFC(Z).
C     ERFC IS THE COMPLEMENTARY ERROR FUNCTION.
C
    COMPLEX Z, ZP
    IF (REAL(Z)) 4,3,3
  3 CALL UP (Z,ECOM)
    RETURN
  4 CALL UP (-Z,ZP)
    ECOM=(2.0,0.0)*CEXP(Z**2)-ZP
    RETURN
    END
```

```
      SUBROUTINE DOWN (A,E)
C
C*** COMPUTES EXP(Z**2)*ERF(Z) USING POWER SERIES.
C
      COMPLEX A,E,U
      IF(CABS(A) - 3.5) 2,2,1
    1 CALL UP(A,U)
      E= CEXP(A**2) - U
      RETURN
    2 Z=REAL (A)
      ZI=AIMAG (A)
      CR=1.128379167*Z
      CI=1.128379167*ZI
      BR=CR
      BI=CI
      Z2R = Z*Z-ZI*ZI
      Z2I = 2.*Z*ZI
      EM=1.5
    6 PR= Z2R*CR-Z2I*CI
      PI = Z2R*CI + Z2I*CR
      CR=PR/EM
      CI=PI/EM
      BR=BR+CR
      BI=BI+CI
      IF((CR*CR+CI*CI)/(BR*BR+BI*BI)-1.E-11)9,9,8
    8 EM=EM+1.0
      GO TO 6
    9 ER=BR
      EI=BI
      E=CMPLX (ER,EI)
      RETURN
      END

      SUBROUTINE UP (A,E)
C
C*** COMPUTES EXP(Z**2)*ERFC(Z) USING ASYMPTOTIC SERIES.
C
      COMPLEX A,E,Z,EP,Z2,GN
      Z=A
      IF (CABS(Z) - 3.5) 1,1,2
    1 CALL DOWN (Z,EP)
      E=CEXP(Z**2) - EP
      RETURN
    2 Z2=-Z*Z
      ZB2=CABS(Z2)
      GN=(0.56418958,0.0)/Z
      EP=GN
      EN=0.5
    5 GN=EN*GN/Z2
      EP=EP+GN
      IF(CABS(GN/EP)-1.0E-005) 7,7,6
    6 EN=EN+1.0
      IF (EN-ZB2) 5,7,7
    7 E=EP
      RETURN
      END
```

```
      FUNCTION OMCOS(X)

***   OMCOS(X) = 1 - COS(X)
      IS ACCURATE FOR ALL X INCLUDING X NEAR 0.

      IF(ABS( X).GT..15) GO TO 40
      IF(X.EQ.0.) GO TO 50
         IF X IS SMALL, SUM TAYLORS SERIES FOR 1-COS(X)
      S = X*X
      T=.5*S
      OMCOS = T
      R = 4.
   10 T=-T*S/(R*(R-1.))
      OMCOS=OMCOS + T
      IF(ABS(T/OMCOS) .LE. .5E-9) GO TO 51
      R=R+2.
      GO TO 10
   40 OMCOS = 1.-COS(X)
      RETURN
   50 OMCOS = 0.
   51 RETURN
      END
      SUBROUTINE ZEXP(A,B,X,Y,MAGTUD)
C
C*** SCALED EVALUATION OF THE EXPONENTIAL FUNCTION
C     IN THE COMPLEX PLANE.
C     INPUT:
C       (A+IB) = THE COMPLEX EXPONENT.
C     OUTPUT:
C       EXP(A+IB) = (X+IY)*(E**MAGTUD)
C
      MAGTUD=A
      SCALE=MAGTUD
      E=EXP( A-SCALE)
      X=E*COS( B)
      Y=E*SIN( B)
      RETURN
      END



      COMPLEX FUNCTION AIRY(ZZ)
C
C*** COMPUTES HUFFORDS NORMALIZATION OF THE AIR FUNCTIONS.
C
      COMMON/MEXP/M
      COMPLEX Z,ZZ,Z1,A,AP,U,ZT,ZA,ZB,ZE,ZR,B0,B1,B2,B3
      COMPLEX AI,AIP,WI,WI1,WIP,WI1P,WI2,WI2P
      DIMENSION X(2),X1(2),XT(2)
      LOGICAL LG(3)
      EQUIVALENCE (X,Z),(X1,Z1),(XT,ZT)
      DATA Z1/(0.,0.)/, A/(0.35502805389,0.)/
      DATA AP/(-0.25881940379,0.)/
      DIMENSION AV( 70)
      COMPLEX AV
```

```
      DATA AV/
     &   (-3.2914517363E-001, 0.0000000000E+000),
     &   (-2.6780035625E+000, 1.4774589547E+000),
     &   ( 3.5076100903E-001, 0.0000000000E+000),
     &   ( 2.4122262158E+000, 6.9865124448E-001),
     &   ( 3.3635531189E+001,-3.4600959696E+000),
     &   ( 3.4449739613E+002,-3.3690890250E+002),
     &   (-7.0265532950E-002, 0.0000000000E+000),
     &   (-5.4818219290E-001,-1.9207365909E+000),
     &   (-1.3383395342E+001,-1.6022590802E+001),
     &   (-2.2967795901E+002,-3.2072452637E+001),
     &   (-1.8040780476E+003, 2.1917675036E+003),
     &   (-3.7881429368E-001, 0.0000000000E+000),
     &   (-1.3491836060E+000, 8.4969077213E-001),
     &   (-6.0453339320E+000, 1.0623175540E+001),
     &   ( 3.1169621695E+001, 9.8813517650E+001),
     &   ( 9.8925349347E+002, 1.3905286008E+002),
     &   ( 2.2740742820E-001, 0.0000000000E+000),
     &   ( 7.1857403459E-001, 9.7809094170E-001)/
      DATA AV(19),AV(20),AV(21),AV(22),AV(23),AV(24)
     &,AV(25),AV(26),AV(27),AV(28),AV(29),AV(30),AV(31)/
     &   ( 6.0621088063E+000, 2.7203014866E+000),
     &   ( 3.6307084828E+001,-2.0961355813E+001),
     &   (-6.7139789190E+001,-3.0904638708E+002),
     &   (-2.8001653691E+003, 4.6649365984E+002),
     &   ( 5.3556088329E-001, 0.0000000000E+000),
     &   ( 9.2407365385E-001,-1.9106560052E-001),
     &   ( 1.8716185961E+000,-2.5743310394E+000),
     &   (-7.2188436328E+000,-1.2924200190E+001),
     &   (-8.1787377840E+001, 3.2087013839E+001),
     &   ( 2.9933948552E+002, 5.6922179258E+002),
     &   ( 3.5502805389E-001, 0.0000000000E+000),
     &   ( 3.1203438104E-001,-3.8845385098E-001),
     &   (-5.2839999360E-001,-1.0976411220E+000)/
      DATA AV(32),AV(33),AV(34),AV(35),AV(36),AV(37)/
     &   (-4.2009351585E+000, 1.1940151191E+000),
     &   ( 7.1858832892E+000, 1.9600912513E+001),
     &   ( 1.0129121011E+002,-7.5951233292E+001),
     &   ( 1.3529241631E-001, 0.0000000000E+000),
     &   ( 3.2618478398E-002,-1.7084872785E-001),
     &   (-3.4215381085E-001,-8.9067646330E-002)/
      DATA AV(38),AV(39),AV(40),AV(41),AV(42),AV(43),
     &AV(44),AV(45),AV(46),AV(47),AV(48),AV(49),
     &AV(50),AV(51),AV(52),AV(53)/
     &   (-1.4509641493E-001, 1.0328015748E+000),
     &   ( 4.1001968523E+000,-6.8936911760E-001),
     &   (-1.3030124036E+001,-1.6910541453E+001),
     &   ( 3.4924130423E-002, 0.0000000000E+000),
     &   (-8.4464726625E-003,-4.2045154421E-002),
     &   (-6.9313268963E-002, 3.5364798705E-002),
     &   ( 1.5227622646E-001, 1.2848454470E-001),
     &   ( 1.0681373184E-001,-6.7766153503E-001),
```

```
     &   (-2.6193432727E+000, 1.5699859905E+000),
     &   ( 6.5911393574E-003, 0.0000000000E+000),
     &   (-3.9443985580E-003,-6.8060106117E-003),
     &   (-5.9820131079E-003, 1.1799010149E-002),
     &   ( 2.9922498406E-002,-5.9772930737E-003),
     &   (-7.7464130231E-002,-5.2292402759E-002),
     &   ( 1.1276585896E-001, 3.5112442431E-001),
     &   ( 9.5156385121E-004, 0.0000000000E+000)/
      DATA AV(54),AV(55),AV(56),AV(57),AV(58)/
     &   (-8.0842995655E-004,-7.6590132690E-004),
     &   ( 1.6147816065E-004, 1.7661755136E-003),
     &   ( 2.0138718363E-003,-3.1976716632E-003),
     &   (-9.5086784440E-003, 4.5377832492E-003),
     &   ( 3.7560191819E-002, 5.7361916864E-004)/
      DATA AV(59),AV(60),AV(61),AV(62),AV(63),AV(64),
     &AV(65),AV(66),AV(67),AV(68),AV(69),AV(70)/
     &   ( 1.0834442814E-004, 0.0000000000E+000),
     &   (-1.0968606480E-004,-5.9902329668E-005),
     &   ( 1.0778191327E-004, 1.5771596227E-004),
     &   (-6.8980937889E-005,-3.7626457370E-004),
     &   (-1.6166126174E-004, 9.7457773280E-004),
     &   ( 9.9476943603E-006, 0.0000000000E+000),
     &   (-1.0956823939E-005,-2.9508799638E-006),
     &   ( 1.4709074502E-005, 8.1042089702E-006),
     &   (-2.4446015180E-005,-2.0638143108E-005),
     &   ( 7.4921288640E-007, 0.0000000000E+000),
     &   (-8.4619068946E-007,-3.6807338399E-008),
     &   ( 1.2183963384E-006, 8.3589199402E-008)/
      DIMENSION APV( 70)
      COMPLEX APV
      DATA APV/
     &   ( 3.4593548728E-001, 0.0000000000E+000),
     &   ( 4.1708876594E+000, 6.2414437707E+000),
     &   ( 3.2719281855E-001, 0.0000000000E+000),
     &   ( 1.0828742735E+000,-5.4928302529E+000),
     &   (-2.3363517933E+001,-7.4901848140E+001),
     &   (-1.0264877579E+003,-5.6707940802E+002),
     &   (-7.9062857537E-001, 0.0000000000E+000),
     &   (-3.8085833358E+000, 1.5129605192E+000),
     &   (-2.6086379081E+001, 3.5540709915E+001),
     &   ( 1.0761838222E+002, 5.1239944904E+002),
     &   ( 6.6597797197E+003, 1.8096186253E+003),
     &   ( 3.1458376921E-001, 0.0000000000E+000),
     &   ( 1.8715425470E+000, 2.0544836557E+000),
     &   ( 2.2591736932E+001, 4.8562995474E+000),
     &   ( 1.6162997879E+002,-1.4335597185E+002),
     &   (-8.0047161665E+002,-2.1527454270E+003),
     &   ( 6.1825902074E-001, 0.0000000000E+000),
     &   ( 1.3019603890E+000,-1.2290774954E+000)/
      DATA APV(19),APV(20),APV(21),APV(22),APV(23),
```

```
&APV(24),APV(25),APV(26),APV(27),APV(28),APV(29)/
&   ( 1.5036118745E-001,-1.1008092874E+001),
&   (-7.0116800393E+001,-4.0480822759E+001),
&   (-4.8317166902E+002, 4.9692755718E+002),
&   ( 4.8970655652E+003, 4.8627290801E+003),
&   (-1.0160567116E-002, 0.0000000000E+000),
&   (-5.4826636454E-001,-7.1365288463E-001),
&   (-4.6749134088E+000,-1.1924245293E-001),
&   (-1.0536397828E+001, 2.4943711387E+001),
&   ( 1.6333770696E+002, 9.0394910688E+001),
&   ( 5.6449455285E+002,-1.4248324426E+003),
&   (-2.5881940380E-001, 0.0000000000E+000)/
 DATA APV(30),APV(31),APV(32),APV(33),APV(34),APV(35),
&APV(36),APV(37),APV(38),APV(39),APV(40),APV(41)/
&   (-4.8620754109E-001, 1.5689924913E-001),
&   (-4.7348131897E-001, 1.7093438130E+000),
&   ( 7.0373840765E+000, 3.6281824918E+000),
&   ( 1.7739586372E+001,-4.0360422402E+001),
&   (-2.9791511956E+002,-3.8408892977E+001),
&   (-1.5914744130E-001, 0.0000000000E+000),
&   (-1.1340423572E-001, 1.9730504925E-001),
&   ( 4.0126209154E-001, 3.9222995820E-001),
&   ( 1.3348652430E+000,-1.4377272421E+000),
&   (-7.9022494720E+000,-4.2063644605E+000),
&   (-1.3892752107E+000, 5.1229416787E+001),
&   (-5.3090384434E-002, 0.0000000000E+000)/
 DATA APV(42),APV(43),APV(44),APV(45),APV(46),APV(47),
&APV(48),APV(49),APV(50),APV(51),APV(52),APV(53)/
&   (-1.6832965528E-003, 6.8366967859E-002),
&   ( 1.3789401334E-001,-1.1613804016E-002),
&   (-1.4713730621E-001,-3.7151985747E-001),
&   (-1.0070196495E+000, 1.1591348425E+000),
&   ( 7.5045049133E+000, 4.6913115383E-001),
&   (-1.1912976706E-002, 0.0000000000E+000),
&   ( 5.1468574932E-003, 1.3660891236E-002),
&   ( 1.8309710537E-002,-1.8808588497E-002),
&   (-6.4461593156E-002,-1.3611794718E-002),
&   ( 1.0516239905E-001, 1.9313053560E-001),
&   ( 2.0520046212E-001,-9.1772617372E-001),
&   (-1.9586409502E-003, 0.0000000000E+000)/
 DATA APV(54),APV(55),APV(56),APV(57),APV(58),APV(59)/
&   ( 1.4695649526E-003, 1.8086384633E-003),
&   ( 5.9709947951E-004,-3.8332699216E-003),
&   (-6.8910893004E-003, 5.4467425272E-003),
&   ( 2.6167927738E-002,-8.4092000294E-004),
&   (-8.8284474192E-002,-4.6475312179E-002),
&   (-2.4741389087E-004, 0.0000000000E+000)/
 DATA APV(60),APV(61),APV(62),APV(63),APV(64),
&APV(65),APV(66),APV(67),APV(68),APV(69),APV(70)/
&   ( 2.3707837404E-004, 1.6461109527E-004),
&   (-1.7465569860E-004,-4.2026783985E-004),
```

```
&   (-1.0394516180E-004, 9.4761844375E-004),
&   ( 1.3004110522E-003,-2.2446656813E-003),
&   (-2.4765200397E-005, 0.0000000000E+000),
&   ( 2.6714870982E-005, 9.8691565027E-006),
&   (-3.3539774178E-005,-2.7113284942E-005),
&   ( 4.9197843140E-005, 6.9349092091E-005),
&   (-2.0081508947E-006, 0.0000000000E+000),
&   ( 2.2671244519E-006, 2.7848508382E-007),
&   (-3.2692132725E-006,-7.3943488682E-007)/
 DIMENSION ASLT(17)
 DATA  ASLT/ 1.1407E+002, 1.1549E+002,
&    1.1779E+002, 1.2124E+002, 1.2619E+002, 1.3319E+002,
&    1.4307E+002, 1.5716E+002, 1.7774E+002, 2.0884E+002,
&    2.5832E+002, 3.4294E+002, 5.0339E+002, 8.5678E+002,
&    1.8336E+003, 5.7270E+003, 3.5401E+004/
 DIMENSION ASV(21)
 DATA  ASV/1.8335766942E+010,
&    1.9293755496E+009, 2.1428803701E+008, 2.5198919876E+007,
&    3.1482574185E+006, 4.1952487519E+005, 5.9892513580E+004,
&    9.2072066015E+003, 1.5331694323E+003, 2.7846508084E+002,
&    5.5622785377E+001, 1.2341573335E+001, 3.0794530307E+000,
&    8.7766696967E-001, 2.9159139927E-001, 1.1609906404E-001,
&    5.7649190421E-002, 3.7993059132E-002, 3.7133487657E-002,
&    6.9444444448E-002, 1.0000000000E+000/
 DIMENSION APSV(21)
 DATA  APSV/-1.8643931093E+010,
&   -1.9635237894E+009,-2.1829342088E+008,-2.5697908389E+007,
&   -3.2145365220E+006,-4.2895240048E+005,-6.1335706678E+004,
&   -9.4463548250E+003,-1.5763573037E+003,-2.8703323717E+002,
&   -5.7508303524E+001,-1.2807293083E+001,-3.2104935853E+000,
&   -9.2047999257E-001,-3.0825376496E-001,-1.2410589605E-001,
&   -6.2662163500E-002,-4.2462830794E-002,-4.3885030868E-002,
&   -9.7222222227E-002, 1.0000000000E+000/
 DIMENSION NQTT(15),NQT(8)
 EQUIVALENCE (NQTT(8),NQT(1))
 DATA NQTT/1,3,7,12,17,23,29,35,41,47,53,59,64,68,71/
 ANM(Z)=ABS( REAL(Z))+ABS( AIMAG(Z))



 ENTRY AI(ZZ)
 LA=0
 GO TO 1



 ENTRY AIP(ZZ)
 LA=0
 GO TO 2



 ENTRY WI(ZZ)
```

```
      ENTRY WI1(ZZ)
      LA=1
      GO TO 1


      ENTRY WIP(ZZ)


      ENTRY WI1P(ZZ)
      LA=1
      GO TO 2



      ENTRY WI2(ZZ)
      LA=-1
      GO TO 1



      ENTRY WI2P(ZZ)
      LA=-1
      GO TO 2
    1 LB=0
      GO TO 3
    2 LB=1
      GO TO 3
    3 Z=ZZ
      IF(LA) 5,7,4
    4 U=(-0.5,0.866025403 78)
      GO TO 6
    5 U=(-0.5,-0.866025403 78)
    6 Z=U*Z
    7 LC=0
      IF (X(2)) 8,9,10
    8 LC=1
      X(2)=-X(2)
      GO TO 10
    9 X(2)=0.
   10 CONTINUE
C*** COMPARE WITH PREVIOUS
      IF(X(1) .NE. X1(1) .OR. X(2) .NE. X1(2)) GO TO 20
      IF (LG(LB+1)) GO TO 400
      IF(LB) 220,210,220
  400 CONTINUE
C*** EXIT
      IF(LB) 402,401,402
  401 ZT=A
      IF (LC.EQ.1) XT(2)=-XT(2)
      IF(LA)404,411,403
```

```
  402 ZT=AP
      IF (LC.EQ.1) XT(2)=-XT(2)
      IF(LA)403,411,404
  403 U=(1.,-1.7320508076)
      GO TO 410
  404 U=(1.,1.7320508076)
      GO TO 410
  410 ZT=U*ZT
  411 AIRY=ZT
      AI=AIRY
      AIP=AIRY
      WI=AIRY
      WI1=AIRY
      WIP=AIRY
      WI1P=AIRY
      WI2=AIRY
      WI2P=AIRY
      RETURN
   20 CONTINUE
C*** AFFINE COORDINATES
      M=0
      Z1=Z
      LG(1)=.FALSE.
      LG(2)=.FALSE.
      LG(3)=.FALSE.
      IF(X(1).LE.-7..OR.X(1).GT.7. .OR. X(2).GT.6.928203232)
     & GO TO 200
      IP=7.-X(1)
      IP=7-IP
      P=IP
      IQ=0.86602540378*X(2)+0.5*(P-X(1))
      Q=IQ
      N=NQT(IP)+IQ
      IF(N.GE.NQT(IP+1)) GO TO 200
  100 CONTINUE
C *** SERIES
      XT(1)=P
      XT(2)=1.1547005384*Q
      U=Z-ZT
      B1=AV(N)
      B3=B1*ZT*U
      AP=APV(N)
      B2=AP*U
      A=B2+B1
      AP=AP+B3
      AN=1.
      DO 110 I=2,3
      AN=AN+1.
      B3=B3*U/AN
      A=B3+A
      B0=B1
```

```
      B1=B2
      B2=B3
      B3=(ZT*B1+U*B0)*U/AN
      AP=B3+AP
      IF(ANM(B2).GT.0.5E-10*ANM(A) .AND.
     & ANM(B3).GT.0.5E-10*ANM(AP)) I=0
  110 CONTINUE
      LG(1)=.TRUE.
      LG(2)=.TRUE.
      GO TO 400
  200 CONTINUE
C*** ASYMPTOTICS
      ZA=CSQRT(Z)
      ZB=0.28209479177/CSQRT(ZA)
      ZT=-0.66666666667*Z*ZA
      T=XT(1)**2+XT(2)**2
      CALL ZEXP(XT(1),XT(2),SX,SY,M)
      ZE=CMPLX(SX,SY)
      ZM=EXP(-FLOAT(M+M))
      ZR=1./ZT
      IF(XT(2) .GT. 0. .AND. XT(1) .LT. 11.8595) LG(3)=.TRUE.
      DO 201 NT=2,18
      IF(T .LT. ASLT(NT-1)) GO TO 202
  201 CONTINUE
      NT=19
  202 IF(LB) 220,210,220
  210 CONTINUE
C*** A
      ZT=ASV(NT-1)
      DO 211 I=NT,21
  211 ZT=ASV(I)+ZT*ZR
      A=ZT*ZE
      IF (.NOT. LG(3)) GO TO 216
  212 ZT=ASV(NT-1)
      DO 213 I=NT,21
  213 ZT=ASV(I)-ZT*ZR
      A=A+(0.,1.)*ZT/(ZE)*ZM
  216 A=ZB*A
      LG(1)=.TRUE.
      GO TO 401
  220 CONTINUE
C*** AP
      ZT=APSV(NT-1)
      DO 221 I=NT,21
  221 ZT=APSV(I)+ZT*ZR
      AP=-ZT*ZE
      IF (.NOT. LG(3)) GO TO 226
  222 ZT=APSV(NT-1)
      DO 223 I=NT,21
  223 ZT=APSV(I)-ZT*ZR
      AP=AP+(0.,1.)*ZT/(ZE)*ZM
  226 AP=ZA*ZB*AP
      LG(2)=.TRUE.
      GO TO 402
      END
```

```
      COMPLEX FUNCTION RGW (MM)
C
C*** CALCULATION OF THE GROUND WAVE
C     INPUT
C       DMIN = DISTANCE BETWEEN TRANSMITTER AND RECEIVER IN KM
C       H1   = HEIGHT OF THE TRANSMITTER IN KM
C       H2   = HEIGHT OF THE RECEIVER IN KM
C     OUTPUT
C       RGW = THE GROUND WAVE CALCULATED WITH THE RESIDUE SERIES
C
      COMMON /WG/ AK1,V,Q,Y1,Y2,COTH,STH,X,H1,H2,FLF,A,MRGWD
      COMPLEX T(200),W(200),G,R12,S,D,Q,W1,DW1,WY1,WY2,GW,S2
      COMPLEX TJY1,TJY2,DWY1
      GW=0.
      GO TO(60,125),MM
C*** MM=1 MEANS THIS IS A NEW CASE. FIND SOLUTIONS TO MODE EQUATION.
C*** MM=2 MEANS ONLY THE DISTANCE HAS CHANGED.
 60   J2=1
      MM=2
C*** LOOP ON TERMS OF RESIDUE SERIES.
 65   DO 100 J=J2,200
C*** TW FINDS THE SOLUTION OF THE MODE EQUATION
C     AND GETS AIRY FUNCTIONS.
      CALL TW( J-1 , Q, T(J), W1, MW1, DW1, MD1, S,M,S,M)
      TJY1=T(J)-Y1
      TJY2=T(J)-Y2
      IF(H1.GT.0)GO TO 80
      IF(H2.GT.0)GO TO 75
      W(J)=1.
      GO TO 85
C*** COMPUTE HEIGHT GAIN FACTORS
 75   CALL CWAIRY(1,T(J)-Y2,WY2,MY2,S,M)
      W(J)=2.7182818**(MY2-MW1)*WY2/W1
      GO TO 85
      CONTINUE
      IF (MRGWD .NE. 1) GO TO 81
C*** COMPUTE DERIVATIVE OF W1(T-Y1)
      CALL CWAIRY(2,TJY1,DWY1,MY1,S,M)
      WY1=-DWY1
      GO TO 82
 81   CALL CWAIRY(1,T(J)-Y1,WY1,MY1,S,M)
      CONTINUE
      W(J)=2.7182818**(MY1-MW1)*WY1/W1
      IF(H2 .LE. 0.) GO TO 85
      CALL CWAIRY(1,T(J)-Y2,WY2,MY2,S,M)
      S=2.7182818**(MY2-MW1)*WY2/W1
      W(J)=W(J)*S
 85   W(J)  =  W(J)/(T(J)  -Q*Q)
C*** W(J) IS THE COEFFICIENT OF THE DISTANCE FACTOR
```

```
C      FOR THE J-TH TERM.
       G=W(J)*CEXP((0.,-1.)*X*T(J))
       GW=GW+G
       IF(J.EQ.1)GO TO 100
       IF( CABS(G/GW)  .GT. 0.0005) GO TO 100
       J1=J
       GO TO 110
  100  CONTINUE
       J2=200
       GO TO 165
  110  IF(J1.LE.J2)GO TO 165
       J2=J1
       GO TO 165
C**** SUM THE RESIDUE SERIES FOR THIS DISTANCE.
  125  DO 140 J=1,J2
       G=W(J)*CEXP((0.,-1.)*X*T(J))
       GW=GW+G
       IF(J.EQ.1)GO TO 140
       IF( CABS(G/GW)  .LT. 0.0005) GO TO 165
  140  CONTINUE
       IF(J2.GE.200)GO TO 165
       J2=J2+1
       GO TO 65
    5  RGW=GW*(FLF*3.1415927 *SQRT(2.*V/(3.1415927*STH))
      & /(2000.*A))*(1.,-1.)
       RETURN
       END



C     SUBROUTINE TW( I, Q, T, W1,MW1, DW1,MD1, W2,MW2, DW2,MD2)
C
C T IS THE I-TH ROOT OF W-SUB-ONE-PRIME - Q*W-SUB-1 =0.
C (W IS THE AIRY FUNCTION.)
C THE ROOTS ARE COUNTED IN ORDER OF INCREASING MAGNITUDE.
C W-SUB-ONE(T) = EXP(MW1)*W1, W-SUB-ONE-PRIME = EXP(MD1)*DW1,
C W-SUB-TWO = EXP(MW2)*W2, ETC.
C
       DIMENSION TZERO(11), TINFIN(11)
       COMPLEX Q,W1,DW1,W2,DW2, PH, A ,T
  W-SUB-ONE-PRIME(TZERO(I)) =0.
       DATA  TZERO/ 1.018793, 3.2481975, 4.8200992, 6.1633074,
      1 7.3721773, 8.4884868, 9.5354490, 10.52766, 11.475057, 12.384788
      2 13.262219/
  W-SUB-ONE(TINFIN(I)) =0.
       DATA  TINFIN / 2.3380997, 4.0879494, 5.5205598, 6.7867081,
      1 7.9441336, 9.0226508, 10.040174, 11.008524, 11.936016, 12.82877
      2 13.691489/
       DATA  PH /(0.5, -0.8660254)/,   CON/ 1.17809724/
```

```
      IF( REAL(Q)**2 + AIMAG(Q)**2 .GT. 1.) GO TO 50
      IF(I .GT. 10) GO TO 10
      TZ = TZERO(I+1)
      GO TO 20
   10 YS = ((4*I+1)*CON)**2
      TZ= YS**0.3333333*(1.-.1458333/YS)
   20 T = TZ*PH
C T IS NOW SOLUTION FOR Q =0.
      T = T+Q/T
      GO TO 100
   50 IF(I .GT. 10) GO TO 60
      TZ = TINFIN(I+1)
      GO TO 70
   60 YS = ((4*I+3) *CON)**2
      TZ= YS**0.33333333*(1.+.1041667/YS)
   70 T = TZ*PH
C T IS SOLUTION FOR Q=INFINITY.
      T = T+1./Q
  100 K=0
   NOW, USE NEWTONS ITERATION TO CONVERGE ON SOLUTION.
C CWAIRY COMPUTES  W(T)  AND  W PRIME(T)
C101 CALL CWAIRY(1,T,W1,MW1,W2, MW2)
      CALL CWAIRY(2,T,DW1,MD1,DW2,MD2)
      A=(2.718281828**(MD1-MW1))*DW1/W1
      A = (A-Q)/(  T -A*Q)
      T = T-A
      K=K+1
      IF(K .GT. 15) GO TO 150
      IF(CABS(A/T) .GT. 0.5E-5) GO TO 101
      RETURN
      WRITE(6,155) I,T,A
      FORMAT('   FAILED TO CONVERGE ON T(',I2,'), T= ',
     1  (E14.6,E14.6),' LAST CORRECTION =',  (E14.6,E14.6))
      RETURN
      END

      SUBROUTINE CWAIRY(KK,T,F1,M1,F2,M2)
C
C     CALCULATION OF THE W(T) AIRY FUNCTIONS.
C     INPUT:
C        KK=1, W(T) OF KIND 1 AND W(T) OF KIND 2 ARE COMPUTED.
C        KK=2, THE DERIVATIVE OF W(T) OF KIND 1 AND THE DERIVATIVE
C              OF W(T) OF KIND 2 ARE COMPUTED.
C        T =   THE COMPLEX ARGUMENT.
C     OUTPUT:
C        F1*(E**M1) = W(T) OF KIND 1 OR THE DERIVATIVE OF W(T)
C                     OF KIND 1 AS INDICATED BY KK.
C        F2*(E**M2) = W(T) OF KIND 2 OR THE DERIVATIVE OF W(T)
C                     OF KIND 2 AS INDICATED BY KK.
C     NOTE.  F1 AND F2 ARE COMPLEX, E=2.718281828..., AND
C     M1 AND M2 ARE EXPONENTS.
```

```
      COMMON/MEXP/M
      COMPLEX F1,F2,WI1,WI2,WI1P,WI2P,T
      GO TO(100,200),KK
  100 F2=WI1(T)
      M2=M
      F1=WI2(T)
      M1=M
      GO TO 300
  200 F2=WI1P(T)
      M2=M
      F1=WI2P(T)
      M1=M
  300 F1=1.7724538509*(0.,-1.)*F1
      F2=1.7724538509*(0.,+1.)*F2
      RETURN
      END
```

Appendix V

LABORATORY SIMULATION STUDIES OF MODULATION EFFECTS

V.1. Introduction

In the present Appendix the effects on TV reception of extraneous modulations of the received signals are investigated by laboratory simulation techniques. The primary purpose of the simulation tests was: (i) to observe and characterize the nature of the interference effects produced and (ii) to establish any possible relationships between the onset and amount of distortion produced and the characteristics of the modulation applied. We have seen earlier that the amplitude modulation of the signals caused by rotating windmills is capable of producing adverse effects on reception, and during the simulation tests emphasis was placed on this type of modulation.

The simulation studies were carried out early in the program prior to the actual field tests at Plum Brook, and yielded results providing some understanding of the effects of the modulation of received signals on TV reception in a controlled environment. The test results proved useful in the design and optimuzation of the methods used in the later field tests, and they also provided important guidelines as to the effects to look for in the field testing of TV reception in the presence of a windmill.

V.2. Experimental Arrangement

Figure V.1 gives the block diagram of the equipment arrangement used in the measurements. A directive antenna with a gain of about 10 dB over an isotropic radiator was mounted on the roof of a five story building. A rotator enabled it to be directed towards the TV transmitter of interest.

Laboratory simulators were designed and built such that the amplitude and phase of the input signals to a TV receiver could be modulated at any of the VHF

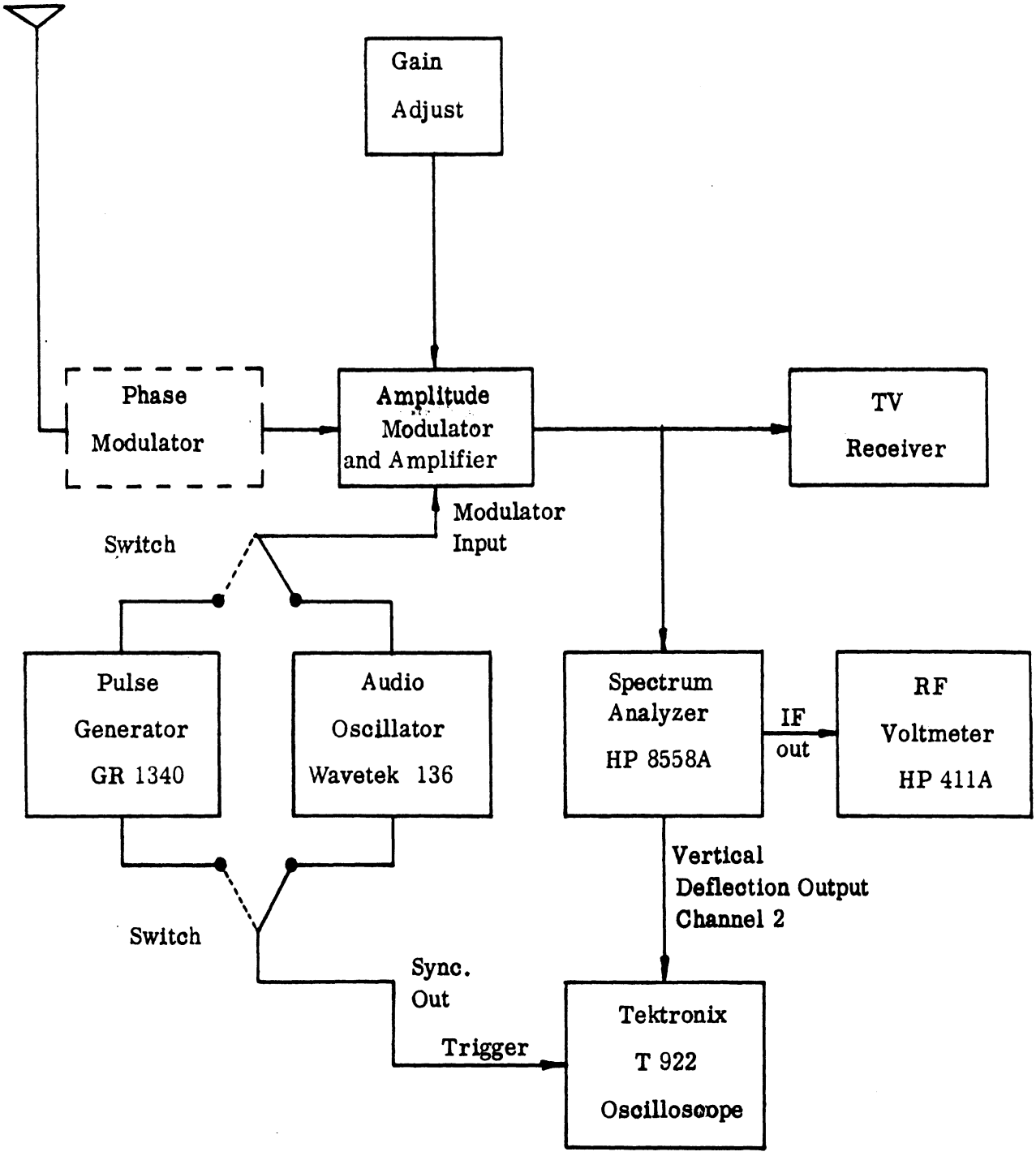

Figure V.1. Equipment and arrangement used in simulated modulation studies.

channel frequencies. An amplifier was included in the amplitude modulator thus making it possible to control the level of the input signal to the receiver. The amplitude modulator applied a continuous sine wave modulation to the incoming signal. The level of amplitude modulation introduced was variable over a 30 dB range at modulation frequencies ranging from zero to one MHz. The phase modulation provided for a $\pm$ 45 degree phase change at low modulation frequencies and up to $\pm$ 90 degrees at higher modulation frequencies. The phase changes over the above ranges could be made slowly or at rates up to several hundred KHz. The pulse generator provided unidirectional repetitive pulse modulation of the received signals. The modulation pulse width and repetition frequencies were variable. Aside from these, the components used were standard and are identified in the block diagram in Figure V.1. Most of the data were obtained using a 1976 Zenith TV receiver. A few tests were also made using a 1974 Magnavox TV receiver.

V.3. Presentation of Results

With the phase modulator in the position shown in Figure V.1, there appeared to be no significant effect as the phase was varied. Hence no data will be presented on the effects of simulated phase modulation. However, it is recommended that further studies be made using a type of phase modulation which would more closely simulate that caused by the rotating windmill.

The results obtained in the amplitude modulation tests are given in a series of tables. For a given TV receiver, tests were performed to determine the received picture quality as the modulation index was increased from zero to a value which resulted in severe distortion. To determine the modulation index, we used the change in amplitude of the level of the audio signal. This is ordinarily constant since the audio information is transmitted with frequency modulation. For sine wave amplitude modulation the modulation index m is obtained from the observed change in the audio signal level using the relation

$$m = \frac{dB^{-1} - 1}{dB^{-1} + 1} , \qquad (V.1)$$

where $dB^{-1} = 10^{\Delta/20}$. (V.2)

Δ is the observed change in the audio carrier signal level expressed in dB.

The pulse modulation produces positive pulses only and in this case the modulation index is obtained from

$$m = 10^{\Delta/20} - 1, \quad (V.3)$$

where Δ is as defined before.

Data were obtained at several TV channel frequencies and as a function of the level of the input signal power, the modulation index and the frequency of modulation. The method of obtaining the data was as follows. The given TV receiver was tuned to the TV channel frequency of interest and the spectrum analyzer, with its resolution set at 300 KHz, was tuned to the audio carrier frequency of the same channel. To determine the modulation index, the output level of the spectrum analyzer was noted, first with zero modulation and then with the audio oscillator (or the pulse modulator) set at the desired level. The resulting change Δ in dB of the audio carrier signal level is used to compute the modulation index. The received picture quality was then studied as a function of Δ. The audio reception was not appreciably effected by the modulations.

The amplitude modulation interferes with the video reception in the form of horizontal dark bars moving vertically through the picture on the TV screen. When the modulation frequency approaches a multiple of the TV vertical sweep frequency, a zero beat is observed, i.e, the bars become stationery. The observed TV pictures are rated qualitatively as follows:

A	unimpared video.	D	intolerable black bars and vertical mirage effects.
B	onset of faint black bars.		
C	non-trivial black bars.	E	pulsating snow caused by signal excursions into the noise level; unacceptable.

Tables V.1 and V.2 show the observed picture quality for sine wave modulation as a function of the input signal power level, the modulation index and frequency for a Zenith TV receiver tuned to Channels 2 and 13 frequencies. The corresponding data for the Magnavox TV receiver are presented in Tables V.3 and V.4. In both sets of data it is seen that the modulation frequency at which picture distortion begins to occur tends to become lower as the modulation index increases. One would expect that video distortion would occur more readily with a decrease in the level of the input TV signal but this is not indicated by the data.

Tables V.5 through V.9 show the threshold of modulation defined to be the modulation index required to produce minimum observable video distortion (Case B) as a function of the input signal level and the modulation frequency. The first three tables are for the Zenith TV receiver and the last two are for the Magnavox. There is a fairly consistent trend in these results showing an earlier incidence of video distortion as the modulation frequency increases, but there is no consistent variation with the level of the input power. Table V.6 gives results for very low modulation frequencies. This case is of interest in that is shows that the TV receiver is vulnerable to modulation frequencies much lower than had been expected. No significant difference was noted in the performance of the Zenith and the Magnavox receivers.

All of the data shown so far has been for sine wave modulation. Table V.10 shows results obtained with pulse modulation of received signals. The modulation pulses were unidirectional rectangular pulses of width τ repeating at time intervals T. Compared to the sine wave modulation data, the present results indicate that video distortion occurs at a much lower level of modulation. The threshold modulation is found to be independent of the signal level. As discussed earlier the windmill does produce a pulse-like modulation of the incident signals. Although the modulation pulses produced by a rotating windmill are approximately sinx/x shape, it is expected that their effect on video reception would be similar to that found here.

V.4. A Mechanical Simulator

Since there was no opportunity early in the program to do any field testing using the actual windmill at Plum Brook, a low cost substitute was developed to

Level of audio carrier in dB over milliwatt	m 0	m 0.058		m 0.112		m 0.226	
	Frequency of Modulation (Hz) and Picture Quality						
-35	A	460	B	190	B	120	B
		8000	C	600	C	360	C
						600	D
-40	A	400	B	150	B	100	B
		2000	C	550	C	300	C
						430	D
-45	A	210	B	170	B	50	B
		1500	C	540	C	300	C
						450	D
-50	A	200	B	120	B	85	B
		1300	C	300	C	300	C
						400	D
-55	onset of snow	210	B	170	B	115	B
		1200	C	400	C	170	C
						380	D
-60	snow	400	B	185	B	145	B
		1000	C	420	C	250	C
						360	D
-65	very snowy	330	B	260	B	190	B
		800	C	490	C	300	C
						600	D

Table V.1. Channel 2 picture quality with sine wave modulation at indicated modulation frequency in Hz. Video carrier frequency = 55.25 MHz, audio carrier frequency = 59.75 MHz. Test receiver is Zenith model 17GC45.

Level of audio carrier in dB over milliwatt	m 0	m 0.058		m 0.112		m 0.226		m 0.330	
	Frequency of Modulation (Hz) and Picture Quality								
-50	A	340	B	160	B	120	B	60	B
		>10K	C	350	C	180	C	140	C
				1100	D	420	D	290	D
-60	A	187	B	162	B	92	B	47	B
		420	C	350	C	130	C	74	C
		4500	D	1180	D	360	D	235	D
-65	onset of snow								

Table V.2. Channel 13 picture quality with sine wave modulation at indicated modulation frequency in Hz. Video carrier frequency = 211.25 MHz, audio carrier frequency = 215.75 MHz. Test receiver is Zenith model 17GC45.

Level of audio carrier in dB over milliwatt	m 0	m 0.058		m 0.112		m 0.226		m 0.330	
	Frequency of Modulation (Hz) and Picture Quality								
-35	A	300	B	183	B	60	B	40	B
		2000	C	600	C	290	C	200	C
				1100	D	450	D	260	D
-40	A	185	B	160	B	110	B	66	B
		1000	C	350	C	365	C	170	C
				680	D	380	D	294	D
-50	A	420	B	190	B	165	B	103	B
		550	C	600	C	290	C	232	C
				730	D	380	D	253	D
-60	onset of snow	250	B	185	B	170	B	110	B
		600	C	420	C	310	C	175	C
				635	D	395	D	305	D
-70	snow			180	B	120	B	120	B
				490	C	300	C	250	C
				650	D	375	D	310	D

Table V.3. Channel 2 picture quality with sine wave modulation at indicated modulation frequency in Hz. Video carrier frequency = 55.25 MHz, audio carrier frequency = 59.75 MHz. Test receiver is Magnavox model CD4220.

Level of audio carrier in dB over milliwatt	m 0	m 0.058		m 0.112		m 0.226		m 0.330	
	Modulation of Frequency (Hz) and Picture Quality								
-40	A	240	B	120	B	115	B	70	B
		775	C	350	C	250	C	240	C
				1100	D	500	D	300	D
-50	A	270	B	195	B	186	B	168	B
		1100	C	550	C	350	C	240	C
				920	D	440	D	340	D
-60	A	190	B	170	B	125	B	111	B
		410	C	280	C	250	C	190	C
				650	D	260	D	200	D
-70	onset of snow			165	B	120	B	120	B
				425	C	165	C	165	C
				600	D	300	D	275	D

Table V.4. Channel 13 picture quality with sine wave modulation at indicated modulation frequency in Hz. Video carrier frequency = 211.25 MHz, audio carrier frequency = 215.75 MHz. Test receiver is Magnavox model CD4220.

Level of audio carrier in dB over milliwatt	Frequency of modulation (Hz)			
	30	50	100	200
	m	m	m	m
-35		0.82	0.60	0.24
-40		0.60	0.52	0.20
-45		0.56	0.24	0.20
-50		0.45	0.23	0.14
-55	onset of snow	0.48	0.24	0.17
-60	snow	0.52	0.43	0.27
-65	very snowy	0.59	0.52	0.48

Table V.5. Modulation index required to produce minimum observable video distortion at Channel 2. Video carrier frequency = 55.25 MHz, audio carrier frequency = 59.75 MHz. Test receiver is Zenith model 17GC45.

Level of audio carrier in dB over milliwatt	m	Frequency of Modulation (Hz)											
		1.5	1.0	2.0	4.0	8.0	16.0	20.0	25.0	30.0	35.0	50.0	64.0
	0	m	m	m	m	m	m	m	m	m	m	m	m
-30	A							0.82	0.75	0.82	0.75	0.59	
-35	A							0.71	0.85	0.59	0.78	0.63	
-40	A							0.80	0.70	0.48	0.48	0.48	
-45	A							0.56	0.48	0.36	0.33	0.28	
-50	A							0.80	0.68	0.50	0.58	0.43	
-55	A	0.70	0.67	0.67	0.73	0.94	0.78	0.48	0.48	0.37	0.33	0.23	0.33
-60	C							0.60	0.52	0.45	0.43	0.37	
-65	C	0.33	0.28	0.23	0.23	0.52	0.48	0.75	0.67	0.61	0.56	0.48	0.38
-70	D							0.89	0.75	0.73	0.70	0.56	

Table V.6. Modulation index required to produce minimum observable video distortion at Channel 7. Video carrier frequency = 175.25 MHz, audio carrier frequency = 179.75 MHz. Test receiver used is Zenith model 17GC45.

Level of audio carrier in dB over milliwatt	Frequency of Modulation (Hz)		
	50	100	200
	m	m	m
-45	0.60	0.52	0.23
-50	0.63	0.52	0.24
-55	0.17	0.17	0.16
-60	0.20	0.20	0.11
-65	0.52	0.33	0.17

Table V.7. Modulation index required to produce minimum observable video distortion at Channel 13. Video carrier frequency = 211.25 MHz, audio carrier frequency = 215.75 MHz, Test receiver is Zenith model 17GC45.

Level of audio carrier in dB over milliwatt	m = 0	Frequency of Modulation (Hz)		
		50	100	200
		m	m	m
-35	A	0.23	0.14	0.14
-40	A	0.52	0.43	0.17
-45	A	0.67	0.59	0.23
-50	A	0.71	0.56	0.23
-55	A	0.87	0.59	0.28
-60	onset of snow	0.75	0.56	0.25
-65	snow	0.73	0.52	0.30
-70	snow	0.69	0.52	0.38
-75	snow	0.52	0.43	0.23

Table V.8. Modulation index required to produce minimum observable video distortion, with sine wave modulation at Channel 2. Video carrier frequency = 55.75 MHz, audio carrier frequency = 59.25 MHz. Test receiver is Magnavox model CD4220.

Level of audio carrier in dB over milliwatt	m = 0	Frequency of Modulation		
		50	100	200
		m	m	m
-40	A	0.43	0.38	0.17
-45	A	0.59	0.52	0.17
-50	A	0.78	0.48	0.23
-55	A	0.87	0.48	0.11
-60	A	0.84	0.48	0.23
-65	A	0.63	0.48	0.17
-70	onset of snow	0.67	0.43	0.14
-75	snow	0.48	0.33	0.23

Table V.9. Modulation index required to produce minimum observable video distortion with sine wave modulation at Channel 13. Video carrier frequency = 211.25 MHz audio carrier frequency = 215.75 MHz. Test receiver is Magnavox model CD4220.

Level of audio carrier in dB over milliwatt	τ = 20 msec T = 1 sec	τ = 30 msec T = 1.5 sec	τ = 40 msec T = 2 sec	τ = 60 msec T = 3 sec
	m	m	m	m
-30	0.14	0.15	0.18	0.16
-40	0.14	0.15	0.18	0.16
-50	0.14	0.15	0.18	0.16
-60	0.14	0.15	0.18	0.16
-70	0.14	0.15	0.18	0.16
-80	0.14	0.15	0.18	0.16

Table V.10. Modulation index required to produce minimum observable video distortion with pulse modulation at Channel 7. Video carrier frequency = 175.25 MHz, audio carrier frequency = 179.75 MHz. Test receiver used is Zenith model 17GC45.

provide a mechanical simulation of at least some of the effects of a windmill on TV performance. The device consisted of a 58.5 cm diameter grid of horizontal metal rods whose spacing was close enough to produce almost complete reflection at VHF and UHF frequencies. The grid could be rotated about a vertical axis at any chosen rate up to about 1500 rpm, the limit being set by excessive vibration. The rotating mechanism was 6 feet high and rested on a 6 foot high platform so that the center of the rotating vane was at the level of the axis of the TV antenna. A photograph of the arrangement is shown in Figure V.2.

It was recognized that the rotating grid was far from an exact simulator of a large windmill, but it did have the ability to modulate the amplitude and phase of the signal received by the TV antenna at rates which were comparable to those that a windmill would provide.

With the grid rotating, no effects were observed on the VHF channels regardless of the position of the grid relative to the antenna. This is not too surprising since the entire grid is electrically small at these frequencies. However, very pronounced effects were seen on the UHF channels. These occurred when the rotating vane was about five feet in front of the end of the antenna with the antenna pointing about 30 degrees away from the direction of the transmitter. As the vane rotated through 180 degrees, the quality of the picture varied from good to completely unacceptable. This behavior was observed with rotation rates which varied from 5 Hz or so up to the highest rates achievable (approximately 25 Hz). There are, of course, two cycles of change for each revolution of the vane, and when the (net) received signals were examined on a spectrum analyzer and associated oscilloscope, it appeared that the modulation index was about 50 percent. No effects were observed when the vane was moved back to 25 feet from the front of the antenna.

It was possible to receive Channel 24 on the back lobe of the antenna, and when the vane was placed in the forward beam of the antenna, there was again a pronounced effect on the TV picture. In yet another arrangement, the antenna was pointed directly at the transmitter, and then the rotating vane had no effect even when placed only five feet in front.

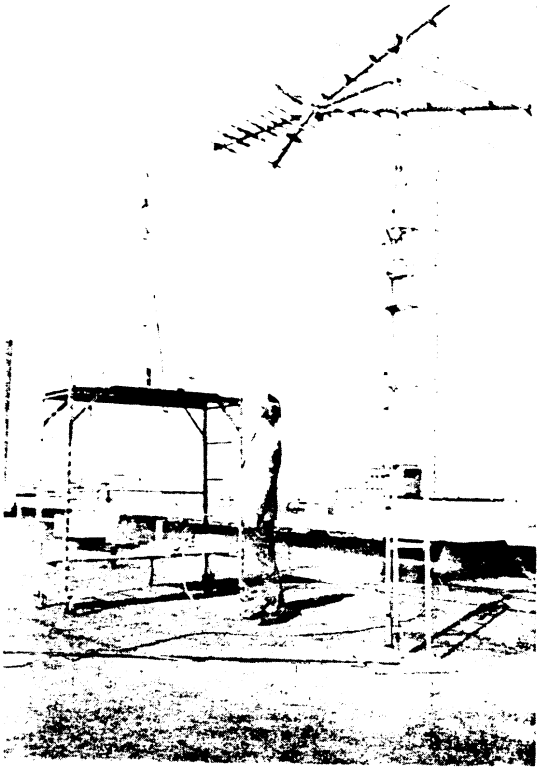

Figure V.2. Rotatable reflector in front of TV antenna.

In all of these tests video distortion occurred only when the major portion of the TV signal was being received indirectly via reflection off the rotating vane. A similar effect was later observed with the windmill at Plum Brook in the field tests, and when it became possible to make field tests, we ceased any further study of the mechanical simulator.

V.5. Discussion

The laboratory simulations demonstrated conclusively that extraneous amplitude modulation of received signals can produce video distortion of TV reception, but no audio distortion was observed with any of the types of modulation used. The level of the observed video distortion depends on the amount and nature of the modulation introduced. Both sinusoidal and pulse modulations appear to produce similar types of video distortion, but the modulation index required for the threshold of distortion is much lower in the latter case. Also, the distortion produced by pulse modulation appears independent of the signal strength, implying that a TV receiver is more vulnerable to pulse modulation. This tends to be true for sine wave modulations also.

Based on these results, the nature of the observed video distortion has been characterized and classified subjectively. In addition, the pulse modulation data served to specify the choice of modulation index for the threshold of distortion to TV reception in the presence of rotating windmill.

Appendix VI

FIELD TESTS

VI.1. Introduction

Field tests associated with the NASA-ERDA 100 kW wind turbine located at the NASA Lewis Plum Brook facility were carried out during the period May to October 1976. The initial tests were made before the laboratory simulations and theoretical calculations were complete and were exploratory in nature. Later tests were aimed at obtaining scattering and operational data, but because of the very intermittent wind conditions throughout the summer, the turbine was in operation for only a few of the tests.

In the following sections we give a brief description of the windmill with particular reference to those features which are important to the field tests. We then indicate the test set-up and procedures used and follow this with a discussion of the three types, i.e., exploratory, scattering and operational, of tests performed. The final section summarizes the results obtained.

VI.2. The Wind Turbine

The windmill has been described in detail in several NASA documents and a sketch of the turbine and tower is shown in Figure VI.1. Of particular importance to our tests are the yawing motion of the turbine, the blade pitch adjustment and the blade rotation.

There are two modes of operation for controlling the yaw, i.e., the azimuthal rotation of turbine nacelle and blades. In the manual mode the turbine can be rotated clockwise or counter-clockwise at a uniform rate of 0.167 revolutions per minute, and this mode was used for all of our scattering measurements. Alternatively there is the auto mode in which the pointing direction is controlled via a servo system. The angular difference between the direction of the nacelle and the wind direction obtained from a sensor on top of the nacelle is used to generate an error signal which activates

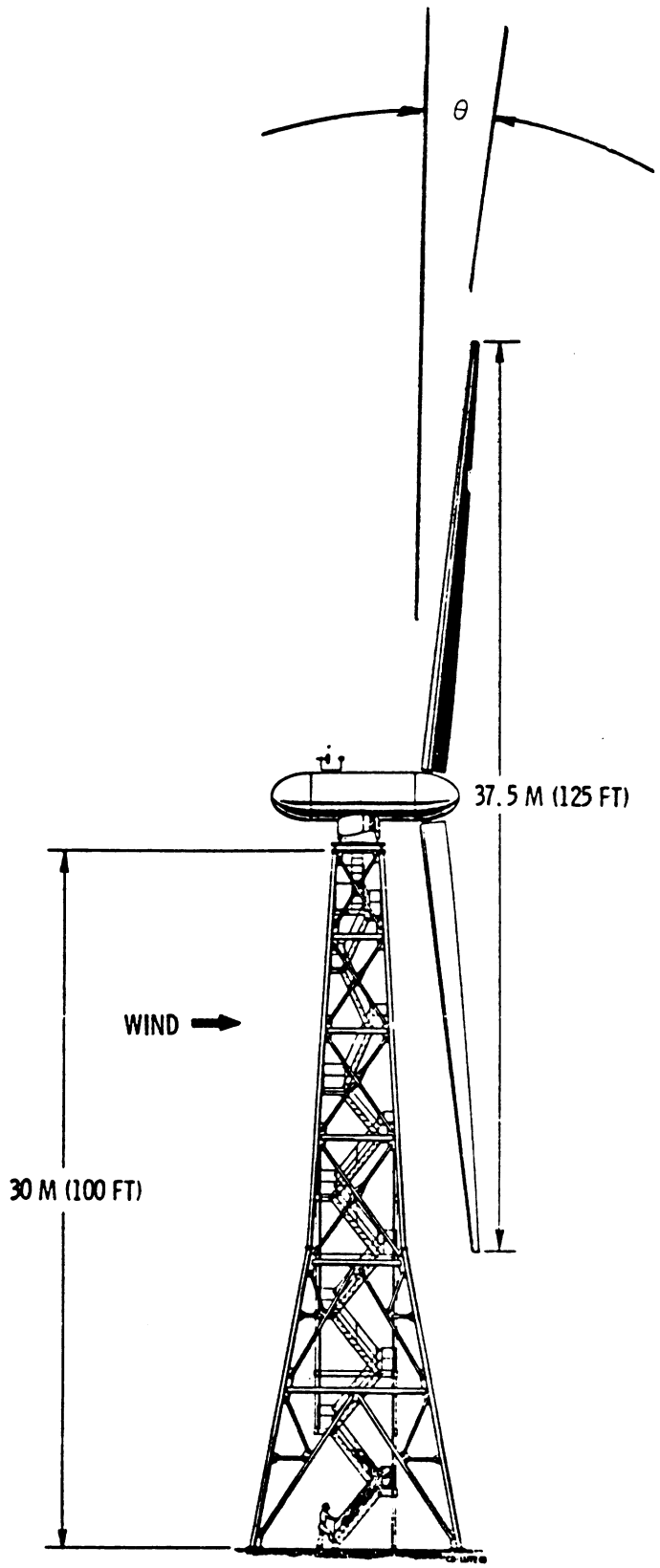

Figure VI.1. 100-kilowatt experimental wind turbine generator.

the yaw drive mechanism to align the nacelle with the wind. A calibrated voltage readout indicates the actual pointing direction at any time. The auto mode was used in all other tests. With both modes of operation a braking system is available to stop the nacelle in any desired (azimuthal) direction.

Manual and auto modes also exist for controlling the pitch angle of the blades from that for zero power to that for maximum power. In the scattering measurements the blades were manually set for maximum power to provide the largest surface for specular reflection of the incident field. The auto mode is based on a servo control system in which the error signal is proportional to the difference between the actual and a pre-set (variable from 0 to 40 rpm) blade rotation speed. The actual blade pitch angle can be obtained from a calibrated voltage readout.

The wind velocity must be at least 6 mph to obtain blade rotation, and the maximum allowable rotation rate is 40 rpm. However, for mechanical reasons, all of our exploratory and operational tests were made with the blades rotating at no more than 20 rpm. A voltage pulse is generated whenever a blade passes through 360 degrees (the zero being when the blade is vertical) and this pulse is available for recording. For the scattering measurements the blades were locked in position parallel to the ground using the blade braking system.

VI.3. Test Procedures

The basic set-up for carrying out the field tests is shown in Figure VI.2. where we have indicated only those instruments which are pertinent to the data gathering. The sources of the RF energy were the television transmitters located in Cleveland (Channels 3 and 43) and Toledo (Channels 13 and 24). With any given station some of the energy was reflected off the turbine blades and this, together with the 'direct' signal, was picked up by the field site antenna and fed simultaneously to a TV monitor and a spectrum analyzer. The audio portion of the signal was taken from the analyzer and recorded on paper tape for later evaluation. The video signal was detected by the TV receiver and fed to a video tape recorder whenever the data was felt worth preserving. At both the field site and the wind turbine control center the WWV time

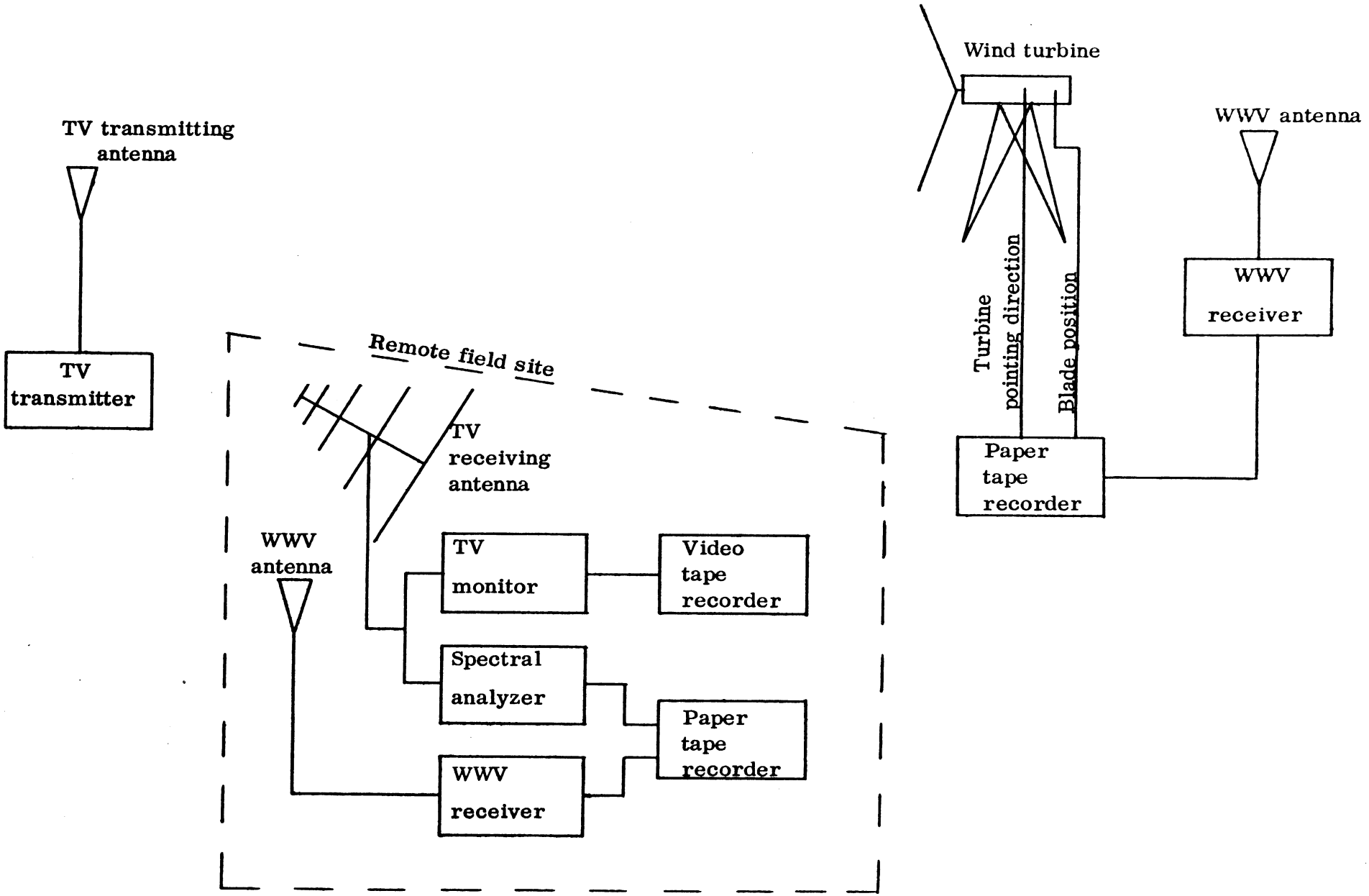

Figure VI.2. Test equipment set up.

code was also received and recorded to permit a subsequent correlation of the field data with the turbine state, i.e., azimuth, blade position, etc.

Additional procedures peculiar to a given type of test will be described in conjunction with those tests.

VI.4. Exploratory Tests

These were conducted at the Plum Brook facility on May 12 and 26, 1976. Being the first tests performed, and carried out ahead of any predictions obtained from the theoretical analyses, the objective was to see if the rotating turbine blades provided any detectable TV interference, and if they did, to examine the nature of the interference.

On the first trip the blades were rotating at approximately 20 rpm and the receiving antenna was positioned only 200 feet from the turbine. This close distance was chosen to maximize the possibility of interference, and when the (directional) antenna was pointed towards the turbine (thereby discriminating against the direct signal), reception on all four TV channels showed periodic interference. The output from the spectrum analyzer indicated that the interference was in the form of a narrow pulse occurring whenever the blades passed through the horizontal. On the second trip the site chosen was approximately 0.25 miles from the turbine. With the antenna pointed towards the turbine, interference was again observed when viewing Channel 43 (Cleveland) and the type of interference was similar to that on the previous trip.

These tests clearly showed that the turbine could interfere with TV reception. We therefore planned a series of further tests whose prime purpose was to study the manner in which the interference depended on the azimuthal orientation of the wind turbine with respect to the locations of the receiving antenna and the TV transmitter. In effect, these were concerned with the scattering of the RF energy off the blades of the turbine.

VI.5. Scattering Tests

Scattering tests were carried out on June 15, July 30, September 1 and October 26, 1976, with the turbine blades locked in a horizontal position. Prior to making the tests, 7 sites were identified and physically checked out at the Plum Brook facility. These are shown in Figure VI.3 and care was taken to ensure that the turbine was visible from each. Six of the sites, numbers 3 through 8, are roughly on a circle of radius 0.5 miles centered on the turbine. Subsequently, two further sites were identified and given numbers 10 and 12 (there is no site 11). Site 10 is approximately 1 mile from the turbine and close to NASA Plum Brook sewage disposal area. It was selected because of its proximity to houses. Sites 12 and 14 are about 0.25 miles from the turbine and are approximately on the radials for sites 6 and 5 respectively.

As a result of the theoretical analyses it had now become evident that the UHF channels would be most susceptible to interference. All of the scattering measurements were therefore made using the available UHF Channels 24 and 43 from Toledo and Cleveland respectively.

The test procedure used was as follows:

(i) Select one of the identified test sites.

(ii) Connect the equipment as shown in Figure VI.2.

(iii) Lock the turbine blades horizontal with their pitch set for maximum power.

(iv) Position the TV antenna to receive Channel 24.

(v) Tune the TV receiver and the spectrum analyzer to this station.

(vi) Rotate the turbine nacelle in azimuth.

(vii) Record the WWV time code at the test site.

(viii) Record the spectrum analyzer signal.

(ix) At the turbine control center, record the WWV time code and the nacelle pointing direction.

(x) Reposition the receiving antenna to point towards the turbine.

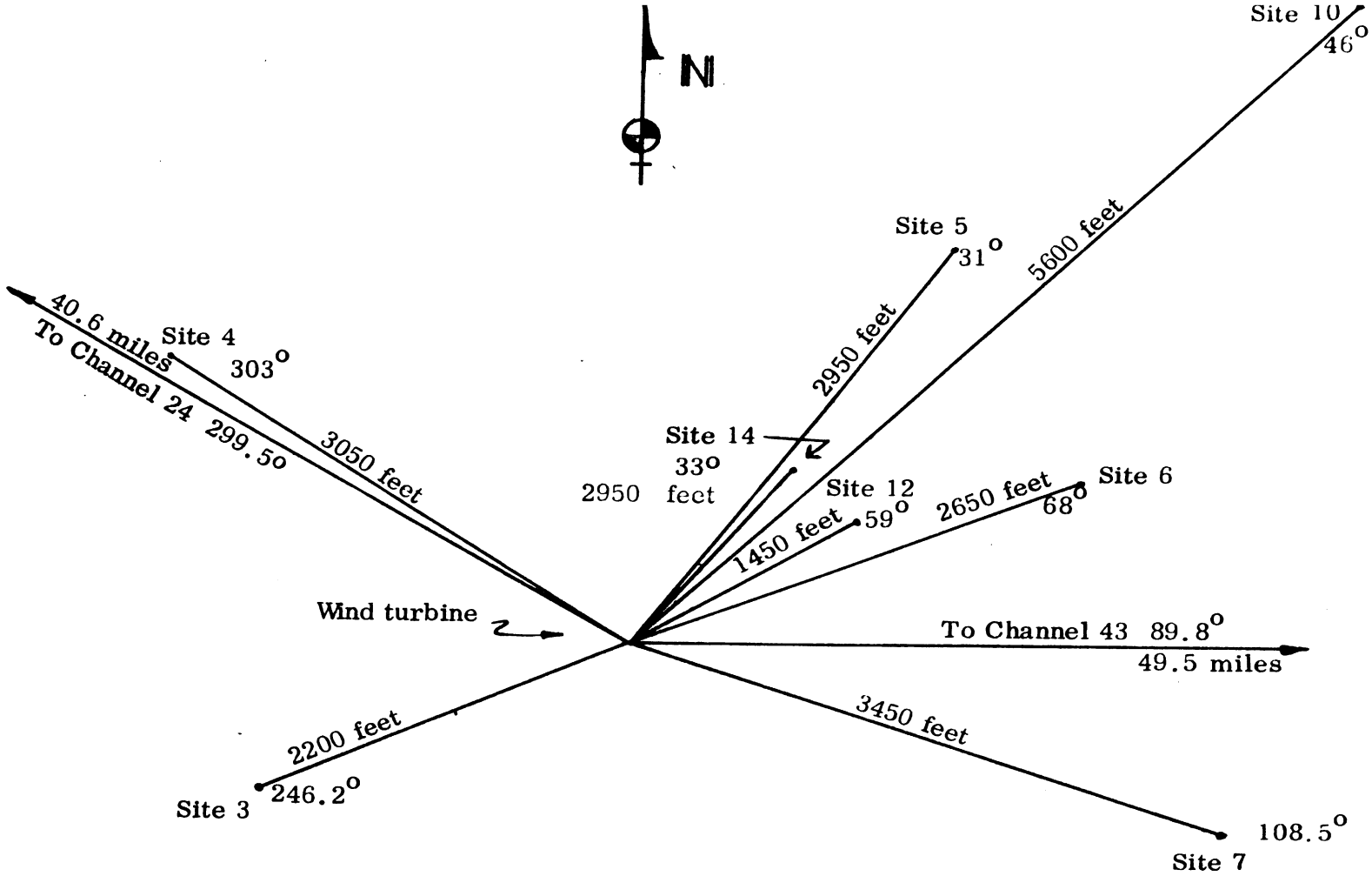

Figure VI.3. Wind turbine test sites.

(xi) Repeat steps (vi) through (ix).

(xii) Position the TV antenna to receive Channel 43.

(xiii) Repeat steps (v) through (xi).

VI.5.1. Scattering Test Results

Scattering test results were obtained at a number of selected sites using TV Channel 24 (video carrier frequency = 531.25 MHz) whose transmitter is located at Toledo as the source of RF signals. Figure VI.4 shows the wind turbine control center strip chart recordings obtained during the site 6 measurements. The top recording gives the turbine nacelle pointing direction as a function of time for a selected interval. The turbine was rotating clockwise in the horizontal plane, and the 0 degree and 180 degree marks refer to the north and south directions respectively. The lower recording shows the WWV time code signals received during the same period. A reduction of the WWV signals [1] indicated that each division in the horizontal scale corresponds to 1 sec.

The TV Channel 24 signals scattered by the wind turbine blades were received at field site 6. The receiving antenna was located 10 feet above the ground with its beam directed towards the turbine. The WWV time code signals and the received TV signals at the spectrum analyzer, observed during the same period of time as in Figure VI.4, are shown in Figure VI.5. The pair of sine wave-like shapes in the spectrum analyzer output are the signals scattered by the blades. Each sine wave may be identified with a turbine blade, and two sine waves appear because the blades are canted at an angle θ of approximately 3 degrees relative to the normal to the nacelle axis (Figure VI.1). As seen from Figure VI.5 the two sine waves are separated by approximately 12 degrees and centered 6 degrees on either side of the nacelle axis direction. On the basis of specular reflection by the blades, the reflected ray direction for each blade would be displaced by an angle 2θ from the nacelle axis in the same direction as the canting of the blade. Thus, the reflected rays from the two blades would be separated by $2\theta \simeq 12$ degrees, as shown in Figure VI.5. The magnitude of the specularly reflected signal received at site 6 is compared with the theoretical values in Appendix VII, with satisfactory agreement.

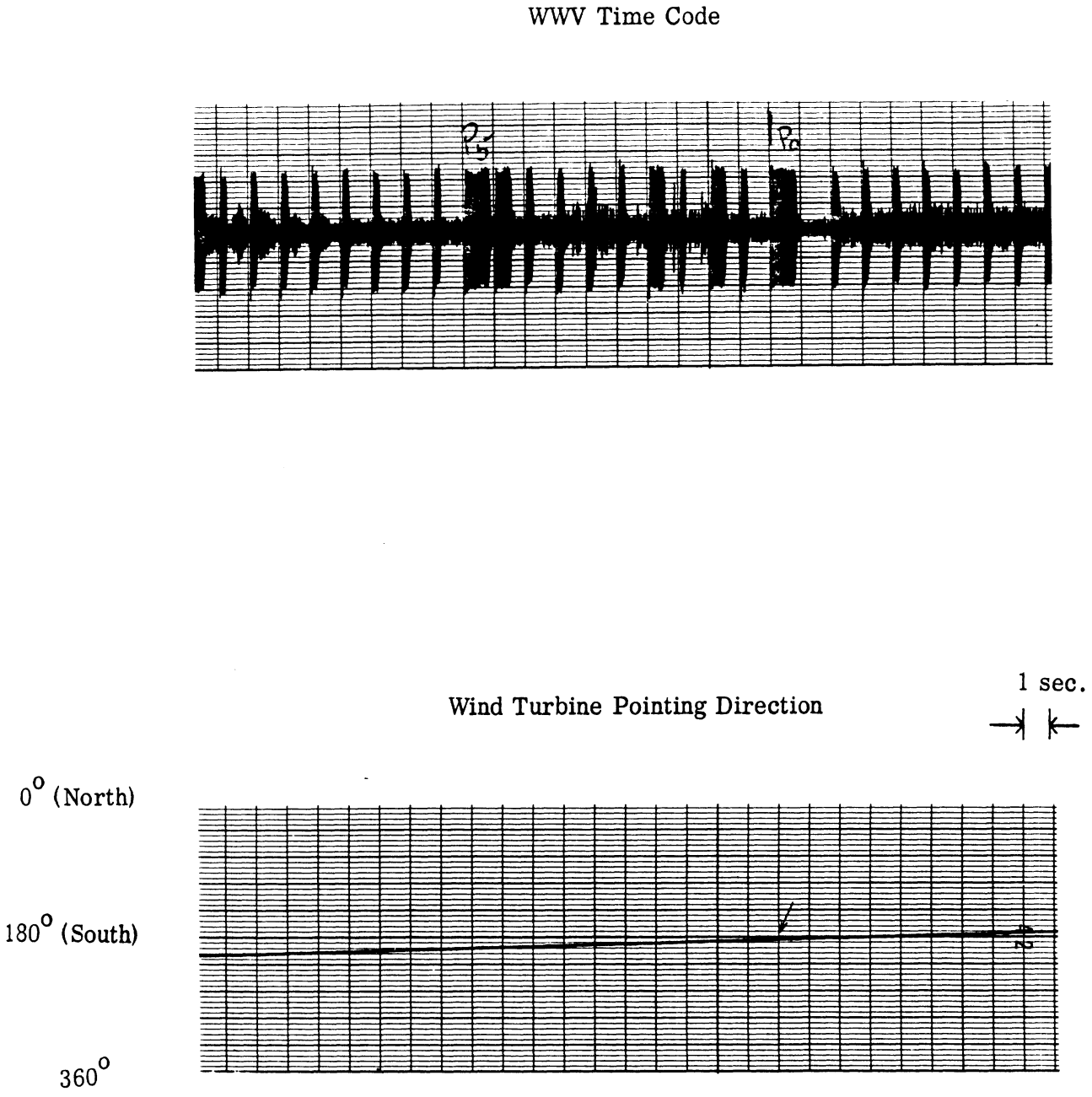

Figure VI.4. Wind turbine control center strip chart recordings during site 6 measurements.

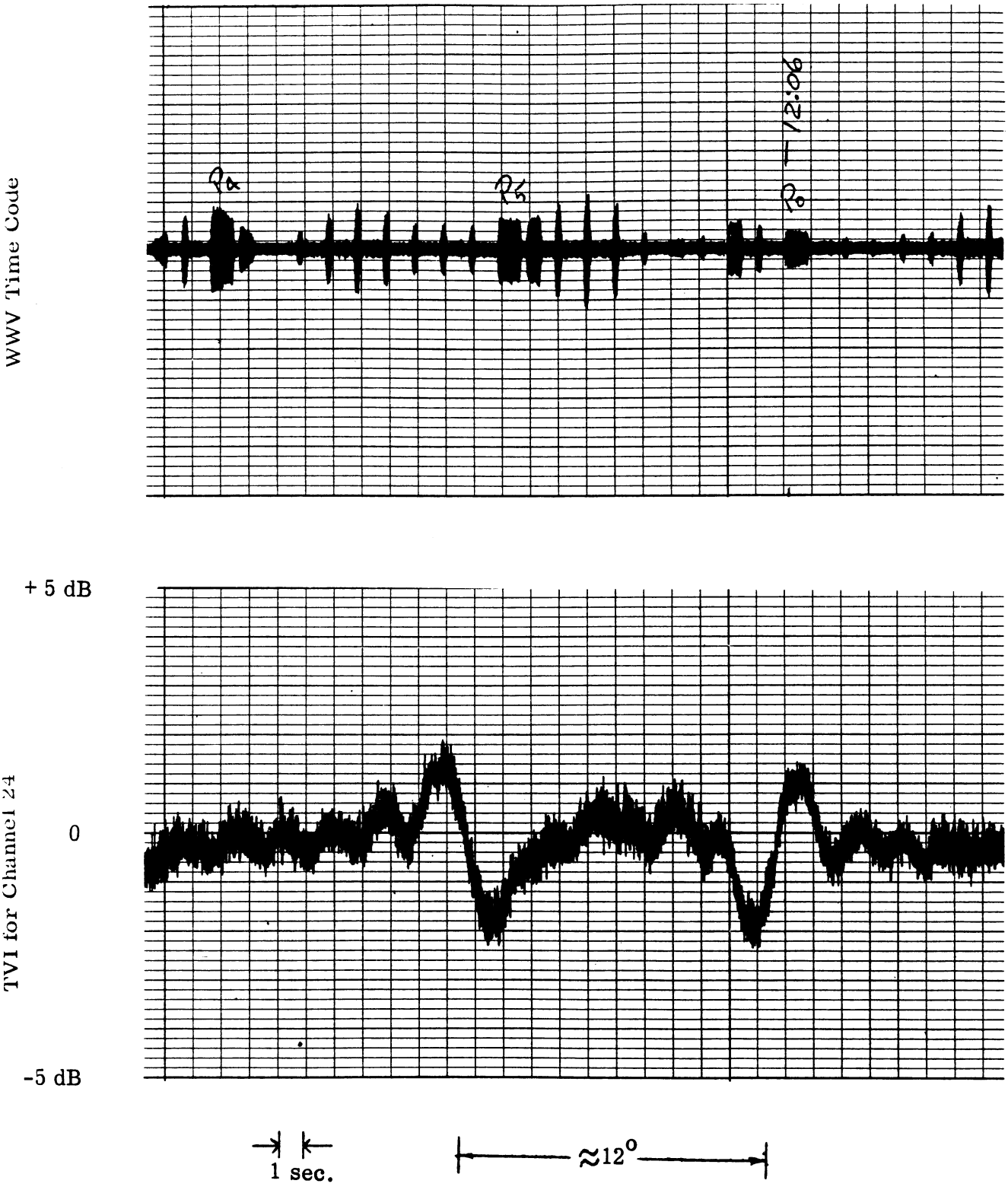

Figure VI.5. WWV time code and scattered Channel 24 signals observed at site 6.

Similar results obtained at site 5 are shown in Figures VI.6 and VI.7. Although the amplitude variations of the scattered signals are smaller than in Figure VI.5, we remark that at site 5 the scattered signal had to traverse a wood to reach the receiving antenna, and the greater attenuation may be due to this.

VI.6. Operational Tests and Results

VI.6.1. Test Procedures

Operational tests were conducted on October 29 and November 2, 1976 to observe and record any video distortion of TV reception caused by the rotating blades of the turbine. The observed results were recorded on both video and paper tapes. The test procedure used was as follows:

(i) Select one of the identified test sites.

(ii) Connect the equipment as shown in Figure VI.2.

(iii) Position the TV antenna to receive Channel 24.

(iv) Tune the TV receiver and spectrum analyzer to Channel 24.

(v) Lock the turbine blades horizontal to the ground and point the turbine nacelle to 0 degrees azimuth.

(vi) Make a 3-minute video tape.

(vii) Allow the turbine blades to rotate.

(viii) Make a 3-minute video tape.

(ix) Record the WWV time code at the test site.

(x) Record the spectrum analyzer signal at the test site.

(xi) At the turbine control center, record the WWV time code, the nacelle pointing direction and the blade position mark.

(xii) Reposition the receiving antenna to point towards the turbine.

(xiii) Repeat steps (v) through (xi).

(xiv) Position the TV antenna to receive Channel 43.

(xv) Repeat steps (iii) through (xiii).

A typical measured horizontal plane pattern of the receiving antenna used at the field test sites is shown in Figure VI.8. Observe that the back lobe maximum of the pattern is about 15 dB down from the main lobe maximum.

WWV Time

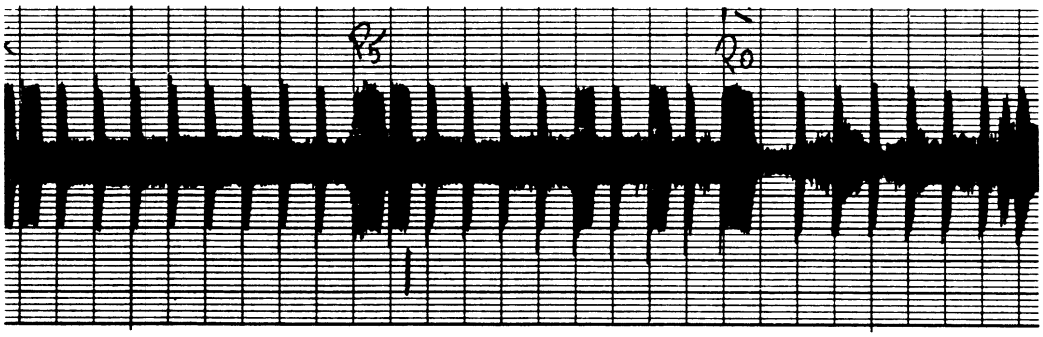

Windmill Pointing Direction

360°

180° (South)

0° (North)

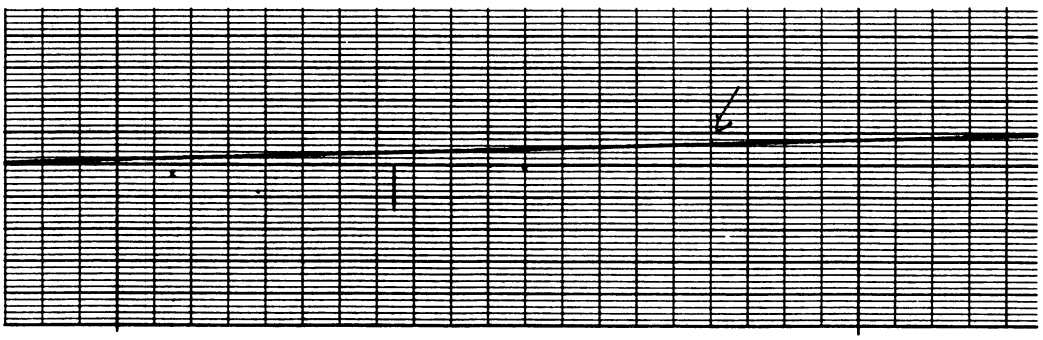

Figure VI.6. Wind turbine control center strip chart recordings during site 5 measurements.

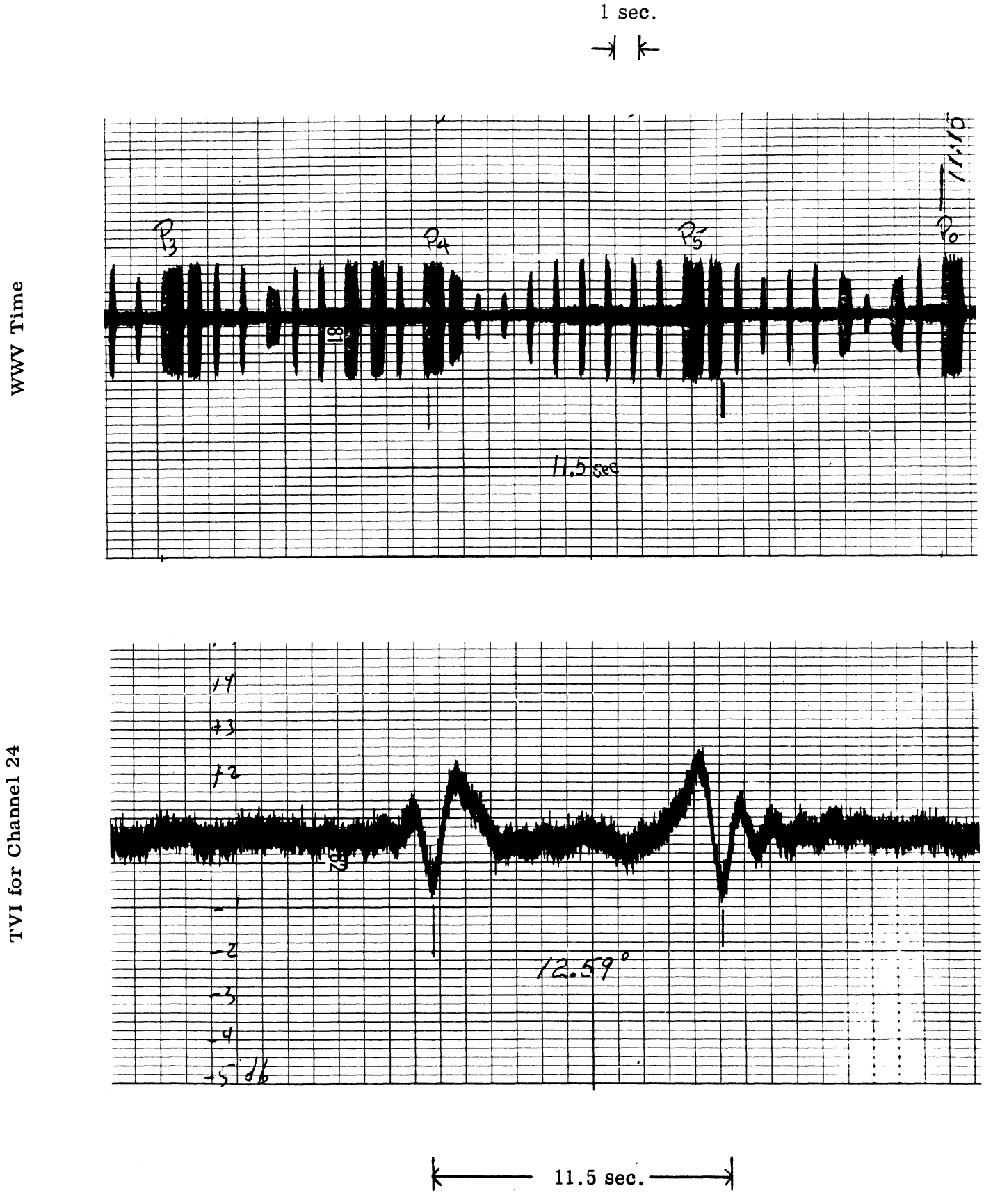

Figure VI.7. WWV time code and scattered Channel 24 signals observed at site 5.

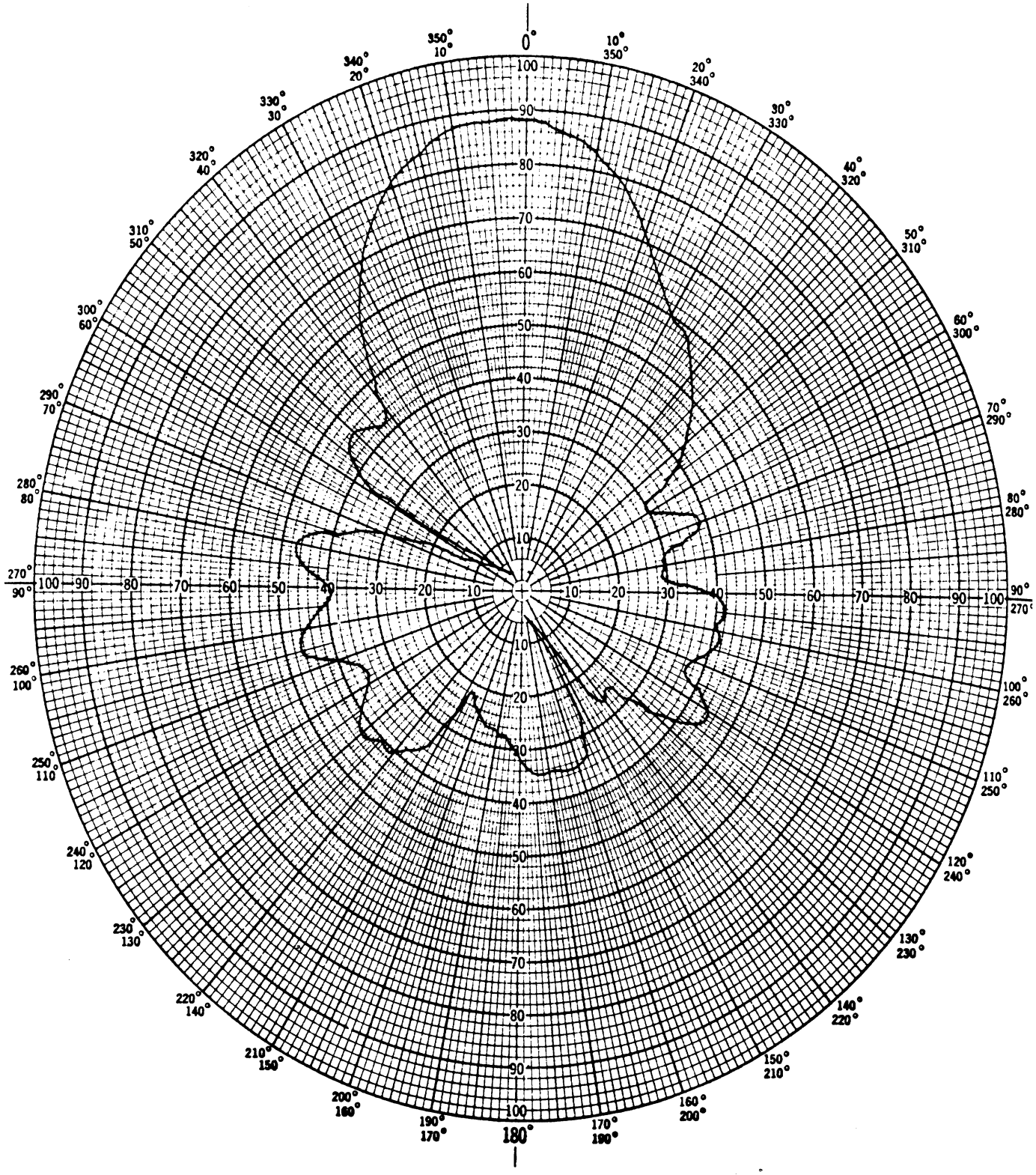

Figure VI. 8. TV receiving antenna pattern (600 MHz).

VI.6.2. Operational Test Results

Tests were carried out at sites 6, 12 and 14 (see Figure VI.3). TV Channels 24 and 43 transmitting stations were both used as signal sources, but no video distortion was observed on Channel 24 at any of the test sites. Also, at sites 6 and 12, no video distortion was observed on Channel 43, but this was attributed to the fact that for the specific orientation of the turbine during the tests, the site and/or antenna were not positioned so as to receive signals specularly reflected from the blades. However, at site 14, Channel 43 signals specularly reflected by the rotating blades of the turbine were received with sufficient strength to produce video distortion, and we discuss below only the results obtained at this site using Channel 43.

In the tests at site 14, the main beam of the receiving antenna was directed towards the Channel 43 transmitter. The locations of the site, wind turbine and TV transmitter were then such (Figure VI.3) that signals specularly reflected off the blades were received on the back lobe of the antenna. Figure VI.9 gives the wind turbine control center strip chart recordings obtained during the test. The top recording shows the turbine nacelle pointing direction as a function of time for a selected interval of time, and the middle recording gives the blade rotation as a function of time over the same period. The rotation period of the blades is 3 sec. The lowest recording in Figure VI.9 is the WWV time code signal from which the time axis is determined. Note that each division in the horizontal axis represents 1 sec.

Figure VI.10 shows the strip chart recordings of the WWV time code and Channel 43 signals received in the presence of the rotating windmill blades. Each division of the horizontal scale represents 250 msec, and the pulse-like modulation of the total received signal produced by the blades is clearly evident in the lower recording in Figure VI.10. The modulation pulses repeat every 1.5 sec (rotation period was 3 sec) and the widths of the individual pulses are approximately 75 msec. Video distortion was found to occur in synchronism with these pulses and the received pictures were recorded on video tape. No audio distortion was heard.

In contrast to the scattering test data (Figure VI.5) the signals received during the operational tests (Figure VI.10) were modulated by single sine wave-like pulses.

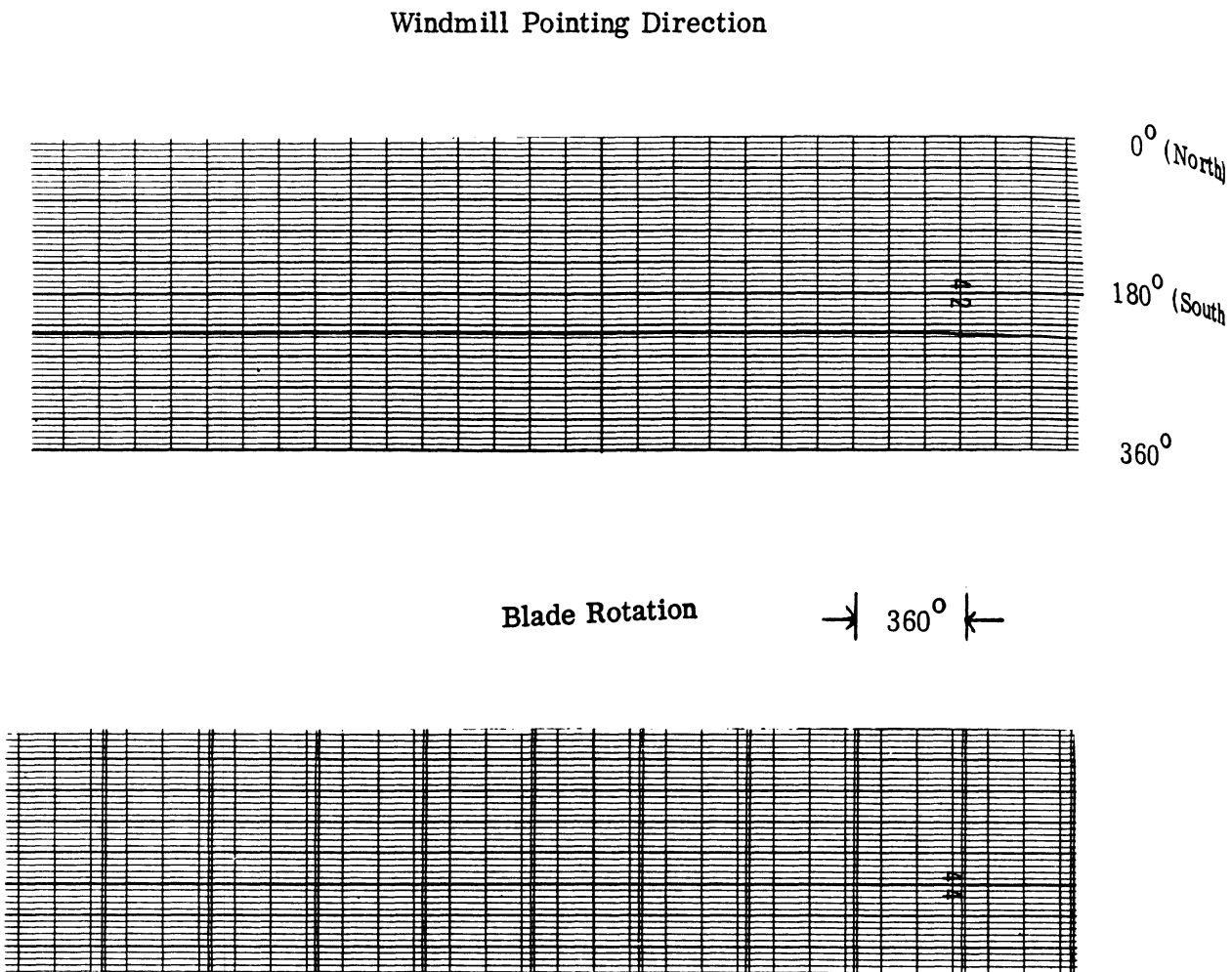

Figure VI.9. Wind turbine control center strip chart recordings during the operational test at site 14.

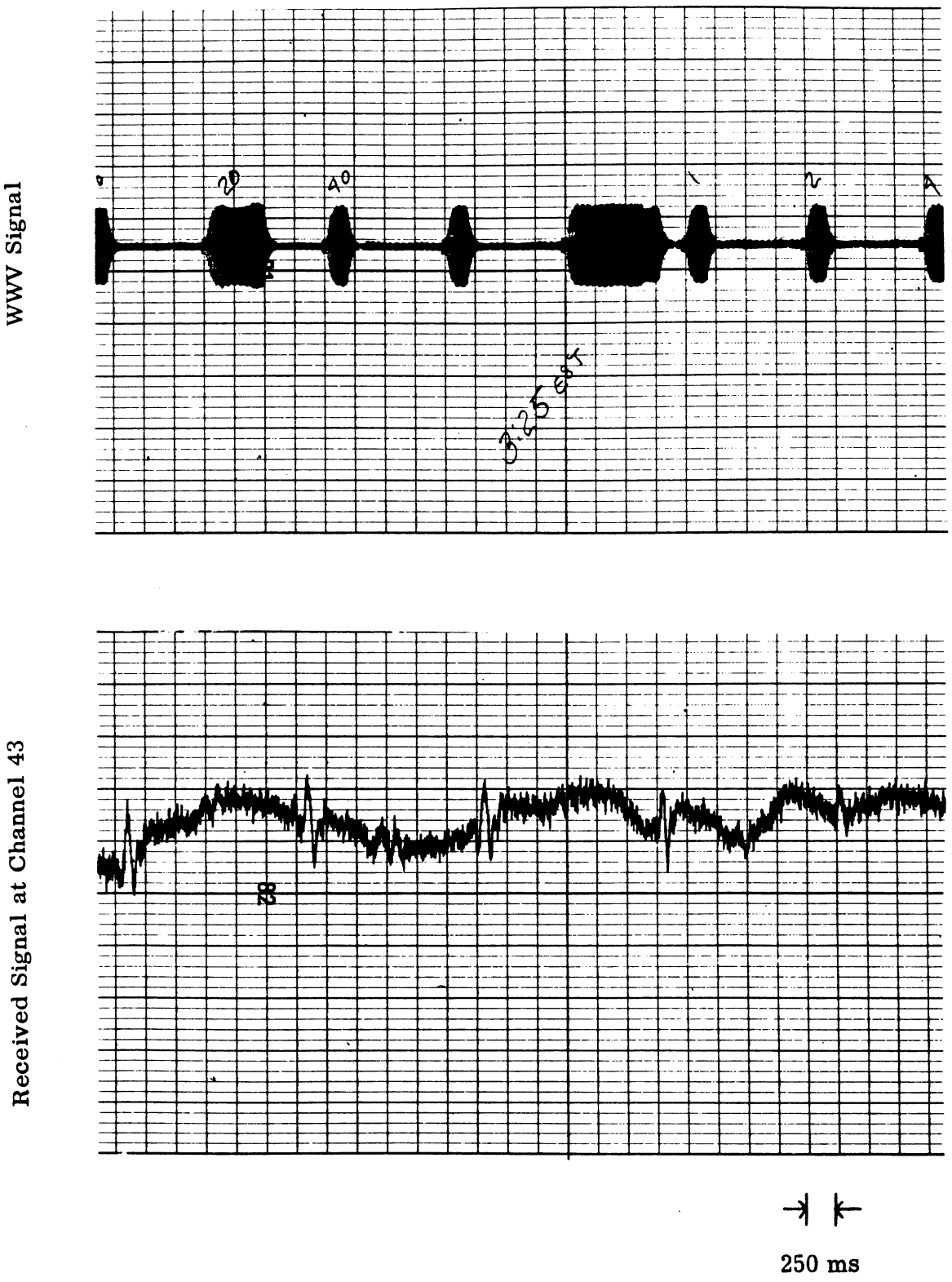

Figure VI.10. WWV time code and received Channel 43 signals during operational tests at site 14.

During the tests it was also observed that the video distortion occurred when the turbine blades were approximately vertical. This was the first time that any distortion had been seen when the blades were vertical. Although the incident fields are horizontally polarized, the large blades (dimensions ~60 x 3 feet; wavelength $\lambda \simeq 1.5$ feet for Channel 43 signals) will act as specular reflectors regardless of their orientation. When the blades are vertical, the upper and lower ones will reflect the incident field in directions approximately 6 degrees above and below the local horizon. The angle between the local horizon and the line joining the phase center of the receiving antenna to the center of the vertically oriented upper blade is approximately

$$\alpha \simeq \tan^{-1}\left(\frac{H_1 - H_2}{R}\right),$$

where H_1 is the height above the ground of the center of the vertically oriented blade; H_2 is the height above ground of the phase center of the receiving antenna, and R is the distance between the wind turbine and the antenna. In the present case with $H_1 \simeq 140$ feet, $H_2 \simeq 10$ feet and $R \simeq 1,350$ feet, $\alpha \simeq 5.5$ degrees. The antenna at site 14 could therefore receive signals scattered by a vertically oriented upper blade, but not those from a lower blade since they would propagate in a direction 6 degrees above the local horizon and would miss the antenna. This explains the occurrence of single modulation pulses in the received signals.

VI.7. Discussion

The field test results showed that the rotating blades of a wind turbine introduce pulse-like amplitude modulations to TV signals received in the vicinity of the turbine. The modulation pulses repeat at half the rotation period of the blades. Significant effects occurred at UHF frequencies and at a distance of approximately 0.25 miles from the turbine in spite of the 15 dB reduction in the scattered signal produced by the polar diagram of the receiving antenna. Severe video distortion was observed on Channel 43 and recorded, but no audio distortion was found.

VI.8. Reference

1. Howe, Sandra L., Editor, "NBS Time and Frequency Dissemination Service", NBS Publications 432, U.S. Dept. of Commerce, NBS, Boulder, Colorado, January 1976.

Appendix VII

ANALYSIS OF RESULTS

VII.1. Introduction

In this Appendix we first examine typical results obtained by numerical computation of the theoretical expressions of Appendix III and compare them with the relevant field test data of Appendix VI. If a windmill is illuminated by such a field, energy will be scattered off the blades, and because of the rotation of the blades, the net field picked up by a TV receiver in the vicinity of the windmill will be amplitude modulated. A method is described for deducing the modulation function and index from the computed field strength data. If the modulation is sufficiently strong, it will produce video distortion, and for any given TV Channel there is a region around the windmill where distortion can occur. This will be referred to as the windmill interference zone and an approximate theoretical method is described for computing its dimensions.

VII.2. Field Strength Variation

In Appendix III expressions were presented for the far zone field of an antenna located above a homogeneous smooth spherical earth, and these can be used to compute the strengths of both the direct and secondary fields. It will be assumed that the antenna is a horizontal electric dipole whose effective radiated power P is 1 kW. As evident from the $\sin\beta$ factor in (III.68), the far field is a function of the azimuthal angle referred to the dipole axis, but since it is sufficient to confine our attention to the direction for maximum field, this factor will be replaced by unity, corresponding to $\beta = \pi/2$. The resulting (maximum) field strength of the transmitter will be denoted by $\left|E_{\phi}^{T}(R)\right|$, where (as always) we are concentrating on the horizontal component.

The variation of the field strength as a function of the great circle distance d_{12} (see Figure III.4) of the receiver from the transmitter is illustrated in Figures VII. 1a, b, c for three different frequencies. The lobing is characteristic of the

interference region and is due to the combination of direct and ground-reflected signals. The magnitudes of the peaks fall off approximately as $1/d_{12}$. Beyond this region the field strength decreases approximately as $1/(d_{12})^2$ and later exponentially. The distance over which the interference region extends decreases with decreasing frequency and transmitter and receiver heights, but otherwise the field strength behavior is similar in all of the cases shown.

The smaller of the two transmitter heights in Figure VII. 1 is typical of a windmill viewed as re-radiator, i.e. the source of the secondary field, and with proper normalization the curves for h_1 = 30 m in Figure VII. 1 show the variation in the strength of the secondary field as a function of distance from the windmill.

To illustrate the manner in which the direct and secondary field strengths vary as a function of the distance d_{32} (see Figure III. 4) of the receiver from the windmill, consider the case of TV Channel 43 (f = 647 MHz) at the NASA Plum Brook site for which the windmill is 79.75 km from the transmitter. The transmitter is assumed to radiate 1 kW effective power, and the strength of the windmill regarded as a transmitter is computed using blades of total area 50 m^2 (see Section VI. 1). The transmitter, receiver and windmill are taken to lie on the same great circle and in Figure VII.2 curves 1 and 2 show the direct field at a receiver on the transmitter side and far side of the windmill respectively. Because the transmitter is at a large distance from the windmill, the direct field varies rather uniformly as a function of d_{32} and is, of course, larger in the first case, whereas the secondary field has a lobe structure out to 1 km or so from the windmill. At distances greater than this the strength of the secondary field relative to the direct one falls off more rapidly at a receiver on the near side of the windmill, implying that the interfering effects of the windmill will extend a shorter distance on this side. We will use these results in a later section.

VII.3. Total Received Field

At a receiving antenna R in the presence of a windmill, the total field can be written as

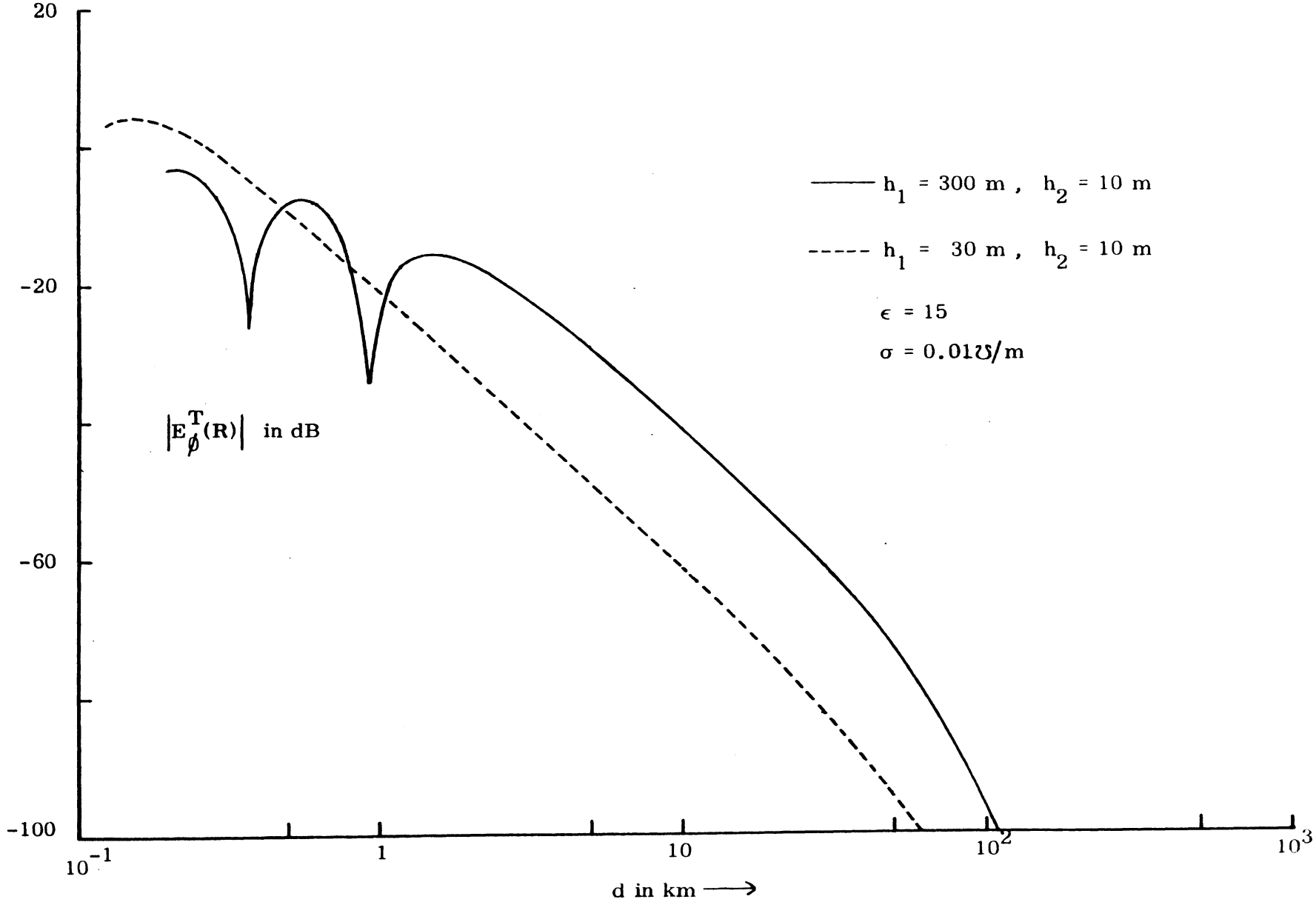

Figure VII. 1(a). $|E_\phi^T(R)|$ vs. d(= d_{12}) for f = 50 MHz.

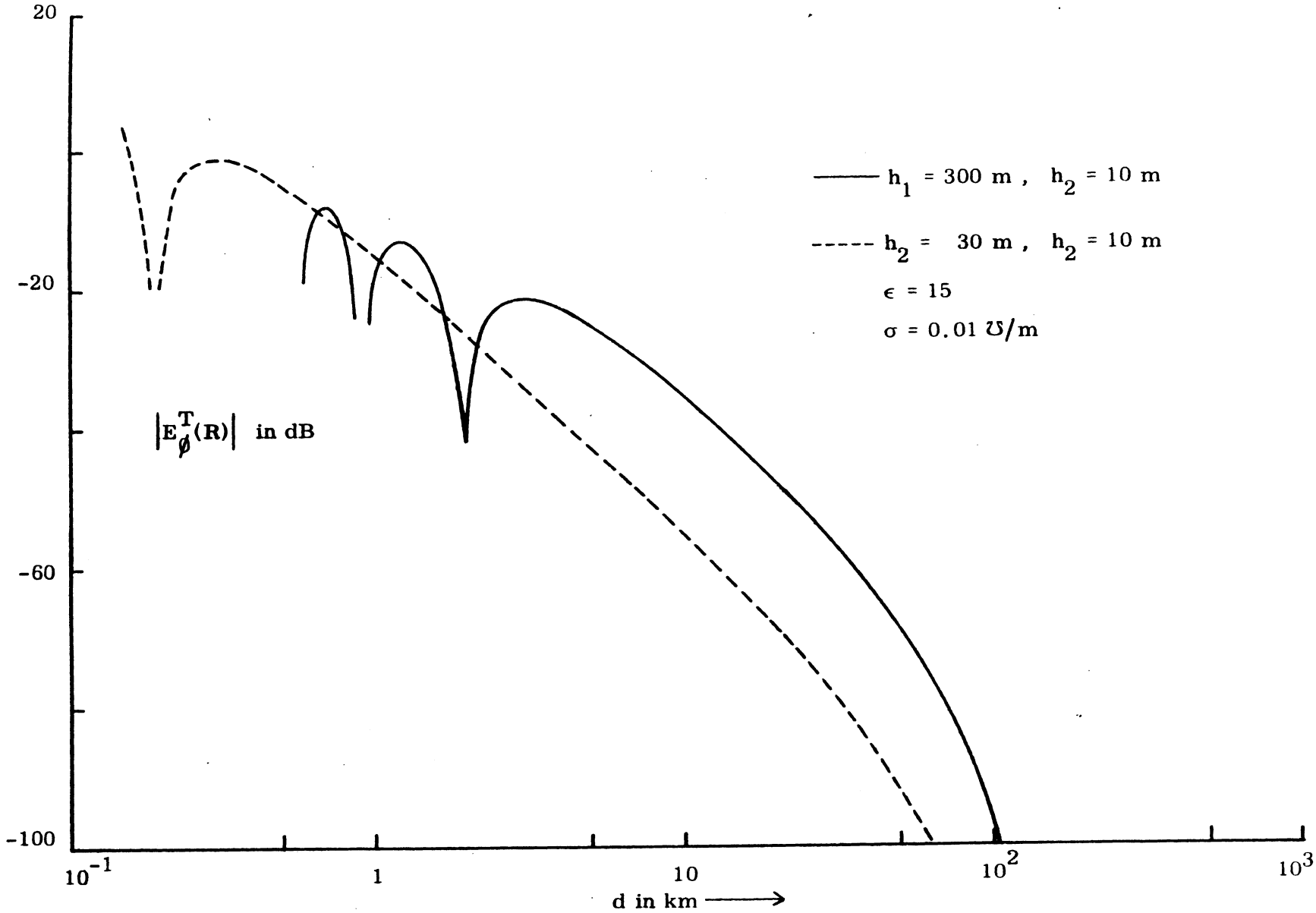

Figure VII. 1(b). $|E_\phi^T(R)|$ vs. $d(= d_{12})$ for f = 100 MHz.

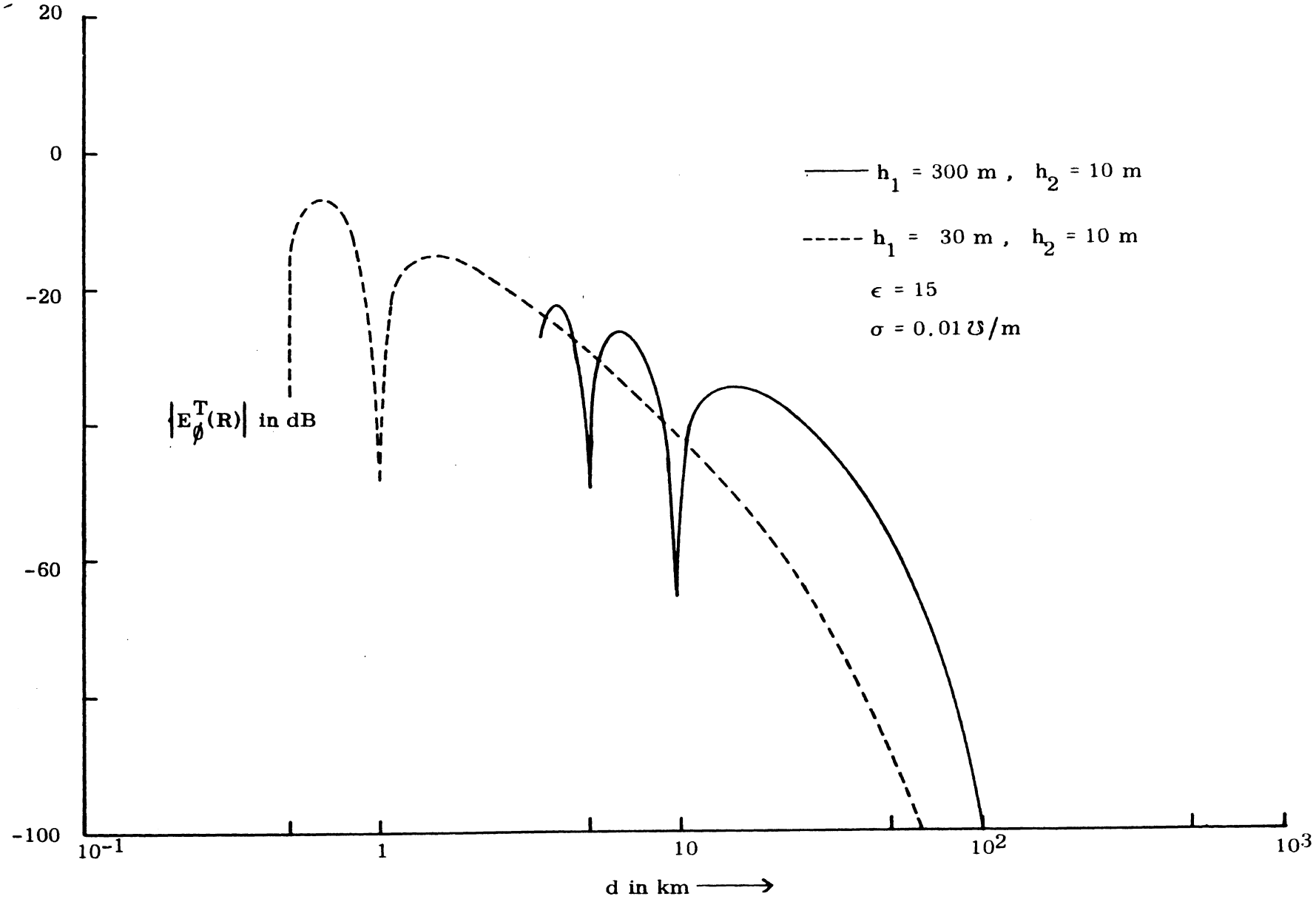

Figure VII.1(c). $|E_\phi^T(R)|$ vs. d(= d_{12}) for f = 500 MHz.

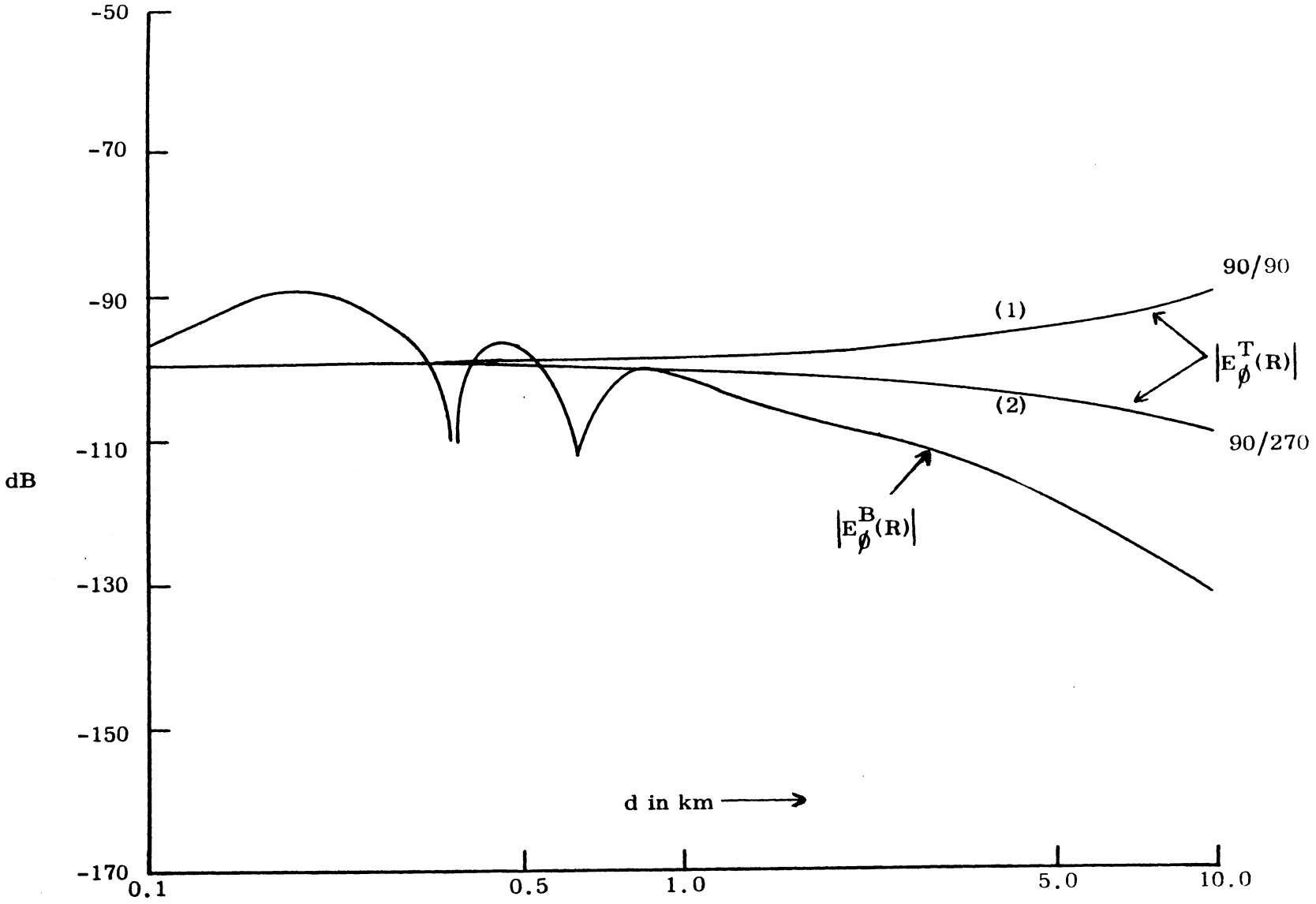

Figure VII.2. $|E_{\phi}^{T}(R)|$ vs. $d(= d_{32})$ and $|E_{\phi}^{B}(R)|$ vs. $d(= d_{32})$ for f = 647 MHz, h_2 = 300 m, h_1 = 10 m, d_{31} = 79.7 km, ϵ = 15, σ = 0.01 $\mho$/m.

$$E_{\phi}(R,\ t) = E_{\phi}^{T}(R) + E_{\phi}^{B}(R, t) \qquad \text{(VII. 1)}$$

where $E_{\phi}^{T}(R)$ is the direct field at R

$E_{\phi}^{B}(R,\ t)$ is the secondary field

and the rf time dependence represented by a factor $e^{i\omega t}$ has been omitted. All of the quantities in (VII. 1) are complex and the time dependence of the secondary field is due to the rotation of the windmill blades. We can separate out this time dependence by writing

$$E_{\phi}^{B}(R,\ t) = \left|E_{\phi}^{B}(R)\right| f_{m}(t)\, e^{i\delta(t)} \qquad \text{(VII. 2)}$$

where $\left|E_{\phi}^{B}(R)\right|$ is the maximum value of the field amplitude during any one rotation of the blades,

$f_{m}(t)$ is the (real) modulation function whose maximum value is unity,

$\delta(t)$ is the time varying phase.

If we also write the direct field as

$$E_{\phi}^{T}(R) = \left|E_{\phi}^{T}(R)\right| e^{i\delta_{o}} ,$$

the expression for the total field becomes

$$E_{\phi}(R,\ t) = E_{\phi}^{T}(R) \left\{1 + m f_{m}(t)\, e^{i\tilde{\delta}(t)}\right\} \qquad \text{(VII. 3)}$$

where $\tilde{\delta}(t) = \delta(t) - \delta_{o}$ (and is the rf phase difference between the scattered and direct signals)

and $$m = \left|\frac{E_{\phi}^{B}(R)}{E_{\phi}^{T}(R)}\right| . \qquad \text{(VII. 4)}$$

Assuming $m << 1$, the amplitude of the total received signal is then

$$\left|E_\phi(R)\right| = \left|E_\phi^T(R)\right| \left\{1 + m f_m(t) \cos \tilde{\delta}(t)\right\} \qquad \text{(VII.5)}$$

and m can now be identified as the modulation index (see also III.73).

Compared with the function $f_m(t)$, $\cos \tilde{\delta}(t)$ is rapidly varying as a function of time and achieves its extreme values ± 1 many times during a single sweep of $f_m(t)$. The envelope of (VII.5) is therefore

$$\left|E_\phi(R, t)\right|_{\text{envelope}} = \left|E_\phi^T(R)\right| \left\{1 \pm m f_m(t)\right\} \qquad \text{(VII.6)}$$

and represents the total received field that is actually observed. As a function of time, the variations (in dB) above and below the ambient field amplitude $\left|E_\phi^T(R)\right|$ of the direct field alone are, respectively,

$$\Delta_1 = 20 \log_{10} \left\{1 + m f_m(t)\right\}$$

$$\Delta_2 = 20 \log_{10} \left\{1 - m f_m(t)\right\} \qquad \text{(VII.7)}$$

implying a maximum-to-minimum variation

$$\Delta = \Delta_1 - \Delta_2 = 20 \log_{10} \left\{\frac{1 + m f_m(t)}{1 - m f_m(t)}\right\} \quad \text{dB} \qquad \text{(VII.8)}$$

VII.4. Modulation Function

The modulation function $f_m(t)$ represents the time dependence of the scattered field amplitude $\left|E_\phi^B(R)\right|$ introduced by the blade rotation. This could be determined by numerically computing the scattered field at every instance of time; however, this would be a very lengthy procedure in any practical case and would not bring out those features which are common to any rotating structure. We shall therefore use instead the physical optics approximation in conjunction with a rectangular plate model for a windmill blade.

VII.4.1. Determination of $f_m(t)$

Consider a rectangular metal plate located in the xz plane of a Cartesian coordinate system and oriented at an angle θ_s with respect to the (vertical) z axis (see Figure VII.3). The origin is also that of a spherical coordinate system and is located at the center of the plate. The plate will later be assumed rotating in the xz plane with angular frequency Ω such that any instant of time

$$\theta_s = \Omega t \, . \tag{VII.9}$$

As noted in Appendix III the transmitted field is predominantly horizontally polarized, implying that the magnetic field incident on the blade is in the z direction. It is therefore assumed that

$$\vec{H}^i = \hat{z} \, H_0 e^{ik(x \sin\theta_0 \cos\phi_0 + y \sin\theta_0 \sin\phi_0 + z \cos\theta_0)} \tag{VII.10}$$

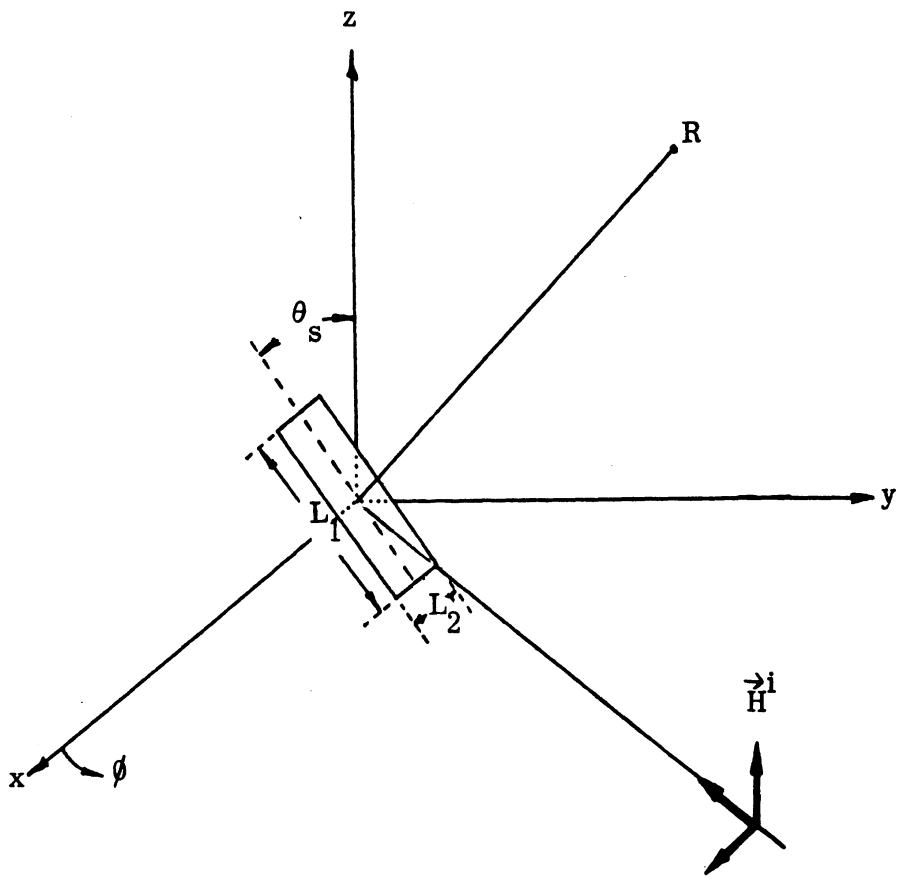

Figure VII.3. Scattering problem for a rectangular plate.

where, as always, a time dependence $e^{i\omega t}$ has been assumed and suppressed. According to the physical optics approximation, the current density at an arbitrary point x', z' on the illuminated side of the plate is then

$$\vec{J}_s = \hat{x}\, 2H_0 e^{ik(x' \sin\theta_0 \cos\phi_0 + z' \cos\theta_0)} \qquad \text{(VII.11)}$$

and is zero on the back. These currents radiate to produce the scattered field and by carrying out the necessary integration, the electric Hertz vector specifying the scattered field at a distant point R is found to be

$$\vec{\pi} = \hat{x}\, \frac{2H_0}{4\pi i\omega\epsilon} \frac{e^{-ikr}}{r} L_1 L_2 \operatorname{sinc}\left\{\frac{L_1}{\lambda}(p \sin\theta_s - q \cos\theta_s)\right\} \cdot \operatorname{sinc}\left\{\frac{L_2}{\lambda}(p \cos\theta_s + q \sin\theta_s)\right\} \qquad \text{(VII.12)}$$

where

$$\left.\begin{aligned} p &= \sin\theta_0 \cos\phi_0 + \sin\theta \cos\phi\,, \\ q &= \cos\theta_0 + \cos\theta\,, \end{aligned}\right\} \qquad \text{(VII.13)}$$

L_1, L_2 are the plate dimensions (see Figure VII.3)

and

$$\operatorname{sinc} X = \frac{\sin\pi X}{\pi X}\,.$$

The scattered electric field at R is given by

$$E_\phi = -k^2 \pi_x \sin\phi\,.$$

It therefore has only the ϕ component

$$E_\phi = i \frac{e^{-ikr}}{r} E_0 \frac{L_1 L_2}{\lambda} \sin\phi \operatorname{sinc}\left\{\frac{L_1}{\lambda}(p \sin\theta_s - q \cos\theta_s)\right\} \cdot \operatorname{sinc}\left\{\frac{L_2}{\lambda}(p \cos\theta_s + q \sin\theta_s)\right\} \qquad \text{(VII.14)}$$

where $E_0 = H_0/\eta_0$

and η_0 is the intrinsic admittance of free space. With the blade rotating, its dependence on time is through the parameter $\theta_s = \Omega t$, and since $|\text{sinc } X| \leq 1$, it follows that the modulation function is

$$f_m(t) = \text{sinc}\left\{\frac{L_1}{\lambda}(p \sin \Omega t - q \cos \Omega t)\right\} \text{sinc}\left\{\frac{L_2}{\lambda}(p \cos \Omega t + q \sin \Omega t)\right\}. \quad \text{(VII.15)}$$

VII.4.2. Nature of $f_m(t)$

Equation (VII.15) shows that for a given incident field direction (θ_0, ϕ_0) the nature of $f_m(t)$ is strongly dependent on the scattering or receiving direction (θ, ϕ). For a plate in the xz plane, the specular and forward scattering directions are $\theta = \pi - \theta_0$, $\phi = \pi - \phi_0$ and $\theta = \pi - \theta_0$, $\phi = \pi + \phi_0$, respectively, and in both cases $p = q = 0$, giving $f_m(t) = 1$. Although these are the directions of maximum scattering, the model that we have used does not reveal any time modulation resulting from the rotation of the plate.

This finding is at variance with actual observations on a windmill, and the defect of our model is not hard to see. Because we have assumed the (planar) blades to lie <u>in</u> the plane of rotation and have, in addition, employed a technique for calculating the scattering which is polarization independent, the directions of maximum scattering are the same regardless of the blade position. When the scattering is a maximum, the modulation is then a minimum, and the modulation will become significant only in directions away from the specular and forward lobes. In a practical situation it may be that the receiver cannot lie in a direction of maximum scattering (and we shall explore this case in a moment), but there is one key particular in which any actual windmill blades must differ from our model: they <u>must</u> lie out of their plane of rotation with, in practice, the two blades turned in opposite directions if they are to function as a turbine. They may, in addition, be aerofoil-shaped (non-planar) and/or coned, but these modifications merely reinforce the effect produced by the twisting

of a planar blade about its axis. If the receiver is in the specular direction for a blade in any given position, the rotation of the blade will now displace the specular lobe and it will not be until the blades complete a full revolution that the receiver again picks up the specular lobe. This leads to the concept of a rotating specular lobe or beam, and for a receiver which is appropriately positioned to pick up the maximum return, the signal has the form of a sinc pulse repeating every revolution of the blades.

We explore this concept further in Section VII.4.3., but it is well to note that even for a planar blade rotating in its plane there will be some modulation of the signal if the receiver is somewhat away from the direction of the maximum (specular) scattering. This may be true for all feasible locations of the receiver in a practical situation. For a transmitter which is far away, the direction of incidence on the blade can be assumed to lie in the plane $\theta_0 = \pi/2$ of the local horizontal (see Figure VII.3). For any given ϕ_0, the specular direction is then $\theta = \pi/2$, $\phi = \pi - \phi_0$, but since the windmill is usually much higher than the receiving antenna, it may be that the closest that can be achieved to this direction is $\theta = \pi/2 + \alpha$, $\phi = \pi - \phi_0$, where α is some small angle. Under these conditions, (VII.15) implies

$$f_m(t) \simeq \text{sinc}\left(\frac{L_1}{\lambda} \sin\alpha \cos \Omega t\right) \text{sinc}\left(\frac{L_2}{\lambda} \sin \alpha \sin \Omega t\right). \qquad \text{(VII.16)}$$

For a blade of high aspect ratio, $L_1 >> L_2$, and the time dependence of $f_m(t)$ is primarily determined by the first factor in (VII.16). The modulation function now has the form of a sinc pulse, and if its width $2t_1$ in time is measured by the separation of the first zeros on either side of the maximum,

$$2t_1 = \frac{2}{\Omega} \sin^{-1}\left\{\left(\frac{L_1}{\lambda}\sin\alpha\right)^{-1}\right\}$$

For a receiver sufficiently displaced from the specular direction, $\frac{L}{\lambda}\sin\alpha >> 1$ and

$$2t_1 \simeq \left(\pi f_B \frac{L_1}{\lambda} \sin\alpha\right)^{-1} \qquad \text{(VII.17)}$$

where f_B is the blade rotation frequency.

Equation (VII. 17) can also be used to predict the spread of the modulation function for scattering in the forward direction.

VII. 4. 3. Rotating Beam Concept

Because of the blades' twist out of their plane of rotation and (possibly) their coning as well, the specularly reflected lobe will sweep out a path through space as the blades rotate, and a stationary receiver so located as to pick up the maximum of the lobe will actually receive a signal only at those times corresponding to a narrow range of the blade rotation angle θ_s . The angular width $\Delta\phi$ of the specularly reflected beam of a stationary blade as measured between the first zeros of the sinc pattern is determined by the narrow dimension L_2 of the blade, and from (VII. 14) with $\theta_0 = \theta = \pi/2$ and $\theta_s = 0$ (blade vertical), we have

$$\Delta\phi = 4 \sin^{-1}\left\{\left(\frac{2L_2}{\lambda}\sin\phi_0\right)^{-1}\right\} \simeq \left(\frac{L_2}{2\lambda}\sin\phi_0\right)^{-1} . \qquad \text{(VII. 18)}$$

Since the beam will rotate with the angular frequency Ω of the blade, the time width $2t_0$ of the observed modulation pulse becomes

$$2t_0 = \frac{\Delta\phi}{2\pi f_B} = \left(\pi f_B \frac{L_2}{\lambda}\sin\phi_0\right)^{-1} \qquad \text{(VII. 19)}$$

c.f. (VII. 17). This will be used later in our analysis of the results observed at Plum Brook.

VII. 5. Interference Zone of a Windmill

The amplitude modulation of a TV signal received in the presence of a windmill comes about because of the sinc type pulses which constitute the scattered field observed at any fixed location. The duration of the pulses depends on the linear dimensions of the blades, their rotation speed, and the angles of observation with respect to

the plane of rotation of the blade. The strength of the pulses and, hence, the modulation depth depends on the scattered field strength relative to the ambient level of the direct (primary) field, and as noted above, both m and $f_m(t)$ are significant in directions close to those of specular and forward scattering. For a receiver so located, the windmill may produce unacceptable levels of video distortion.

From the results of the laboratory studies described in Appendix II it was concluded that the distortion would be unacceptable if $m \geq 0.2$. All other things being equal, m is a (not necessarily uniformly) decreasing function of distance from the windmill, and the specification $m \geq 0.2$ will therefore locate a zone around the windmill within which video distortion can occur. This will be called the windmill interference zone, but it should be emphasized that the situation is not 'black and white'. The distortion decreases with increasing distance and the boundary of the zone is simply the place where the distortion is judged as having passed from unacceptable to tolerable. With this caveat, the boundary of the zone is defined by the threshold 0.2 of the modulation index m .

Within the zone distortion will occur only with the passage of the rotating scattered beam through the receiving point, implying that for any given transmitter location the plane of rotation of the blades is such that this can take place. Our calculations of the zone will be carried out under the assumption that for given locations of the transmitter and receiver, the plane of blade rotation is oriented to direct the maximum scattered signal to the receiver. It does not therefore follow that video reception within the zone will be adversely affected at all times: at any given moment, video reception will depend on the orientation of the windmill.

The actual shape of the interference zone is a rather complicated function of the propagation and scattering characteristics, and, in general, can only be determined numerically taking into account the parameters appropriate to the specific situation. We show later an example in which the zone shape has been computed, but for convenience of description most of our calculations have been directed at the radius of an equivalent circular zone around the windmill. Nevertheless, by suitable (albeit drastic)

approximation, it is possible to arrive at an analytic specification of the zone, and we shall discuss this case first before going on to a more precise numerical determination later.

VII.5.1. Simplified Model

The simplified model ignores the directional scattering characteristics of the blades and the effect of the earth on the propagation. In effect, therefore, we assume omnidirectional scattering as well as omnidirectional transmitting and receiving antennas, and regard the entire problem as a free space one; but in spite of these assumptions, the model is able to predict the maximum distance from the windmill at which interference can occur, and also provides a valid qualitative picture of the interference.

In Figure VII.4, T, B and R are respectively the transmitter, windmill blades and receiver all located in the xy plane of a Cartesian coordinate system (x, y, z) whose origin is at B. The transmitter is at a large distance D from the windmill, and the receiver is at a distance d from the windmill in a direction making an angle ϕ with the positive x axis. On suppressing the usual time dependence, the direct field at R can be written as

$$E^T(R) \simeq K \frac{e^{-ik(D - d \sin \phi)}}{D(1 - \frac{d}{D} \sin \phi)} \qquad \text{(VII.20)}$$

where K is some constant. The direct field at B is similarly

$$E^T(B) = K \frac{e^{-ikD}}{D} \qquad \text{(VII.21)}$$

and if the effective scattering area of the blades is A independent of ϕ, the scattered field at R is

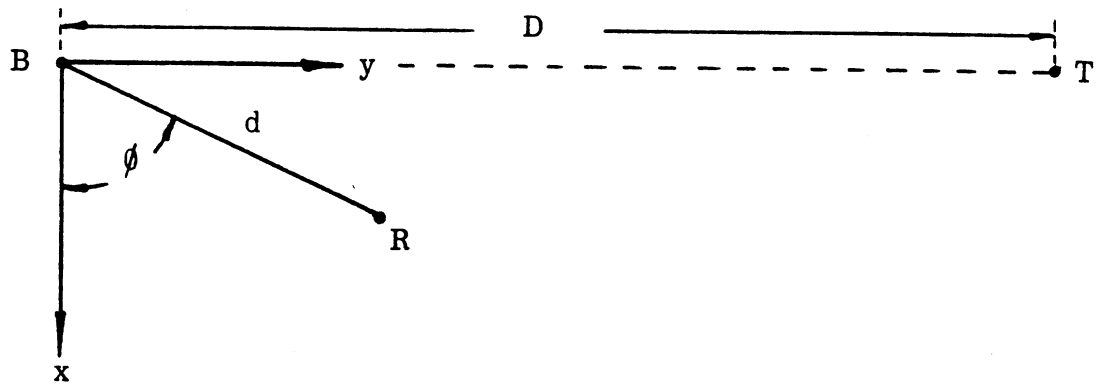

Figure VII.4. Simplified model for interference zone calculations.

$$E^B(R) = \frac{A}{\lambda} E^T(B) \frac{e^{-ikd}}{d}$$

$$= \frac{KA}{\lambda d} \frac{e^{-ik(D+d)}}{D} . \qquad \text{(VII.22)}$$

The modulation index is therefore

$$m = \left| \frac{E^B(R)}{E^T(R)} \right| = \frac{A}{\lambda d} \left(1 - \frac{d}{D} \sin \phi\right) , \qquad \text{(VII.23)}$$

and since in most practical situations $A << m\lambda D$, (VII.23) can now be solved to give

$$d = \frac{A}{m\lambda} \left(1 - \frac{A}{m\lambda D} \sin \phi\right) . \qquad \text{(VII.24)}$$

With m = 0.2, (VII.24) defines the interference zone around the windmill. The zone is sketched in Figure VII.5 and is approximately circular of radius $A/m\lambda$ but with the center of the circle displaced a distance $A/m\lambda D$ from the windmill in the direction away from the transmitter. As A increases and/or λ decreases, the radius and the center shift both increase. In the limiting case of a transmitter at infinity, the zone is exactly a circle of radius $A/m\lambda$ centered on the windmill.

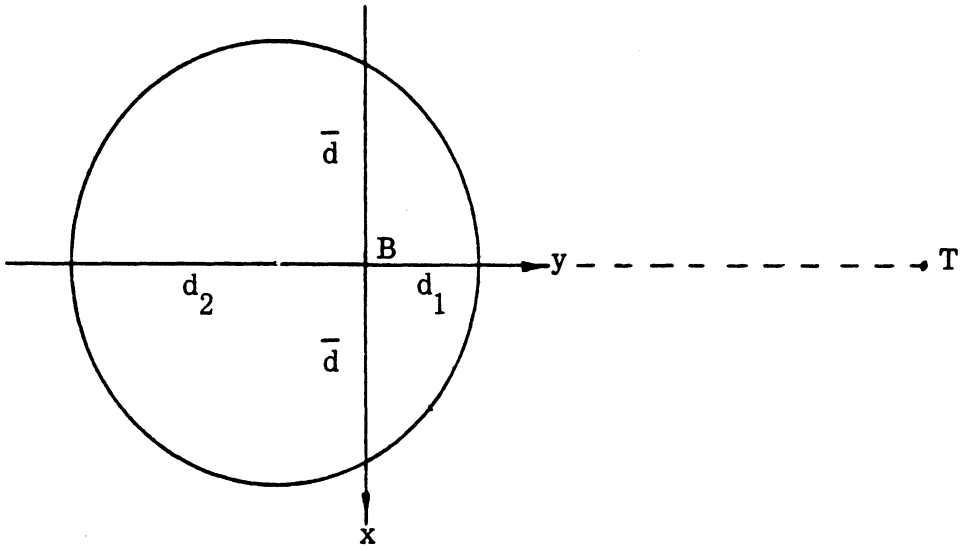

Figure VII.5. Interference zone based on the simplified model:

$$d_1 = \frac{A}{m\lambda}\left(1 - \frac{A}{m\lambda D}\right),\ d_2 = \frac{A}{m\lambda}\left(1 + \frac{A}{m\lambda D}\right),\ \bar{d} = \frac{A}{m\lambda}.$$

VII.5.2. Improved Model

A large rectangular plate does not scatter isotropically, and as a first improvement to the simplified model discussed above, we now introduce the actual scattering characteristics of the plate.

The plate is again assumed to lie in the xz plane of a Cartesian coordinate system and to rotate in the same plane (see Figure VII.3). To simplify the discussion, the directions of incidence and scattering are taken to be in the (horizontal) xy plane, implying $\theta = \theta_0 = \pi/2$. In the particular case $\phi_0 = \pi/2$ representing normal incidence on the blade, the directions of specular and forward scattering are $\phi = \pi/2$ and $\phi = 3\pi/2$ respectively, and the isotropic scattering model is directly applicable with the parameter A in (VII.22) equal to the physical area of the blades. The scattering pattern

then consists of two identical sinc distributions centered on $\phi = \pi/2$ and $3\pi/2$, and if we confine attention to just the main lobe of the distribution, the scattering as a function of the angle ϕ of reception consists of two lobes centered on the line joining the transmitter to the windmill. This in turn leads to the interference zone shown in Figure VII.6.

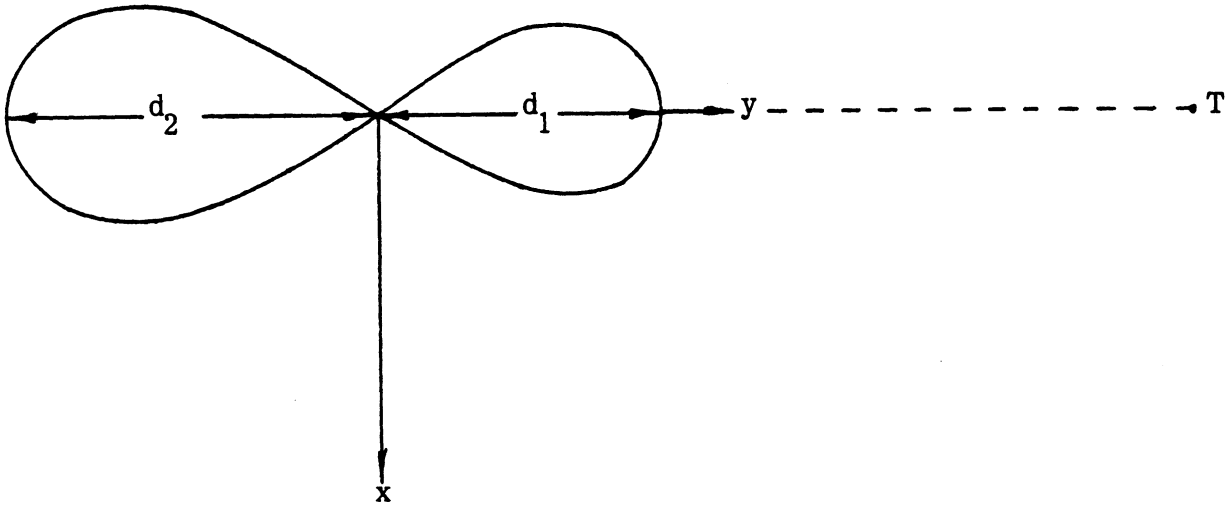

Figure VII.6. Interference zone for incidence normal to the plane of blade rotation.

The dimensions d_1 and d_2 are the same as in Figure VII.5 and the widths of the regions as specified, for example, by the 3 dB points, are determined by the electrical dimensions of the blades.

A more general case is that in which the transmitter is in a direction $\phi \neq \pi/2$. The specular direction is then $\phi = \pi - \phi_0$ and as evident from (VII.14) the effective area of the blades is reduced to A sin ϕ_0. The situation is unchanged if instead of displacing the incident direction from $\phi_0 = \pi/2$ we rotate the plane in which the blades lie; and by observing that the angle between the directions of incidence and reflection is $\pi - 2\phi_0$, the effective area of the blades for maximum scattering in a direction ϕ

relative to the x axis is A cos ($\pi/4 - \phi/2$). The distance d to which the interference zone extends in this direction is therefore

$$d(\phi) = d_1 \cos\left(\frac{\pi}{4} - \frac{\phi}{2}\right) \qquad \text{(VII.25)}$$

where d_1 is as defined before. The zone is a cardioid and is sketched in Figure VII.7.

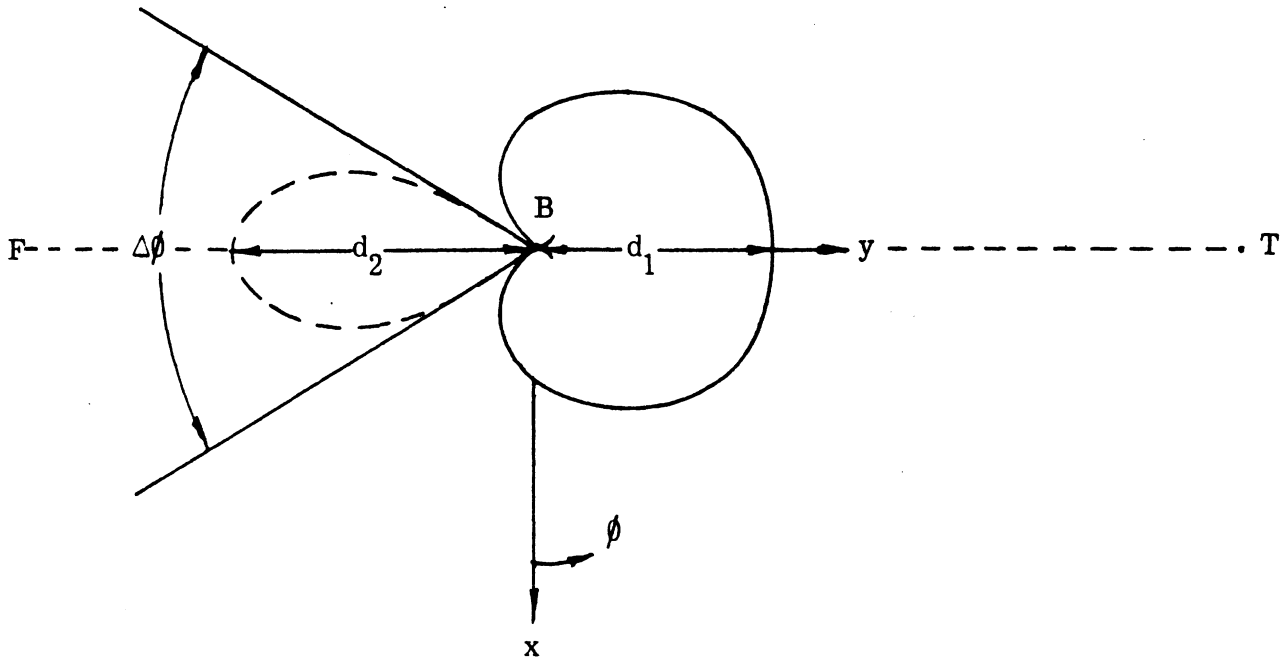

Figure VII.7. The specular (———) and forward (-----) scattering portions of the interference zone of a windmill.

In addition, however, there is still the forward scattering lobe of Figure VII.6. Its position is determined only by the direction of incidence and for a transmitter located as shown, the lobe is always centered on the direction BF of Figure VII.7. The maximum interference distance d_2 in the forward direction is achieved when the blades rotate in a plane perpendicular to this, i.e. in the xz plane, and for rotation in a plane making an angle α with the xz plane, the forward interference distance d_f is

$$d_f = d_2 \cos \alpha . \qquad \text{(VII.26)}$$

The total angular width (see Figure VII.7) of the forward zone is

$$\Delta\phi = \frac{2\lambda}{L_2 \cos \alpha} \qquad \text{(VII.27)}$$

where L_2 is the smaller dimension of the blade, but since our specification of windmill interference is based on the selection of that orientation of windmill which produces maximum interference in any chosen direction, it is sufficient to take $\alpha = 0$ as regards the forward scattering. We then have $d_f = d_2$ and in general $d_2 > d_1$.

The complete interference zone is therefore the union of the cardioid produced by specular scattering off the blades and the left hand lobe of Figure VII.6 attributable to forward scattering. Though our analysis has used only the simplified model in which the propagation effects of the earth are ignored, the inclusion of these effects does not significantly change the shape of the zone.

VII.5.3. Interference Zone Calculation

We now present a systematic method for computing the interference zone around a windmill in a fixed location with respect to a TV transmitter. In contrast to the method discussed in the previous section, we now use the expressions in Appendix III to take into account the effect of a homogeneous spherical earth on the propagation of both the primary (direct) and secondary (scattered) fields. Since the coordinate system used in the analysis of the scattering and modulation function differs somewhat from that in Appendix III, it is necessary to relate the two systems.

In the propagation analysis, the origin of coordinates was taken at the center of the earth (see Figure III.4) with the polar (z) axis aligned along the axis of the windmill tower and the blades rotating in the xz plane. The polar coordinates θ, ϕ defining the locations of the transmitter, receiver and windmill blade center were then identified by the subscripts 1, 2 and 3 respectively. In the present Appendix it proved more convenient to place the origin at the center of rotation of the windmill. The z axis was again vertical and the blades were rotating in the xz plane as before, but relative to our new origin of coordinates, the polar angles specifying the locations of the transmitter and receiver were taken as θ_0, ϕ_0 and θ, ϕ. The two sets of angles are related as follows:

$$\phi_0 = \phi_1 , \qquad \phi = \phi_2$$

whereas θ_0 is related to θ_1 and θ to θ_2 using the transformation relations of Appendix III, for example (III.41).

To determine the interference zone the following steps must be performed:

(i) Identify TV Channel frequency
transmitter coordinates h_1, ϕ_1
transmitter-windmill great circle distance d_{31}
transmitted power P (in kW)
receiver coordinates h_2, ϕ_2
windmill tower height ρ_o
blade (geometric) area A.

With T, B and R denoting the transmitter, windmill blade and receiver respectively

(ii) Use (III.68) with $\beta = \pi/2$ to compute

$$\left|E_\phi^T(R)\right| \quad \text{vs} \quad d(= d_{32}) \quad \text{for (a) } \phi_1 = \pi/2,\ \phi_2 = \pi/2 ;$$

$$\text{(b) } \phi_1 = \pi/2,\ \phi_2 = \pi/2 .$$

(iii) Use (III.60) with dS' = A to compute

$$\left|E_\phi^B(R)\right| \quad \text{vs} \quad d(= d_{32}) .$$

(iv) From (iia) and (iii) find the maximum value of $d(= d_1)$ for which

$$\left|E_\phi^B(R)\right| \Big/ \left|E_\phi^T(R)\right| = 0.2 .$$

(v) From (iib) and (iii) find the maximum value of $d(= d_2)$ for which

$$\left|E_\phi^B(R)\right| \Big/ \left|E_\phi^T(R)\right| = 0.2 .$$

Based on the isotropic scattering model, the interference zone is then a circle of radius $\frac{1}{2}(d_1 + d_2)$. This is the quantity that has been computed in all our studies of interference at specific windmill sites.

To obtain a more realistic estimate of the actual shape of the interference zone, it is necessary to take into account the scattering behavior of the blades. Based on the planar blade model, the following additional steps must be performed:

(vi) Compute $d(\phi') = d_1 \cos\frac{1}{2}\phi'$, $0 \leq \phi' < \pi$, where ϕ' $(= \phi_2 - \pi/2)$ is the angle between the lines joining the windmill to the receiver and the windmill to the transmitter.

(vii) Compute $d(\phi') = d_2 \operatorname{sinc}\left(\frac{L_2}{\lambda}\sin\phi'\right)$, $\pi - \sin^{-1}\frac{\lambda}{L_2} < \phi' \leq \pi$, where L_2 is the (average) smaller dimension of the blades.

Steps (vi) and (vii) respectively determine the specular and forward scattering portions of the interference zone, and the complete zone is then the union of the two. Although this should be a closer approximation to the actual interference zone, we caution that it is still only an approximation. In particular, the procedure described has ignored the change in the primary field at the receiver as ϕ' changes.

The above also assumes that the receiving antenna is isotropic (or, in practice, has the same gain as regards the primary and secondary fields), and if this is not so the interference zone will be affected. To illustrate, suppose the main beam of the receiving antenna is always directed at the transmitter. If ϕ'' is the angle* between the lines joining the receiver to the transmitter and the receiver to the windmill and if $f(\phi'')$ is the pattern function of the receiving antenna in the plane of observation, with $f(0) = 1$,

(viii) multiply the distance d in steps (iv) through (vii) by $f(\phi'')$.

This completes the interference zone calculations for a given transmitter location. For a different frequency and/or transmitter location, all relevant steps must be repeated.

---

* For a remote transmitter, $\phi'' \simeq \pi - \phi'$.

An example of the results obtained based on the isotropic scattering model is as follows:

TV Channel frequency : $f = 647$ MHz

$h_1 = 300$ m , $d_{31} = 79.7$ km, $P = 1$ kW

$h_2 = 10$ m, $\rho_o = 30$ m, $A = 50\ m^2$.

By referring to Figure VII.3 and carrying out steps (i) through (v), it is found that

$$d_1 = 2.73 \text{ km}, \quad d_2 = 4.90 \text{ km} .$$

VII.6. Comparison of Calculated and Observed Results

To assess the validity and accuracy of the various models and expressions used in the theoretical analyses, we shall now compare some of the predicted and observed results. All of the experimental data used was obtained during the field tests on the 100 kW wind turbine at Plum Brook (see Appendix VI). Each blade has the following dimensions:

length (L_1)	=	18.3 m (60 ft.)
width (max)	=	1.36 m (4.5 ft.)
(min)	=	0.46 m (1.5 ft.)
(av. = L_2)	=	0.92 m (3.0 ft.)

The area of a blade is $A \simeq 17\ m^2$. During the tests at Plum Brook the secondary signal observed at any instant of time was the field scattered specularly off a single windmill blade. In the following we shall therefore use the scattering from one blade only to compute the secondary field at the receiver.

VI.6.1 Scattering Tests

Scattering tests were performed at sites 5 and 6, but since the field scattered by the windmill had to traverse a heavily wooded area to reach the receiver at site 5, we confine attention to the site 6 results alone. The source of the signal used here was

TV Channel 24 having frequency f = 533 MHz and wavelength λ = 0.56 m. The pattern of the receiving antenna is shown in Figure VI.8. The main beam was directed at the windmill, thereby reducing the signal due to the primary field by 7 dB. Other pertinent parameters are:

$h_1 = 300$ m, $\phi_1 = 25^o$, $d_{31} = 65.3$ km; P = 1 kW,

$h_2 = 10$ m, $\phi_2 = 155^o$, $d_{32} \simeq 0.8$ km,

windmill tower height $\rho_o = 30$ m.

The details of the calculations are as follows:

Computer outputs:

$$\left|E_\phi^T(R)\right| = -59.68 \text{ dB} \qquad \text{for } \phi_1 = \pi/2,\ \phi_2 = \pi/2,\ d_{32} = 0.8 \text{ km}$$

$$\left|E_\phi^B(R)\right| = -99.34 \text{ dB m}^{-2} \qquad \text{for } \phi_1 = \pi/2,\ \phi_2 = \pi/2,\ d_{32} = 0.8 \text{ km}$$

In the present case

$$\left|E_\phi^T(R)\right| = -59.68 - 7.00 = -66.68 \text{ dB}$$

and in the direction $\phi_1 = \pi/2$

$$\left|E_\phi^B(R)\right| = -99.34 + 20 \log_{10} A$$

$$= -99.34 + 20 \log_{10} 17 = -74.73 \text{ dB}.$$

Hence

$$\left|\frac{E_\phi^B(R)}{E_\phi^T(R)}\right| = 0.40$$

which would be the modulation index for $\phi_2 = \pi/2$. To convert to $\phi_2 = 155^o$, multiply by sin 155^o to obtain

$$m = 0.40 \sin 155^o = 0.17.$$

The predicted field strength changes above and below the ambient level are therefore

$$\Delta_1 = 20 \log_{10} 1.17 = 1.36 \text{ dB}$$

and $$\Delta_2 = 20 \log_{10} 0.83 = -1.62 \text{ dB}$$

compared with the observed values (see Figure VI.5)

$$\Delta_1 = 1.3 \text{ dB}$$

$$\Delta_2 = -2.2 \text{ dB} .$$

The agreement is good.

VII.6.2. Operational Tests

These were performed at site 14 using TV Channel 43 (f = 647 MHz, λ = 0.46 m) as the source. Relevant parameters are

$$h_1 = 300 \text{ m}, \quad \phi_1 = 67.5^\circ, \quad d_{31} = 79.7 \text{ km}; \quad P = 1 \text{ kW},$$

$$h_2 = 10 \text{ m}, \quad \phi_2 = 112.5^\circ, \quad d_{32} = 0.47 \text{ km} .$$

The receiving antenna was pointed with its main beam towards the transmitter thereby reducing the scattered signal from the windmill by about 11.5 dB. The computation of the signal fluctuations is similar to the one described above, and the calculated and observed (see Figure VI.10) modulations are as follows:

	Calculated	Observed
Δ_1	0.9 dB	0.8 dB
Δ_2	-1.01 dB	-1.0 dB
m	0.11	0.10

The agreement is excellent.

It is also of interest to examine the time duration of the modulation pulses. We can use either of two methods to estimate it. From (VII.17) with L_1/λ = 39.8,

$\alpha = 5.5^{o}$ and $f_B = 1/3$ we obtain $2t_1 \simeq 250$ ms. On the other hand, from (VII.19) with $L_2/\lambda = 2$, $\phi_0 = \phi_1 = 67.5^{o}$ and $f_B = 1/3$ we find $2t_0 \simeq 517$ ms. The two times are rather different, but if we measure the width of the rotating beam between its 3 dB points (which is usual in practice) rather than between its nulls (as was done in VII.19), the duration $2t_0$ is halved to become 259 ms, which is in good agreement with the value for $2t_1$. The calculated and observed (see Figure VI.10) durations of the received modulation pulses are then:

	Calculated	Observed
$2t_1$	250 ms	~250 ms

The agreement is again excellent.

VII.7. Discussion

The results we have obtained confirm that for a fixed (distant) TV transmitter, a windmill will interfere with the reception of video signals in its vicinity. The interference is most severe in directions close to those of specular and forward scattering off the moving blades, but as the windmill slews in azimuth, these directions will encompass a complete region about the windmill. On the assumption of a receiving antenna which is omnidirectional, the shape of the interference region has been defined and techniques developed for computing its dimensions. We remark that if it is possible to use a directional antenna to discriminate against the windmill-scattered signals, the level of interference can be markedly reduced.

The agreement between the theoretical and observed results indicates that the theoretical model we have assumed is capable of providing a quantitative explanation of the interference phenomenon. As regards the field tests themselves, we have shown that

(i) at a given instant of time, only one of the windmill blades is scattering energy to the receiving point;

(ii) the windmill produces a sinc-type pulse modulation of the received signal; and

(iii) the threshold of modulation for significant (objectionable) interference on Channel 43 is approximately 0.1 .

In calculations of interference distances performed earlier in this study we set the threshold of modulation at m = 0.2. This value was chosen based on laboratory simulations using sinusoidal modulation of the signal, and prior to our present knowledge of the actual modulation introduced by a windmill. However, we also took the effective scattering area of the windmill to be A = 50 m^2 , and the interference distance is proportional to A/m . Since the results now indicate that A should be identified with the area of a single blade (17 m^2) and m taken to be 0.1 as judged by the Plum Brook data, our previous calculations of interference distance are too large by 30 percent.